Separation of racemates via host-guest chemistry

by

Baganetsi Karabo Sebogisi

Thesis submitted in fulfilment of the requirements for the degree

Magister Technologiae: Chemistry

in the Faculty of Applied Science

at the

CAPE PENINSULA UNIVERSITY OF TECHNOLOGY

Supervisor: Associate Professor A. Jacobs
Co-supervisor: Professor L. R. Nassimbeni

Cape Town
January 2012

TABLE OF CONTENTS

DECLARATION

I, Baganetsi Karabo Sebogisi, declare that the contents of this thesis represent my own unaided work, and that the thesis has not previously been submitted for academic examination towards any qualification. Furthermore, it represents my own opinions and not necessarily those of the Cape Peninsula University of Technology.

_____ _____

Signed Date

ABSTRACT

Chirality is very important to the pharmaceutical industry as enantiomers have the same macroproperties except for their optical and pharmacological activity. Industrial research has thus focused to find the most effective resolution technique. However, our aim was to obtain more information regarding the discrimination process. In this project the structures of the hydrates of di-quininium *L*-malate, **(2QUIN^{+})(*L*-MA^{2-})•2H$_2$O** and the di-quininium *D*-malate, **(2QUIN^{+})(*D*-MA^{2-})•2H$_2$O** have been investigated. (-)-Quinine (QUIN) did not show selectivity between the *D* and *L* malic acid and the structure of **(2QUIN^{+})(*DL*-MA^{2-})•2H$_2$O** was obtained. Effect of solvents was demonstrated in the study and the structure of **(QUIN^{+})(*D*-MA^{-})•H$_2$O)** was reported. The relationship between C-O bonds of the carboxylate and carboxylic moieties and ΔpKa was explored in salt and co-crystal formation.

Kinetics of absorption was conducted for the reaction of (+)-deoxycholic acid (DCA) with *n*-propylamine and DCA with racemic *sec*-butylamine. The rate constants of the reactions were determined. Kinetics of desolvation was performed on the powder samples of mixtures of DCA and sec-butylamine and DCA with di-n-butylamine. Non-isothermal methods were used where a series of TG analyses was carried out at different heating rates (2, 4, 10, 32 K min^{-1}). The structures of DCA with *n*-propylamine and di-*n*-butylamine were elucidated.

The selectivity of DCA was investigated. The host compound was found to be able to successfully resolve racemic *sec*-butylamine (2-BUAM) and 2-amino-3-methylbutane (MeBUAM). The structures of DCA with enantiomers of these guests are reported in the study. The structures of *R*-BUAM and *S*-BUAM were solved in different space groups while *R*-MeBUAM and *S*-MeBUAM crystallized in the same space group.

ACKNOWLEDGEMENTS

I wish to express my gratitude to Assoc. Prof. Ayesha Jacobs, Prof. Luigi R Nassimbeni and Dr. Nikoletta Báthori for the continuous guidance, time, advice, support and encouragement throughout my study. It has been a privilege to work with them, as they have taught me to resolve complex problems throughout my project and all I have learned from them will be very useful tools in my future career.

I thank my colleagues Amina Sayed, Nothemba Silwana, Mawonga Mei and Yav Kabwit for the support.

I am grateful for my family and friends who supported me throughout.

The Financial assistance of the Cape Peninsula University of Technology Postgraduate office towards this research is acknowledged. Opinions expressed in this thesis and the conclusions arrived at, are those of the author and are not necessarily to be attributed to the Cape Peninsula University of Technology Postgraduate office.

DEDICATION

Sebogisi and Mogomela families

LIST OF FIGURES

LIST OF TABLES

ABBREVIATIONS

CSD	Cambridge Structural Database
TGA	Thermogravimetric Analysis
DSC	Differential Scanning Calorimetry
PXRD	powder X-ray diffraction
R	universal gas constant
E_a	activation energy
ΔT	temperature difference
T	temperature
FT-IR	Fourier transform infra red
G	guest
H	host
IR	infra red
kJ mol^{-1}	kilojoules per mole
HNMR	proton nuclear magnetic resonance
T	temperature
QUIN	(-)-quinine
DCA	(+)-deoxycholic acid
CA	(+)-cholic acid
NSAID	non-steroidal anti-inflammatory drug
API	active pharmaceutical ingredients
T_{on}	onset temperature
R	correlation coefficient
k	rate constant
P	vapour pressure
l	liquid
g	gas
s	solid
DL-MA	*DL*-malic acid
D-MA	*D*-(+)-malic acid
L-MA	*L-(-)*-malic acid
ACE	acetone
PPA	1-propylamine
2-BUAM	(*R, S*)-*sec*-butylamine
R-BUAM	(*R*)-(-)-*sec*-butylamine
S-BUAM	(*S*)-(+)-*sec*-butylamine
1-BUAM	*n*-butylamine
ETAM	diethylamine
DIBUAM	di-*n*-butylamine
MeBUAM	(*R, S*)-2-amino-3-methylbutane
R-MeBUAM	(*R*)-(+)-2-amino-3-methylbutane
S-MeBUAM	(*S*)-(-)-2-amino-3-methylbutane
R2	decreasing area
R3	decreasing volume
PF (%)	percentage packing factor
RMS	root mean square
RMSD	root mean square deviation

POSTER PRESENTATIONS

1. Baganetsi K. Sebogisi, Ayesha Jacobs, Nikoletta B. Báthori & Luigi R. Nassimbeni**,** Structures of Quininium (*L*)-Malate and Quininium (*D*)-Malate – A subtle discrimination, 40th SACI Convention incorporating the 15th Inorganic Conference (INORG2011) and the 3rd FASC Congress 16-21 January 2011, University of Witwatersrand, Johannesburg, South Africa.

2. Baganetsi K. Sebogisi, Ayesha Jacobs, Nikoletta B. Báthori & Luigi R. Nassimbeni**,** Structures of Di-quininium (*L*)-Malate and Di-quininium (*D*)-Malate – A subtle discrimination, Cape Peninsula University of Technology Research Day, 2nd December 2011, Cape Town.

CHAPTER 1

INTRODUCTION

1.1 Supramolecular Chemistry

Steed *et al*[1] defined supramolecular chemistry as the study of systems that are made up of groups of molecules or ions that are bonded by non-covalent interactions. These interactions are electrostatic interactions, hydrogen bonding, dispersion interactions and solvophobic effects. It has also been defined by phrases such as 'chemistry beyond the molecule'[2] and 'the chemistry of the non-covalent bond' as well as 'the non-molecular chemistry'.[3]

Supramolecular chemistry blossomed in the late 1960s and early 1970s with host-guest systems in which metal ions were complexed to crown ethers and small guest molecules were bound to larger host molecules by non-covalent interactions.[2&4] However, the history of supramolecular compounds dates back to the 1800s (**Table 1.1.1**) with the discovery of the clathrate chlorine hydrate by Sir Humphrey Davy in 1810.[3]

Table 1.1.1: Summary of the history of supramolecular chemistry

Year	Event
1810	Discovery of chlorine hydrate by Sir Humphrey Davy
1823	Formula of chlorine hydrate by Michael Faraday
1841	Study of graphite intercalates: C. Schafhäutl
1849	F. Wöhler: β-quinol H_2S clathrates
1891	Villiers and Hebd: cyclodextrin inclusion compounds
1893	Alfred Werner: Co-ordination chemistry
1894	Emil Fischer introduced the lock and key concept
1906	Paul Ehrlich introduced the concept of a receptor
1937	K. L. Wolf: the term Übermolecüle is coined to describe organised entities arising from the association of co-ordinately saturated species, e.g. the acetic acid dimer.
1939	Linus Pauling: hydrogen bonds are included in the groundbreaking book "*The nature of the chemical bond*"
1940	M. F. Bengen: urea channel inclusion compounds
1948	H. M. Powell: X-ray structures of β-quinol inclusion compounds; coins the term 'clathrate' to describe compounds where one component is enclosed within the framework of the other
1949	Brown and Farthing synthesise [2,2]paracyclophane
1953	Watson and Crick discover the structure of DNA
1956	Dorothy Crowfoot Hodgkin: X-ray crystal structure of vitamin B_{12}
1959	Donald Cram attempted the synthesis of cyclophane charge transfer complexes with $(NC)_2C=C(CN)_2$
1961	N. F. Curtis: first Schiff's base macrocycle from acetone and ethylenediamine
1964	Busch and Jäger: Schiff's base macrocycles
1967	Charles Pedersen: crown ethers
1968	Park and Simmonds: *katapinand* anion hosts
1969	Jean-Marie Lehn: synthesis of the first cryptands
1969	Jerry Atwood: liquid clathrate from alkyl aluminium salts
1973	Donald Cram: spherands hosts produced to test the importance of pre-organisation
1978	Jean-Marie Lehn: introduction of the term supramolecular chemistry
1979	Gokel and Gokahara developed the lariat ethers.
1981	Vögtle and Weber: podand host and developed nomenclature
1987	Donald J. Cram, Jean-Marie Lehn and Charles J. Pedersen received the Nobel prize for chemistry for their contributions to supramolecular chemistry.
1996	Atwood, Davies, MacNicol and Vögtle: publication of *Comprehensive Supramolecular Chemistry* containing contributions from almost all the key groups and summarising the development of the discipline.
1996	Kroto, Smalley and Curly: Nobel Prize for chemistry for their work on the fullerenes

Source: Steed J. W. & Atwood J. L. (2000). *Supramolecular Chemistry.* Singapore: John Wiley & Sons.

Supramolecular chemistry is a fast growing field that entails a number of study disciplines. A lot of work in supramolecular chemistry is targeted at synthesizing inclusion compounds with certain properties. The most widely studied hosts include crown ethers, spherands, calixarenes and cyclodextrins with guests such as metal cations and small organic molecules.[3]

It is a broad field that involves other fields of chemistry such as inorganic chemistry and organic chemistry that are needed to synthesize novel supramolecular compounds as well as physical chemistry which is required in understanding the properties of the supramolecular compounds. The multidisciplinary nature of supramolecular chemistry has brought together physicists, synthetic organic chemists, biochemists, computational modellers, inorganic and solid state chemists.[1&3]

1.1.1 Molecular recognition

Emil Fischer[5] postulated that binding must be selective. He used the 'lock and key' model (an enzyme mimicking system) of steric fit to describe this recognition. The guest must have a geometric size or shape that complements the receptor or host. Molecular recognition, which is the discrimination by the host between several guests, was established. This chemical occurrence is responsible for all processes taking place in biology and asymmetric synthesis is based upon the potential of molecules or substrates to be selective.[3&5]

The role of complementarity is evident not only in supramolecular systems; it also has an important role in biological systems, e.g. the enzyme and the substrate. In order for the host and the guest to form a supramolecule, they must have common spatially and electronically complementary binding sites. The binding sites on both the host and the guest must also correspond chemically in order to form strong and selective binding.[1]

Chirality is also one of the unique characteristics of things in both the macroscopic and the microscopic worlds. Chirality, just like molecular recognition, existed on earth since the origin of life but the phenomena is not well understood.

1.2 Chiral chemistry

Chirality is the term used to describe the handedness of objects. The term is derived from the Greek word *cheir*, which means hand. Mirror images of chiral objects are nonsuperimposable.

Chirality is also observed in molecules. Compounds that differ in the way their atoms are arranged in space are called stereoisomers or configurational isomers. Two kinds of these isomers are known; *cis*-*trans* and asymmetric centres. The presence of an asymmetric centre or chiral centre is the most common cause of chirality in molecules. An example of an asymmetric centre is a tetrahedral carbon that is bonded to four different groups. **Figure 1.2.1** illustrates the asymmetric centre or chiral centre.

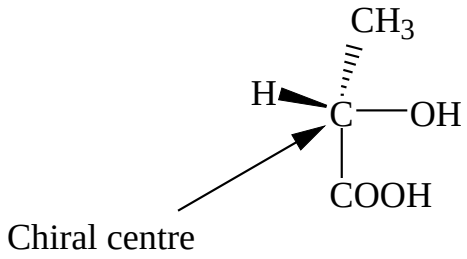

Figure 1.2.1: Chiral centre of lactic acid

Chiral centres were associated with the asymmetry that was found responsible for the rotation of plane polarised light in two different directions. The French physicist Jean-Baptiste Biot[6] discovered (in 1815) that certain natural organic compounds have different effects on plane polarised light and he correlated that to the asymmetry of the molecules. It was later established by Van't Hoff and Le Bel[6] that the asymmetry was related to the molecules having one or more chiral centres.

Asymmetric centres are not only limited to carbon. Nitrogen and phosphorus can also be asymmetric centres, as long as they have four different groups attached to them.[6]

The other cause of chirality is conformation. Simplistic rotations about a single bond can give rise to different conformations. These are distinct molecular arrangements that differ in spatial arrangements. Different conformations can be separated when the rotations about single bonds are restricted by steric factors. This type of stereoisomerism that depends upon restricted bond rotation is called atropisomerism. This sort of isomerism results in numerous molecules being chiral even though they do not have an asymmetric centre, e.g. allenes, spiranes and biaryls.[7&8]

Molecules that are mirror images of each other and are nonsuperimposable are referred to as enantiomers. Chirality is the property of the entire molecule; therefore each member of the nonsuperimposable images (pair of enantiomers) is chiral. **Figure 1.2.2** shows the two stereoisomers that are mirror images of each other.[6]

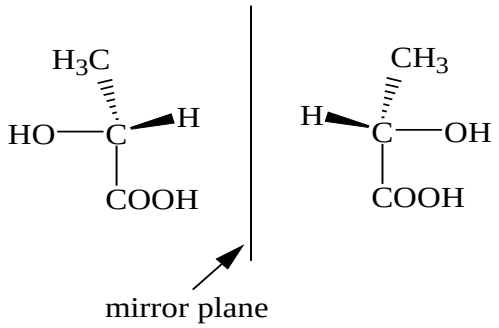

Figure 1.2.2: Mirror images of Lactic acid

R/ S configuration is the Cahn-Ingold-Prelog convention used to describe the stereochemical configuration around the chiral carbon. The letters are derived from Latin, *R* for *rectus*, which means to the right or clockwise and S is for *sinister*, which means to the left or anti-clockwise[9] It is attained by assigning priorities to atoms attached to the chiral carbon in order of decreasing atomic number. The atom with the highest atomic number gets the first priority. The next atoms in each substituent are compared if the first atoms are the same. This is continued until the first point of difference is attained. The molecule is then adjusted such that the atom or group of least priority is pointing directly backwards. If the motion from the substituents of the highest priority through the second to the third is clockwise, the chirality centre has the *R* configuration and if the movement is anticlockwise, the chirality centre has the *S* configuration. The assignment of configuration is shown in **Figure 1.2.3** (A).[10]

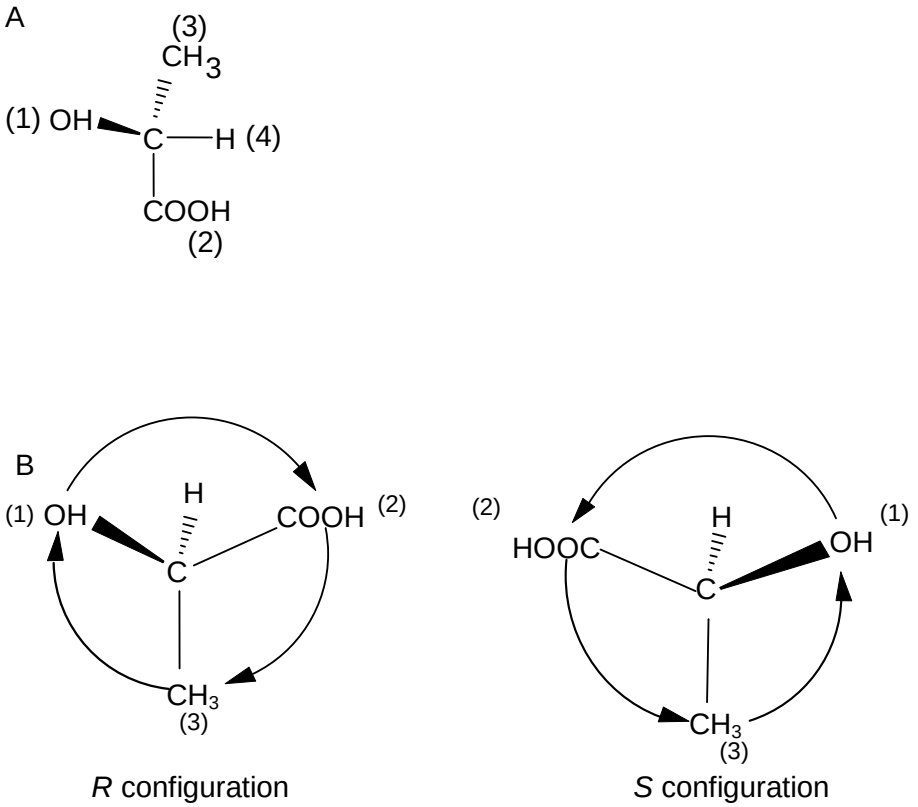

Figure 1.2.3: The assignment of priorities in lactic acid (A) and assignment of configurations (B)

Enantiomers were discovered around the 1850's by the French microbiologist and chemist, Louis Pasteur.[11] He unravelled the mystery about the nature of tartaric acid. He performed an experiment on the sodium ammonium salts of tartaric acid and found that the crystals of this salt have hemihedral faces which allow them to be separated by hand (triage). The crystals are mirror images of each other and behaved differently when exposed to polarized light. These two forms

rotated light in opposite directions and the equimolar mixture of the two forms (racemic mixture) had no effect on polarized light.

Enantiomers have many properties in common. Most physical features of these compounds are the same apart from those arising from how the groups are bonded to the chiral centre. They have identical boiling points, melting points and solubility characteristics. Specific rotation is one property that is different for the enantiomers; they interact with plane polarised light differently.

Compounds with more than one chiral centre are called diastereomers. They are stereoisomers but are not mirror images of each other, therefore they are not enantiomers. These compounds differ quite significantly in physical properties as well as chemical activities. The specific rotations of these compounds can differ in magnitude and sign. Their chemical reactivity can differ and can even lead to entirely different products, depending on the nature and mechanism of the reaction.[8]

Racemates (racemic mixtures) are equimolar mixtures of enantiomers.[12] Pasteur[13] wrote: "Most natural organic products, the essential products of life, are asymmetric and possess such asymmetry that they are not superimposable on their images." Racemic mixtures behave differently from the individual constituents and it is important to comprehend their properties and differences in order to design an efficient method for resolution.

Chirality plays a very important role in the lives of both flora and fauna. It has not only been significant to the chemical industry, agricultural and pharmaceutical industries have also benefited. Many drugs and pesticides synthesised are chiral and are marketed as racemic mixtures. On the other hand, natural chiral compounds are enantiopure, e.g. (-) amino acids and (+) natural sugars.[14]

1.3 Chirality in drug design and development

The occurrence of enantiomers has been very significant to the pharmaceutical industry and is quite common amongst biologically active agents. These agents demonstrate an elevated extent of selectivity in their action. They have the capacity to discriminate or to distinguish their molecular sites of action, particularly receptors or enzymes on which they work. It is because of this discriminatory behaviour of bioactives that complementarity is necessitated between the agent and the site of action. This explains the physicochemical properties of the groups in the molecule that take part in the interaction and their arrangement in space.

Most biochemical processes are stereoselective and natural products are obtained in an optically active form; however most of the organic synthetic drugs are racemic and are therefore optically

inactive. It is vital to note that isomers have different physical and chemical properties and can also show different pharmacological activity. The stereoselectivity of the bioactives means that only one isomer in the racemic drug will be therapeutically active and the other one might not just be inactive but can also cause severe side effects, hence regarded as the impurity.[15] For this reason it will be suitable to deem the two enantiomers as separate drugs with dissimilar characteristics except if confirmed otherwise.[16]

Recently, the significance of stereochemistry in drugs has been recognised and the outcomes of using them as racemates or single enantiomers have been recurrently conferred to in the pharmaceutical industry. The different pharmacological profiles displayed by the isomers of a racemic drug are expressed by their affinity for certain receptors subtypes/ enzymes, distribution rates, metabolism and excretion. Even though the isomers show different pharmacological profiles, some drugs are still administered as racemates.[13] Anti-depressants such as tranylcypromine, citalopram, fluoxetine and trimipramine are still available in racemic mixtures, while single enantiomers of bupropion are being formulated. Zupiclone and some methylphenidate are also some of the drugs in psychiatric practice that are still administered as racemates.[16]

For the reason that most of the chiral drugs are still in racemic mixtures, preparative separations of enantiomers are still vital. Resolution of enantiomers is one of the important topics in scientific research.[17]

1.3.1 Actions of isomers

Because many of the biological macromolecules in humans are chiral, this led to stereoselectivity of drugs or biological actives, (bioactives). For a drug to be effective there has to be some chemical complementarity between the drug and the active site of action. This implies that in a racemic drug, only one enantiomer will be effective, the question arising will be what happens to the other enantiomer?

The difference in pharmacological activity of the enantiomers has led to the creation of two terms, “eutomer” for the potent isomer and “distomer” for the less potent one depending on the pharmacological effect being considered because different isomers may have different pharmacological effects for different activities. The terms are used to refer to one single most obvious effect.[18&15]

Several things can happen to or because of the inactive drug, ranging from the inactivity of the drug resulting in it getting excreted to the enantiomer causing side effects. The possible actions of isomers are as follows;

1. One enantiomer may possess the therapeutic action while the other may contribute to the side effects. This has been demonstrated by thalidomide, **(Figure 1.3.1)**.

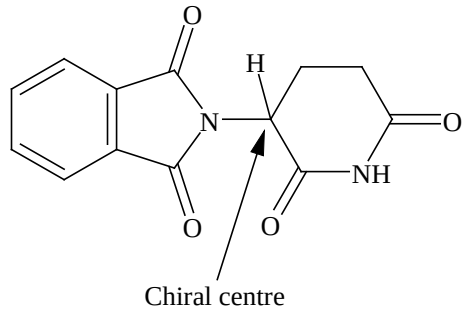

Figure 1.3.1: The molecular structure of thalidomide (2-2,6-dioxopiperidin-3-yl)-1H-isoindole-1,3-dione)

Thalidomide was initially marketed more than 50 years ago for treatment of epilepsy and it was discontinued because of its lack of effectiveness and efficiency. Eventually it was prescribed to women during pregnancy as a sedative and anti-nausea agent. The (*S*)-enantiomer of the drug was thought to cause foetal abnormalities and the (*R*)-enantiomer was responsible for sedative properties. This led to attempts to separate the drug into pure enantiomers which failed because of its ability to racemise on standing. Later the rabbit model in New Zealand showed that both enantiomers were actually responsible for the malformations of the embryo. The use of the drug as a sedative was brought to a stop in the 1960s because of the alarming rates of deformities it caused in children.[19,20&21]

Another drug that is still distributed as a racemate though it has one bioactive enantiomer is ibuprofen (**Figure 1.3.2**). This is a synthetic drug that is used as a non-steroidal anti-inflammatory drug (NSAID) for treatment of pains, inflammation and fever. It is produced as a racemic mixture.

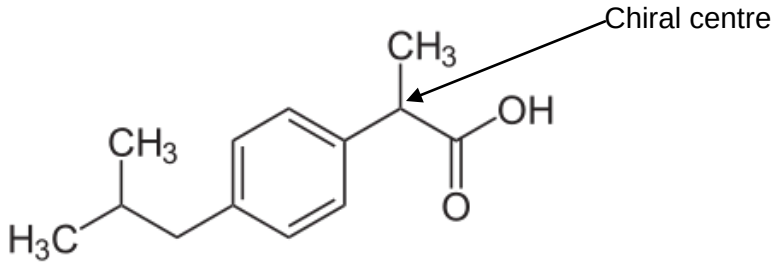

Figure 1.3.2: Molecular structure of ibuprofen [2-(4-isobutyl-phenyl) propionic acid]

The (*S*)-enantiomer of the drug was found to be therapeutically active and the (*R*)-enantiomer was inactive and caused side effects such as stomach ulcers and damage to the kidneys.[22] Efforts to purify the drug enantiometrically are quite challenging and there is ongoing research

on techniques to resolve it. The drug was also found to undergo *in vivo* isomerization, from the *R*-enantiomer to the *S*-enantiomer.[23,24&25]

It is possible that the two enantiomers might have equal biological activity. This has been demonstrated by some antidepressants such as fluoxetine and some immunosuppressive agents like cyclophosphamide. This behaviour of enantiomers has also been observed in anti-malarial drugs, e.g. mefloquine and enpiroline. Enantiomers of agents used for the treatment or prevention of cardiac arrhythmias (flecainide and propafenone) also showed little or no difference in their potency.[14]

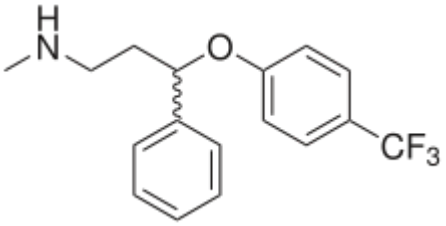

Fluoxetine: *N*-methyl-3-phenyl-3-[4-(trifluoromethyl)phenoxy]propan-1-amine

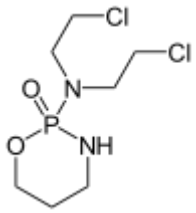

Cyclophosphamide*: N*,*N*-bis(2-chloroethyl)-1,3,2-oxazaphosphinan-2-amine 2-oxide

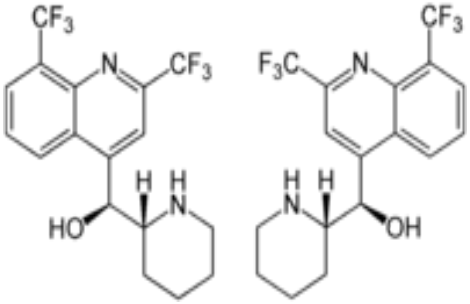

Mefloquine: (*R**,*S**)-2,8-bis(trifluoromethyl)quinolin-4-yl]-(2-piperidyl)methanol

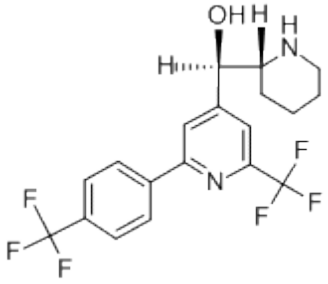

Enpiroline:(*R*)-[(2*R*)-piperidin-2-yl]-[2-(trifluoromethyl)-6-[4-(trifluoromethyl)phenyl]pyridin-4-yl]methanol

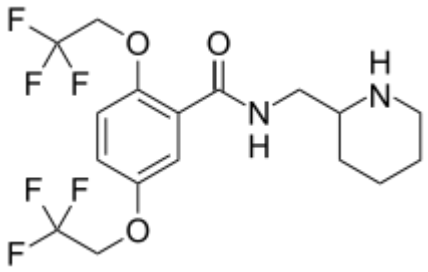

Flecainide: (*R,S*)-*N*-(piperidin-2-ylmethyl)-2,5-bis(2,2,2-trifluoroethoxy)benzamide

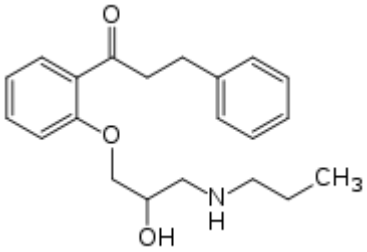

Propafenone: 1-{2-[2-hydroxy-3-(propylamino)propoxy]phenyl}-3-phenylpropan-1-one

2. The potential for enantiomers of racemic drugs to have opposite therapeutic effect have been reported.

3. Cases whereby different isomers have different therapeutic effects are also heard of in the pharmaceutical industry. The enantiomers were found to act as eutomers at different sites.

1.3.2 Global overview of Chiral Drugs

From above, it is clear that the enantiomers of a chiral drug will vary in bioavailability, metabolism rate, metabolites, excretion, potency and selectivity for the receptors, transporters and enzymes and toxicity and this qualifies them to be considered separate drugs. The accessibility of single enantiomer drugs to the medical industry is increasing and sometimes the drugs are available as both single enantiomers and racemates. It is critical to make a distinction between single enantiomers from the racemic mixture as their effectiveness, aftermath profiles and sometimes even the designated applications differ.[16]

There are reasons that stimulate the efforts to obtain enantiopure drugs. These are:

a. If one enantiomer is responsible for most of the therapeutic effects of the drug and the other one cause side effects, separating them will not just eliminate the side effects, but it will also result in administering a lesser dose of the therapeutic enantiomer.
b. Separation of stereoisomers will expose the patient to less body load and this will reduce metabolic drug load.
c. It will be easier to assess physiology, disease and drug co-administration effects.
d. Obtaining enantiopure drugs will lower drug interactions and avoid enantiomer-enantiomer drug interactions.
e. Administering of enantiopure drugs will enable their assessment of efficiency and toxicity *via* pharmacokinetic/ pharmacodynamic monitoring with ease.

These are just specific justifications that are required for decision making. The decision to develop and formulate the drug as a racemate or single enantiomer is entirely up to the manufacturer.

Research on the trend in the development of chiral drugs, shows that there has been an increase in the number of enantiopure drugs approved as compared to racemates. **Table 1.3.1** and **Figure 1.3.3** illustrate the annual distribution of chiral drugs (racemates, single enantiomer) and achiral drugs over a 20 year period, (1983-2002).

Table 1.3.1: Annual distribution of chiral and achiral drugs for the years 1983-2002[14]

Year	Racemates %	Enantiopure %	Achiral %
1983	37	26	37
1984	28	26	46
1985	38	22	40
1986	26	26	48
1987	18	49	33
1988	26	39	35
1989	29	26	45
1990	33	35	32
1991	20	40	40
1992	21	44	35
1993	16	45	39
1994	38	38	24
1995	21	46	33
1996	9	41	50
1997	24	30	46
1998	15	50	35
1999	13	52	35
2000	9	62	29
2001	0	68	32
2002	6	55	39

Even though enantiopure drugs offer greater health benefits, their development and manufacturing is costly and this can be viewed as a barrier for pharmaceutical developers. Cost-effective rationalization for approval or rejection of new therapeutic drugs will be appropriate as it will not be practical to pay an increased amount for only an insignificantly increased effectiveness.[26&18]

1.4 Resolution of racemates

Homochiral and heterochiral are the terms used to illustrate how chiral classes of compounds correlate. Homochiral interactions are the intermolecular non-bonded interactions between the molecules of the same chirality whereas the heterochiral interactions occur between the molecules that have opposite chirality.

The two interactions are demonstrated in the reversible reaction equations below.

Homochiral:

$$R + R \rightleftharpoons R\cdots R$$

Heterochiral:

$$R + S \rightleftharpoons R\cdots S$$

These interactions can be different in strength, direction and accounts for the differences in physical properties of racemates and the pure enantiomers. This is referred to as enantiomer discrimination.

Diastereomer discrimination arises when the interactions of a certain enantiomer of one compound and the two enantiomers of another kind give a diastereomeric pair. This is demonstrated in the reaction below.

$$(R_1, R_1) + (R_2, S_2) \rightleftharpoons R_1\cdots R_2 + R_1\cdots S_2$$ [27]

There are several methods that have been developed for the resolution of enantiomers.[28] These include the following:

a. Conversion to diastereomers

The racemates are converted to diastereomeric mixtures by reacting them with an optically active (resolving agent). The resultant diastereomeric products can be separated and reconverted to the pure enantiomers by reversing the initial chemical transformation as illustrated in **Scheme 1**.[7]

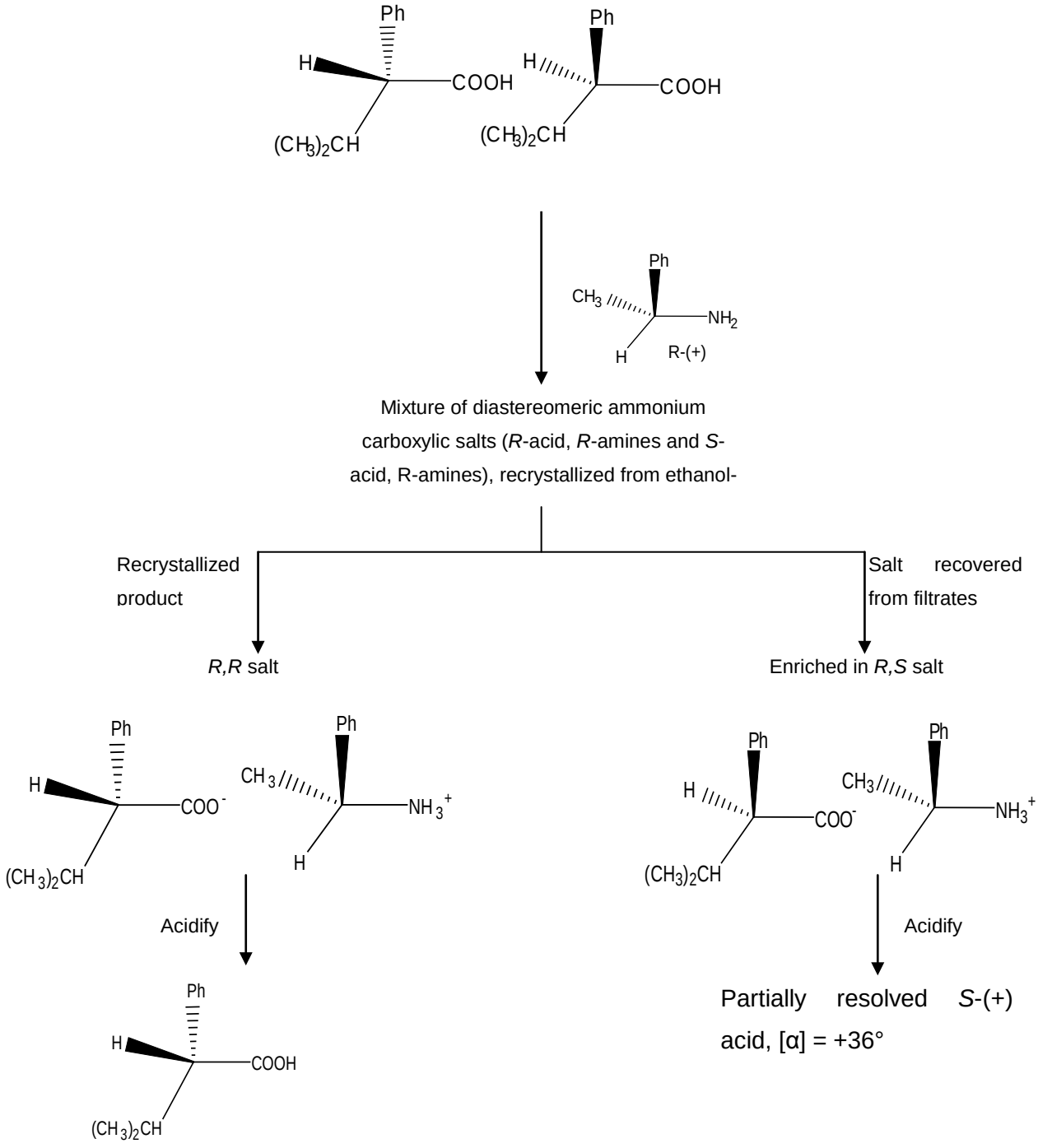

Scheme 1: Conversion of racemic acids to diastereomers

Fractional distillation is the traditional method employed to separate the resultant diastereomeric compounds generated. Chromatographic methods (gas chromatography and high performance liquid chromatography) are also useful since the diastereomeric compounds have differential absorption on achiral materials. Chromatographic techniques can be used on gases and liquids. The conversion to diastereomers technique is often applied to carboxylic acids; a molecule without

a carboxylic group can be converted to a carboxylic acid prior to resolution. Basic racemates can also be changed to diastereomeric salts with appropriate chiral acids. Other functionalities such as alcohols, esters and amino alcohols can be converted to diastereomers.

b. Mechanical separation

This method was used by Pasteur[29] to separate the racemic mixture of sodium ammonium salts of tartaric acid. The enantiomers of sodium ammonium tartrate were crystallised separately. The crystals are nonsuperimposable and distinguishable and therefore can be separated by tweezers. The method rarely works because very few compounds can form distinguishable crystals. The seeding approach has been applied to the method; a seed crystal added to the racemic mixture that will trigger crystallisation of one enantiomer. Sublimation has also been found to provide unprompted resolution. This was observed in the norborneol derivatives; the two enantiomers crystallised separately when the racemic solid was exposed to sublimation.

c. Enzymatic transformations

Biological processes usually are very stereoselective and therefore can lead to a high extent of resolution. Enzyme-catalysed reactions can be used to resolve organic compounds. The enzymes are derived from L-amino acids and are homochiral. Their interaction with one enantiomer bears a diastereomeric relationship to the interaction of the enzyme with the other enantiomer, and this makes one enantiomer more reactive. They are greatly resourceful, act as very selective catalysts and can carry out a variety of conversions. The high degree of selectivity between the two enantiomers is brought about by the specific fit to an active site property of enzymes.

Enzymes that catalyse the hydrolysis of esters and amides and those oxidising alcohols to ketones or aldehydes have been extensively studied. The reactions can also be carried out by brewing the reactants with a micro-organism that generate a suitable enzyme.

The method is limited by the need to find the proper organism and the other enantiomer can be destroyed in the process.[29]

d. Kinetic Resolution

This method is based on the fact that enantiomers can react with chiral compounds at different rates and can even lead to different products as stated before. The difference in the rate of reaction of the two enantiomers with a chiral reagent can be used as a resolution method. The process relies on the difference in transition state energies of the diastereomeric transition states $\boldsymbol{R_1 \cdots R_2}$ and $\boldsymbol{R_1 \cdots S_2}$. The degree of the difference of the reaction rate and the extent of the reaction

determine the level of the resolution that can be accomplished. The enantiomeric purity of the reacted and the unreacted enantiomer will be elevated if the difference in the rate of the equation is large. The degree of conversion can be controlled which will in turn control the level of enantiomeric purity; partial separation can be achieved by discontinuing the reaction before completion. This technique is elaborated in **Scheme 2**.[7]

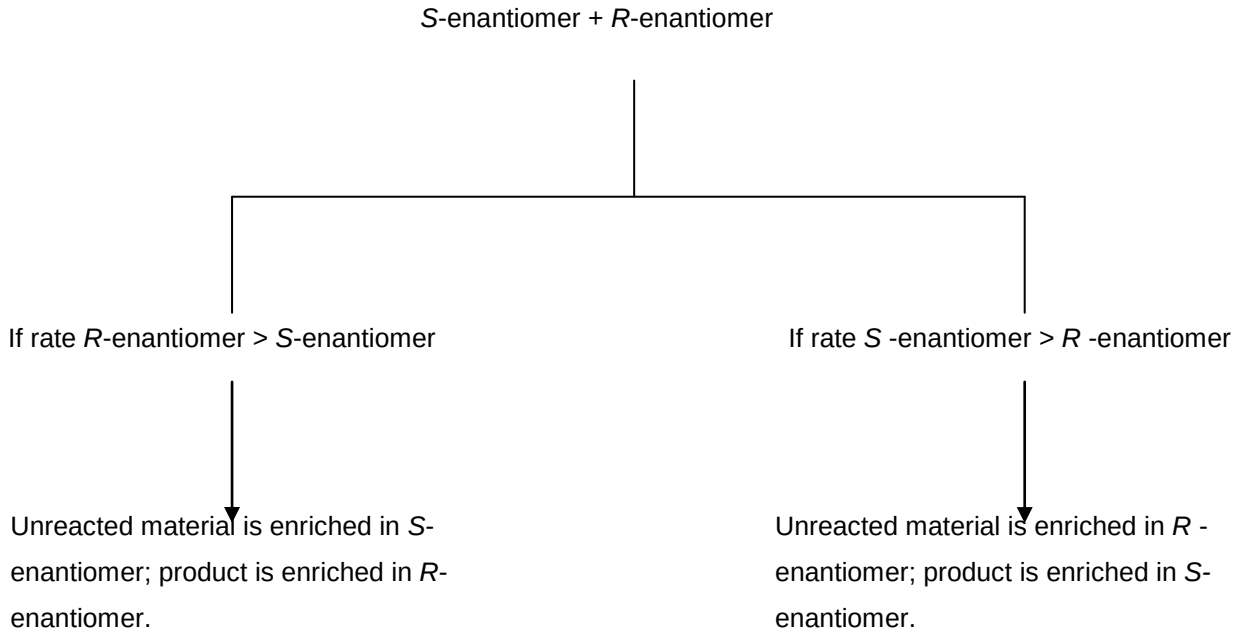

Scheme 2: Separation of racemates by kinetic resolution

Alkenes cannot be easily converted to diastereomers and this method has shown to be useful in resolving racemic alkenes using the optically active diisopinocamphenylborane.

e. Differential Absorption/ Chromatographic method

The method is based on the difference between the two enantiomers in non-covalent bonding to a chiral substance. A homochiral stationary phase is used. Most forms of chromatography; paper, column, thin layer and liquid chromatography provided successful results. The weak bonding between the two enantiomers and the homochiral stationary phase creates diastereomers with different binding affinities. This causes the difference in the rate of motion of the two enantiomers through the column, hence separation. This is quite an old technique and has only been developed recently. It has been found to be the most practical method. Columns with excellent separation capacity have been developed for HPLC and coupling this with chiral column packing materials has made this technique the best technique for separation and analysis of enantiomers.[7&29]

f. Dutch resolution

Other methods such as the Dutch resolution[30] have been developed whereby structurally related resolving agents are used. Resolving agent mixtures were developed and showed to be fast and efficient in resolving a variety of salt forming racemates. The resolution of racemic mixtures *via* diastereomeric salt formation has been the most commonly used industrial technique.[31]

g. Chiral resolution

Chiral host compounds are used to form diastereomers. The host can form an inclusion compound with one enantiomer of the racemic guest- chiral recognition. The host compounds have cavities or arrange to form a cavity that can fit one enantiomer and not the other. Chiral molecules have been successfully resolved by host-guest chemistry. Naturally occurring optically active chemicals have shown to be good resolving agents hence the design of synthetic derivatives of these natural chemicals helped improve the choice of application offered by the natural agents. The design of synthetic resolving agents is based on the co-ordination assisted clathrate formation between hosts with particular functionalities (e.g. –OH and –COOH) and polar guest molecules.[32]

Compounds such as crown ethers, cryptands, cyclodextrin and cholic acid have been used in this kind of resolution.[29]

1.5 Host-guest chemistry

1.5.1 History of inclusion compounds

Even though the concept of supramolecular chemistry was only established a few decades ago, the history of inclusion compounds or host-guest compounds dates back to 1778 when J. Priestley[33] observed the formation of today's "clathrates". 'Clathrates' is the word coined by H. M. Powell[34] (the father of inclusion compounds) in 1948; he elucidated the X-ray crystal structures of β-quinol inclusion compounds. This term is derived from a Latin word 'clathratus' meaning closed or surrounded from all sides and 'inclusion compounds' was introduced by W. Schlenk[33], for channel compounds of urea and thiourea.

Prior to 1947 inclusion compounds or clathrates were prepared, but were not clearly understood. These include the preparation of the chlorine hydrate in 1810, the preparation of cyclodextrin inclusion compounds in 1891 and clathrates of Dianin compound.[34]

1.5.2 Inclusion Compounds

Inclusion compounds can be divided into two groups:

- Where the host is a single molecule possessing cavities and the guest molecule(s) is or are partially enclosed into the cavity within the host resulting in a molecular inclusion.
- Where there is more than one host that pack in such a way as to form voids and the guest resides in the resultant void. This is called crystal lattice inclusion.[1&3] **Figure 1.5.1** illustrates the formation of a molecular inclusion and crystal lattice inclusion.

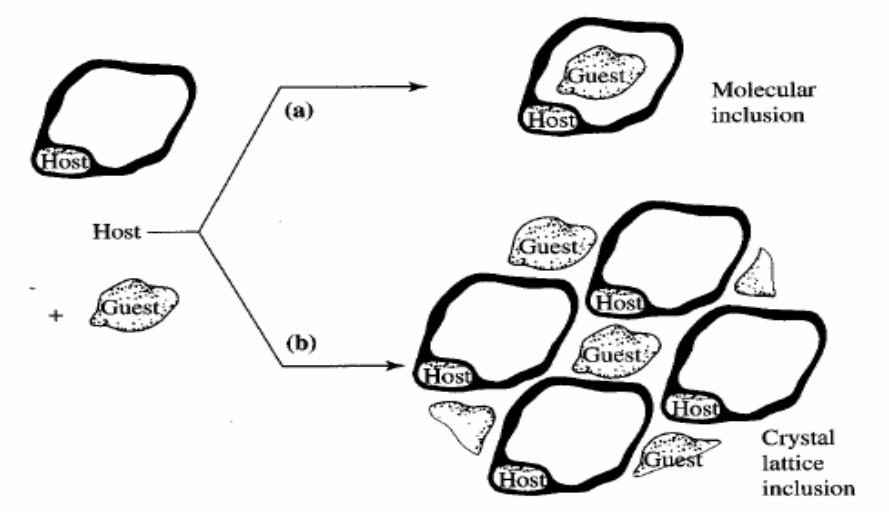

Figure 1.5.1: Illustration of the difference between molecular and crystal lattice inclusion[35]

Host-guest compounds are also referred to as inclusion compounds.

The general formula

$$\mathbf{H_{(s,\alpha)} + nG_{(l)or(g)} \rightarrow H{\cdot}G_{n\,(s,\beta)}}$$

represents the formation of host-guest compounds where:

α is the non-porous phase of the host, the apohost

β is the phase of the host-guest compound with a host guest ratio n

l is the liquid phase

g is the gas phase

s is the solid phase[36]

Successful host molecules are generally large, heavy and rigid and contain functional groups that can bind to suitable guests.[37]

1.5.3 Interactions of supramolecular chemistry

Supramolecular chemistry deals with non-covalent bonding interactions. These interactions are weaker than covalent interactions and they include a number of attractive and repulsive forces discussed below.[1&3]

a. Ion – Ion interactions

These interactions are non-directional.[1] It is the only non-covalent interaction with a strength that can be compared to that of a covalent bond, (418.7 – 1256.1 kJ mol^{-1}).[3] **Figure 1.5.2** shows an example of an ion– ion interaction in tetrabutylammonium chloride.

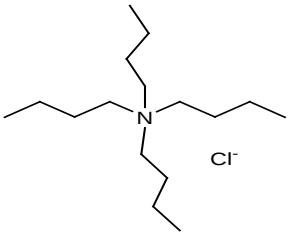

Figure 1.5.2: Illustration of the ion-ion interactions[1]

b. Ion – Dipole interactions

These are observed in bonding of ions with polar molecules both in the solid state and in solution. In complexes of alkali metals with crown ethers, the lone pairs of electrons on the oxygen are attracted to the positively charged ion. It is a directional interaction therefore for it to occur the two components must be arranged such that the interactions occur in the most favourable direction.[1&3]

c. Dipole – Dipole interactions

These occur when one dipole arranges with a neighbour such that the opposite poles are aligned. Just like the ion-dipole interactions they are directional but are considerably weaker. Only complementary species are allowed to form a collective.[1] **Figure 1.5.3** shows dipole-dipole interactions of adjacent carbonyl groups.

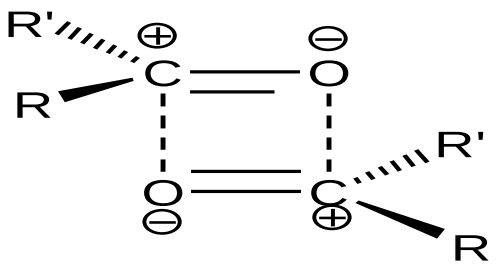

Figure 1.5.3: Illustration of dipole-dipole interactions between carbonyl groups[3]

d. Cation-π interactions

These are interactions between a cation and the face of a simple π-system, e.g. benzene **(Figure 1.5.4)**. They are considered electrostatic since the positively charged metal ion is drawn to the negative electrostatic face of the π-system. Studies reveal that smaller ions bind more readily than the bigger ones. The consequences of the cation-π interactions are entirely separate from aromaticity. The effect of the ions on the binding strength is associated with the ionic radius and the binding energy.

The origin of the electrostatic effect is because of the sp^2 carbon that is more electronegative than hydrogen resulting in $C^{\delta-}$-$H^{\delta+}$ bond dipoles, that combine to form a resultant negative moiety, e.g. C_6H_6 to which the cation binds.

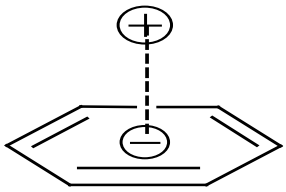

Figure 1.5.4: Illustration of cation-π interaction[38]

Cation-π interactions have been effective as the major design element in supramolecular systems.

Cation-π interactions are important not only to supramolecular chemists, they are also essential in biological systems where they are responsible for stabilizing protein structures.

Research has shown that cation-π interactions are non-covalent bonding forces in gas, solution and biological systems.[38]

e. π-π stacking

These are weak electrostatic interactions observed in aromatic rings in cases where one has poor electron density and the other one is rich in electrons.[3] Aromatic rings are flat and have delocalized π-electrons. The polarisability of the π-electron enables the stabilizing dispersion interactions between aromatic molecules and its surroundings. The directionality of the interaction comes from the electrostatic constituent of the intermolecular stabilization.

The C-H bonds of the aromatic rings are polarized and a molecule with opposite charges is obtained. The centre of the molecule is slightly negative while the edges are slightly positive.

These concepts then introduce the preferable directions of the relatively positive and negative areas of the molecule.[39]

There are two (2) general types of stacking observed in aromatic systems.

i. Face to Face

The molecules are parallel to each other and slightly offset (**Figure 1.5.5**) so that oppositely charged areas of the molecule are closest.[39]

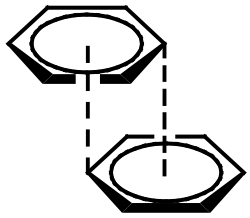

Figure 1.5.5: Illustration of the off-set face-to-face π-π stacking[3]

ii. Edge to Face

The relatively positive hydrogen edge is directed to the slightly negative centre of π electron density as illustrated in **Figure 1.5.6**.[39]

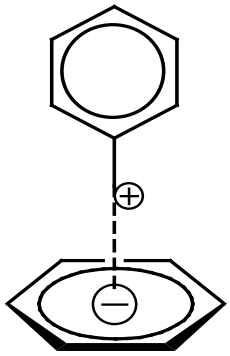

Figure 1.5.6: Illustration of the edge-to-face π-π stacking[3]

f. Hydrogen bond

Laurence and Berthelot[40] described the hydrogen bond as, "an attractive interaction between a hydrogen bond donor, XH, and the hydrogen bond acceptor in the same molecule or between different molecules". The XH···Y presentation is used to describe this interaction, where X represents the electronegative hydrogen donor and Y is the electron rich hydrogen acceptor. Hydrogen bonding by means of the π-system is also possible.

The geometrical parameters d, D, θ and r can be used to describe the hydrogen bond.

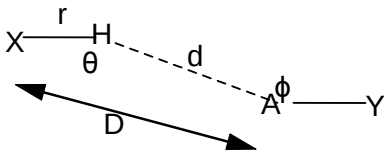

Figure 1.5.7: Geometric description of a hydrogen bond[41]

Desiraju (2004)[41] found that when the hydrogen extends towards the hydrogen acceptor, the angle ϕ increases. Research carried out by Taylor and Kennard[42] shows that the hydrogen bond length, D is determined by the properties of the donor and the acceptor. The length is related to the number of hydrogen bonds that the acceptor is subjected to, i.e. if a hydrogen bond acceptor is involved in a single bond the distance will be shorter than when it is involved in multiple bonds. This is explained by the steric effect. The researchers also observed that the charge of the species plays a role in the bond length and deduced that shorter bonds are formed for charged species and longer ones for the uncharged groups.

For the hydrogen bond to have certain strength, length and of certain qualities, the geometry of the hydrogen bond and the type of the donor and acceptor groups play a role. They influence the characteristics of the hydrogen bond.[1]

Hydrogen bonds are categorised according to their strength based on their ability to determine and control supramolecular structures.

- The very strong hydrogen bonds have bond energies in the range 62.8-167.5 kJmol^{-1}. They often occur between an acid and its conjugate base or between a base and its conjugate acid. They have a more noticeable effect on the crystal packing and their use to crystal engineering is not well understood.
- Strong hydrogen bonds are mostly electrostatic interactions with bond energies of 16.7-62.8 kJmol^{-1}. They have an easily recognizable effect on the crystal packing, can control and modulate supramolecular structures and are very useful in crystal engineering.
- Weak hydrogen bonds have bond energies less than 16.7 kJmol^{-1}. Dispersive and covalence components that are greatly influenced by the character of the donor and acceptor groups changes the electrostatic nature of this interaction. Their effect on the crystal packing is variable and they are of little use to crystal engineering.[41]

The strength and the directionality of the hydrogen bond make it the interaction of choice in supramolecular chemistry. “Strength is a symbol of cohesion and stability while the directionality implies topological control and selectivity”; therefore reproducibility to the supramolecular assembly is guaranteed.[43]

1.6 Forms of inclusion compounds

Inclusion compounds are classified further into co-crystals and salts as shown by **Figures 1.6.1** and **Figure1.6.2**.

Different authors have defined a co-crystal in numerous ways. A co-crystal according to Aakeröy *et al*[44] is most commonly considered to be an arrangement of homogenous crystalline compounds that have two or more neutral constituents that are present in specific stoichiometric quantities. Bhatt *et al*[45] described the co-crystal as “a crystalline material comprised of two or more unique solids at room temperature each containing distinctive physical characteristics such as structure, melting point and heats of fusion.”

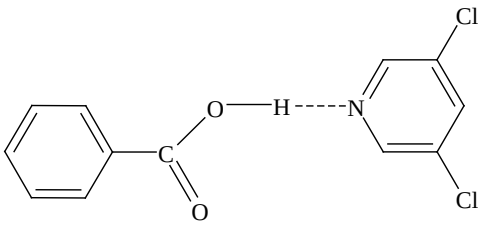

Figure 1.6.1: Illustration of a co-crystal

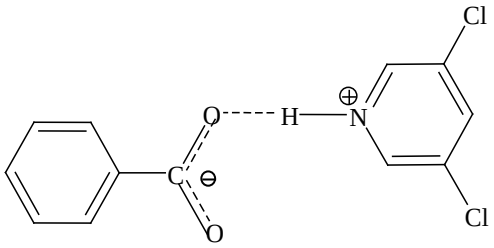

Figure 1.6.2: Illustration of a salt

Substantial discussions surrounding the definition of a co-crystal are on-going with regard to the constituents involved. The argument is based on what kind of constituents really make a co-crystal, since crystals can be obtained from combinations of solids, liquids as well as gases. Terms such as solvates or pseudo-polymorphs have been used to refer to multi-component crystalline material formed from one or more solids and a liquid. This raises questions of what to call multi-component crystals composed of solids and gases or combinations of liquids and even liquids and gases.[46] Bond[46] also highlighted suggestions that co-crystals consist of two or more components that form a unique crystalline structure having unique properties. This definition will include most multi-component compounds such as solvates, inclusion compounds, channel compounds, molecular complexes and clathrates. This is the definition that will be adopted in this study and attention will be drawn to the difference between co-crystals and salts.

Hydrogen bonding has always been used as a mode of preparing co-crystals as shown in **Figure 1.6.1 and 1.6.2** above. The hydroxyl group acts as the hydrogen bond donor and the heterocyclic nitrogen is the acceptor. However it is also possible that an acid-base reaction can occur, whereby a proton is transferred from the acid to the base, (**Figure 1.6.2**), in this manner a salt is obtained and a charge assisted hydrogen bond occurs.

1.7 Host compounds for enantiomer resolution

Host-guest chemistry has been employed in resolving chiral molecules, hence an increased interest of researchers in understanding its mechanism. Toda[47] and other researchers developed a method of resolution *via* inclusion complexes.[48] Naturally occurring optically active chemicals have shown to be good resolving agents hence the design of synthetic derivatives helped improve the choice of application offered by the natural agents. The design of synthetic resolving agents was based on the co-ordination assisted clathrate formation between hosts with particular functionalities (e.g. –OH and –COOH) and polar guest molecules.[49] However host-guest complexes of synthesised polar host TOD 3 **(Figure 1.7.1)** with non-polar guests such as benzene, toluene, p-xylene and ethylbenzene have also been reported.[50]

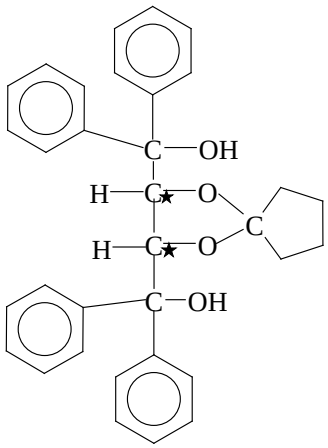

TOD 3

Figure 1.7.1: TOD 3 (*R*,*R*)-(-)-*trans*-2,3-bis(hydroxydiphenylmethyl)-1,4-dioxaspiro(4,4)nonane

Designed synthetic host molecules have been used to resolve a broad variety of substrates *via* clathrate formation. TADDOLS are some of the synthetic resolving agents that have been investigated. These are derivatives of tartaric acid that were synthesised by Toda[51] with the aim of designing a host molecule in which hydroxyl groups were incorporated into a bulky rigid framework and have optical activity. TADDOLS have been extensively explored.[52]

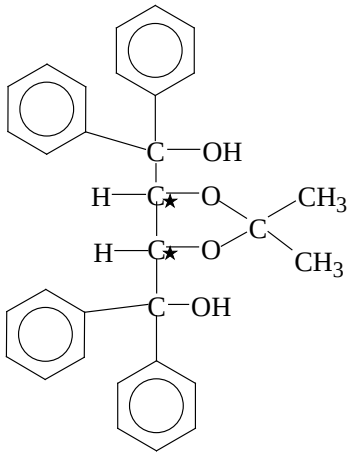

TOD 2

Figure 1.7.2: TOD 2 (*R,R*)-(-)-2,2-Dimethyl-4,5-bis(diphenyl(hydroxy)methyl)-1,3-dioxolane

TOD 2 (**Figure 1.7.2**) was able to form clathrates with several achiral guest molecules and a stable structure was obtained because of the hydrogen bonds formed by the hydroxyl groups and the interactions formed by the bulky phenyl groups. Enantiomeric excess (*ee*) percentages of up to 100 % have been obtained when resolving two chiral bicyclic enone guests with TOD 2 by inclusion complexation.[51]

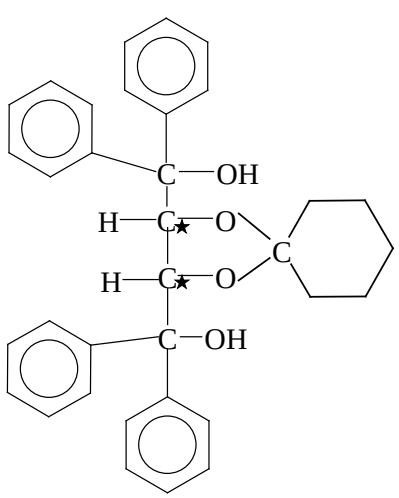

TOD 4

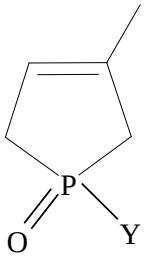

Y = Ph 1a
2-MePh 1b
4-MePh 1c
naphthyl 1d
ethyl 1e
propyl 1f
ethoxy 1g
isopropyl 1h

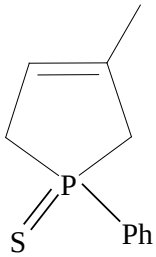

1i

Figure 1.7.3: TOD 4, ((*R,R*)-(-)-*trans*-bis(hydroxydiphenylmethyl)-1,4-dioxaspiro(4,5)decane) and P=O derivatives

TOD 2 and its analogue (TOD 4) (**Figure 1.7.3**) were used in successful resolution of 1-substituted-3-methyl-3-phospholene derivatives, 1a-1i, in **Figure 1.7.3**. Complexes with host-guest ratios of 1: 1 were obtained in most cases, except for **TOD 3• (+) 1f** where the host-guest ratio is 2: 1. The enantiomeric purity of (-)-1a-1h was between 10-96 % *ee*. The enantiomeric excess was

improved to more than 99 % by re-crystallising the complexes in a mixture of ethyl acetate and hexane.[53]

Toda *et al*[54] explored the ability of the TADDOLS in preparation of optically active 5-alkoxyfuran-2-(5H)-ones and dihydrofuran-2-(3H)-one. The resolving agents provided a straightforward and effective preparation of the optically active compounds with the % *ee* of up to 100 %.

Host compounds being investigated in this work are (-)-quinine (QUIN) and (+)-deoxycholic acid (DCA). The structure of QUIN is presented in **Figure 1.7.4**.

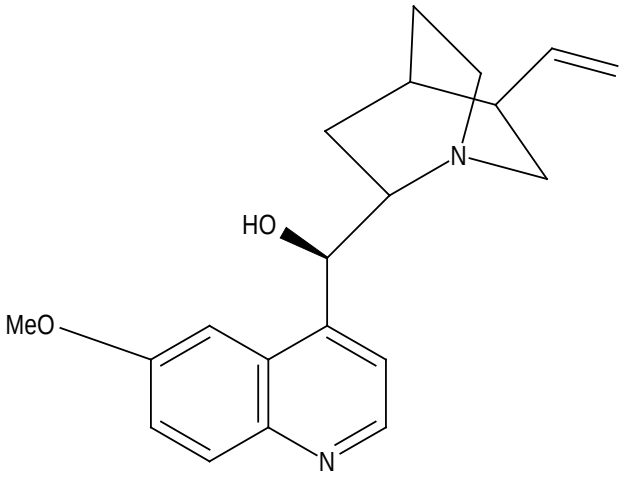

Figure 1.7.4: Structure of QUIN

(-)-Quinine is the most commonly used anti-malarial drug. The optically active derivatives of (-)-quinine are used in asymmetric synthesis.[55]

(-)-Quinine and (+)-quinidine have been used as resolving agents for acidic racemates through formation of diastereomeric salts.[56]

The Cambridge Structural Database[57] survey of (-)-quinine shows that it is one of the active pharmaceutical ingredients (API) that have been explored extensively. The structures of (-)-quinine with organic acids such as tartaric acid[58] and S-mandelic acid[56] have been reported. Salicylic acid[59] and saccharine[45] also formed complexes with (-)-quinine. **Figure 1.7.5** is the structure of DCA.

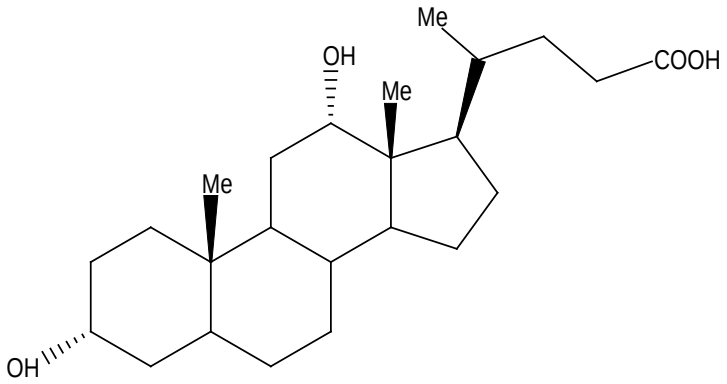

Figure 1.7.5: Structure of DCA

Another host compound investigated is (+)-deoxycholic acid, (DCA). This is one of the aliphatic bile acids produced by vertebrate animals. The structure is comprised of the steroidal frame with two hydroxyl groups below (hydrophilic face) and two methyl groups above (lipophilic face) the steroidal plane. A good number of inclusion compounds of DCA with various guest compounds such as ketones[60,61,62&63] and esters[64] acids have been reported with the first structure being reported with acetic acid by Craven and DeTitta.[65,66] DCA was found to crystallize in an orthorhombic crystal system with the host arranged in cumulated bilayers forming channels. The host compound can arrange in a parallel fashion on the hydrophilic faces and anti-parallel on the lipophilic face. [67]

Structures of (+)-deoxycholic acid with alkyl ammonium guests were reported by Miyata, *et al*[68] these inclusion compounds were salts. The alkyl ammonium cations were found to partially fill the channels formed by the deoxycholate anions.

The attention of crystal engineering to improving the physicochemical properties of active pharmaceutical ingredients have caught the attention of Ikonen *et al*[69] They investigated the inclusion compounds of bile acids with melamine and reported the structure.

Many inclusion compounds of (+)-deoxycholic acid have been reported but very little information on the investigation of (+)-deoxycholic acid as a resolving agent is available.[52] Tahir *et al*[70] reported the successful ability of (+)-deoxycholic acid to distinguish between the *R*- and *S*-enantiomers of camphorquinone and endo-(1)-3-bromocamphor and only the *S*-enantiomers from a racemic mixture were included in the crystal.

1.8 Research Aim

The purpose of this research was to investigate chiral discrimination which will lead to the understanding of separation of enantiomers. It therefore will be helpful to the pharmaceutical industry which is interested in obtaining an effective method for resolving racemates.

Bile acids ((+)-deoxycholic acid & (+)-cholic acid) and (-)-quinine were chosen as hosts for the study because they are large chiral molecules that have the potential to form hydrogen bonds. The hosts were selected because of their pharmacological importance as quinine has been used as an anti-malarial drug. Their chirality is known and they are also well known as chiral resolving agents. During the study the chiral hosts will be exposed to the racemic guest molecules and allowed to crystallise. The thermal decomposition of the resultant crystals will be studied by thermal analysis. The kinetics of desolvation will also be established by non-isothermal methods where possible. Kinetics of absorption will also be studied. X-ray diffraction data will be collected for structural analysis.

Structures of the resultant complexes of DCA and QUIN have been correlated to their chiral discrimination. The use of QUIN and DCA to separate selected racemic mixtures will be studied. It is envisaged that this research will lead to a better understanding of the mechanism of enantiomeric resolution. It is important to note that no extraction of the resolved compounds has been conducted in this project.

REFERENCES

[1] Steed J. W., Turner D. R. & Wallace K. J. (2007). *Core concepts in Supramolecular Chemistry and Nanochemistry*. Singapore: John Wiley & Sons.

[2] Weber, E. (2004). Classification and nomenclature of supramolecular compounds. *Encyclopaedia of supramolecular Chemistry,* Ed: Atwood, J. L. & Steed, J. W., Vol 1: 261-273. New York, Taylor & Francis.

[3]Steed J. W. & Atwood J. L. (2000). *Supramolecular Chemistry.* Singapore: John Wiley & Sons.

[4] Menger, F. M. (2002). Supramolecular chemistry and self assembly. *Perspective* 99:4818-4822.

[5] Desiraju G. R. (2001), Chemistry beyond the molecule, *Nature,* Vol. 412:397-400.

[6] Bruice PK, 2007, Organic Chemistry, 5th Edition, pg 200-250.

[7] Carey, FA. and Sunberg, RJ. (1990), Advanced organic chemistry, 3rd Edition Pg 67-116.

[8] Oki, M., Top. Stereochem. 14, 1 (1983).

[9] McConathy, J. & Owens, M. J. (2003). Stereochemistry in Drug Action. *Primary Care Companion J. Clin. Psychiatry,* Vol. 5:70-73.

[10] McMurry, J. (2004), Organic Chemistry, 6th Edition, Australia, (pg 281- 287).

[11] Anandamanoharan, P. (2010), Isolation of enantiomers via Diastereomer crystallisation, (pg 16), University College London.

[12] Morrison, R. T. & Boyd, R. N. (1992), Organic Chemistry, 6th Edition, New Jersey, (pg 133-141).

[13] Shafaati, A. (2007), Chiral Drugs: Current Status of the Industry and Market, *Iranian Journal of Phamaceutical Research*, Vol. 6: 73- 74.

[14] Kasprzyk-Hordern, B. (2010), Pharmacologically active compounds in the environment and their chirality, *Chem. Soc. Rev.,*39, 4466-4503.

[15] Ariëns, E. J. (1984), Stereochemistry, a Basis for Sophisticated Nonsense in Pharmacokinetics and Clinical Pharmacology, *European Journal of Clinical Pharmacology*, Vol. 26: 663-668.

[16] McConathy, J. & Owens, M. J. (2003). Stereochemistry in Drug Action. *Primary Care Companion J. Clin. Psychiatry,* Vol. 5:70-73.

[17] Jiao, F. P., Chen, X. Q., Yang, L. & Hu, Y. (2008), Enantioselective Extraction of Mandelic Acid Enantiomers Using Ester Alcohol L-Tartrate as Chiral Selector, *Latin American Applied Research,* Vol. 38: 249-252.

[18]Davies, N.M. & Teng, X.W. (2003), Importance of chirality in drug therapy and pharmacy practice: Implications for psychiatry, *Advances in Pharmacy*. Vol. 1: 242-252.

[19] Melchert M. & List A. (2007), The thalidomide saga, *The International Journal of Biochemistry & Cell Biology,* Vol. 39: 149-1499.

[20] Anandamanoharan, P. (2010), Isolation of enantiomers via Diastereomer crystallisation. (pg 16), University College London.

[21] Legrand, S. (2006), Stereoselectivity and regioselectivity in organic chemistry: Novel systems and applications, University of Kalma, Sweden.

[22] Park, D., Lee, J. K., Kim, S-Y, Song, T. & Suh, S-S. (2002), Comparative Optical Separation Of Racemic Ibuprofen By Using Chiral Stationary Phase, C*hinese J. Chem. Eng.,* Vol. 10: 681-685.

[23] Carvalho, P.O., Cass, G.B., Calafatti, S.A.,Contesini, F.J. & Bizaco,R. (2006), Review-Alternatives for the Separation of drug enantiomers: Ibuprofen as a model compound, *Brazilian Journal of Chemical Engineering,* Vol.23:291-300.

[24] Crupi, C., Guela,C., Majolino, D., Mancini,I., Rossi, B., Stancalleni, R., Venuti, V., Verrocchio, P & Viliani, G. (2011), A Phase Solubility Study On The Chiral Discrimination Of Ibuprofen By B-Cyclodextrin Complexes, *Food Biophysics,* Vol. 6:267:273.

[25] Cretu, G., Ionică, M., Dănet, A. F., Aboul-Enein, H., Macovei, R. & Buleandră, M. (2005), Separation of the enantiomers of ibuprofen by a gas chromatographic-mass spectrometric method, *Acta Chromatographica,* No. 15: 315-321.

[26]DePalma, A. (2001), Chirality Companies Broaden Their Approaches: Successful Films Expand Beyond Single-Carbon Transformations, *Genetic Engineering News,* Vol. 21, Number 9, May 1.

[27] Eliel, E. L., Wilen, S. H. & Mander, L. N. (1994), Properties of stereoisomers. Stereoisomer Discrimination, Stereochemistry of Organic Compounds, (pg 153-159), New York.

[28] Báthori N. B. & Nassimbeni, L. R. (2010), Selectivity and Enantiomeric Resolution in Inclusion Chemistry: A Systematic Study of Chiral Discrimination through Crystallisation, *Crystal Growth & Design,* Vol. 10: 1782-1787.

[29] Smith, M.B. & March, J. (2007). March's Advanced Organic Chemistry: Reactions, mechanisms and structures. 6th Edition (136-181).

[30] Vries, T., Wynberg, H., van Echten, E.,Koek, J., ten Hoeve, W., Kellogg, M. R., Broxterman, Q. B., Minnard, A., Kaptein, B., van der Sluis, S., Hulshof, L. & Kooistra, J. (1998), The Family Approach to the Resolution of Racemates, *Angew. Chem. Int. Ed.* Vol. 37: 2349-2354.

[31] Müller, S., Afraz, M. C., de Gelger, R., Ariaans, G. J. A., Kaptein, B., Broxterman, Q. B. & Bruggink, A. (2005), Design and evaluation of inclusion resolutions, based on readily available host compounds, *Eur. J. Org. Chem,* 1082:1096.

[32] Goldberg, I., Stein, Z., Weber, E., Dorpinghaus, N. & Franken, S. (1990), Exploring the Inclusion Properties of New Clathrate Hosts Derived From Tartaric Acid. X-ray Structural Characterisation of the Free Ligands and their Selective Interaction Modes with Alkylamine Guests, *J. Chem. Soc. Perkin Trans. 2*, 953:963.

[33] Dyadin, Y. A. & Terekhova, I. S. (2004). Classical descriptions of inclusion compounds. *Encyclopaedia of supramolecular Chemistry,* Ed: Atwood, J. L. & Steed, J. W., Vol 1: 253-260. New York, Taylor & Francis.

[34]Davies, J. E. D., Kemula, W., Powell, H. M. & Smith, N. O. (1983). Inclusion compounds- Past, present and future. *Journal of Inclusion Phenomena and Macrocyclic Chemistry*, 1: 3-44.

[35] Vögtle, F., Löhr, H.-G., Franke, J. & Worsch, D. (1985), Host/Guest Chemistry of Organic Onium Compounds—Clathrates, Crystalline Complexes, and Molecular Inclusion Compounds in Aqueous Solution, *Angew. Chem. Int. Ed. Eng.*Vol. 24: 727–742.

[36]Nassimbeni, L. R. (2004). Inclusion compounds: Selectivity, Thermal Stability and Kinetics. *Encyclopaedia of Supramolecular Chemistry*, Ed: Atwood, J. L. & Steed, J. W., Vol. 1:696-704.

[37]Nassimbeni, L. R. (2003). Physicochemical Aspects of Host-Guest Compounds. *Accounts of Chemical Research*, 36:631-637.

[38] Dougherty, D. A. (2004). Cation-π interactions. *Encyclopaedia of Supramolecular Chemistry*, Ed: Atwood, J. L. & Steed, J. W., Vol. 1:214-218, New York, Taylor & Francis.

[39] Dance, I. (2004). π-π Interactions: Theory and scope. *Encyclopaedia of Supramolecular Chemistry*, Ed: Atwood, J. L. & Steed, J. W., Vol. 2:1076-1092. New York, Taylor & Francis.

[40]Laurence, C & Berthelot, M. (2000). Observation of the strength of hydrogen bonding. *Perspectives in Drug Discovery and Design,* 18:36-60.

[41]Desiraju, G. R. (2004). Hydrogen Bonding. *Encyclopaedia of Supramolecular Chemistry*, Ed: Atwood, J. L. & Steed, J. W., Vol. 1:658-664. New York, Taylor & Francis.

[42]Taylor, R. & Kennard, O. (2002). Hydrogen-bond in organic crystals. *Accounts of Chemical Research*, 17: 320-326.

[43]Braga, D. & Grepioni, F. (2004). Crystal engineering with hydrogen bonds. *Encyclopaedia of supramolecular chemistry,* Ed: Atwood, J. L. & Steed, J. W., Vol.1: 357-363. New York, Taylor & Francis.

[44] Aakeröy, C. B., Fasulo, M. E. & Desper J. (2007), Cocrystal or Salt: Does it really matter? *Molecular Pharmaceutics* Vol. 4: 317-32.

[45] Bhatt, P. M., Ravindra, N. V., Banerjee, R. & Desiraju G. R. (2005), Saccharin as a salt former. Enhanced solubilities of saccharinates of active pharmaceutical ingredients, *Chem. Commun.,* 1073-1075.

[46] Bond A. D. (2007), What is a co-crystal? *CrystEngComm,* 9:833-834.

[47] Toda, F. (Ed). (2004) Enantiomer Separation, Fundamentals and Practical Methods, Kluwer.

[48] Müller, S., Afraz, M. C., de Gelger, R., Ariaans, G. J. A., Kaptein, B., Broxterman, Q. B. & Bruggink, A. (2005), Design and evaluation of inclusion resolutions, based on readily available host compounds, *Eur. J. Org. Chem,* 1082:1096.

[49]Goldberg, I., Stein, Z., Weber, E., Dorpinghaus, N. & Franken, S. (1990), Exploring the Inclusion Properties of New Clathrate Hosts Derived From Tartaric Acid. X-ray Structural Characterisation of the Free Ligands and their Selective Interaction Modes with Alkylamine Guests, *J. Chem. Soc. Perkin Trans. 2*, 953:963.

[50] Nishikawa, K., Tsukada, H., Murata, M & Yasuoka, N. (1999), Inclusion properties of (R, R)-(-)-trans-2,3-bis(hydroxydiphenylmethyl)-1,4-diaxospiro[4,4]nonane for Aromatic Components, *Journal of Chemical Crystallography,* Vol. 29: 137-144.

[51] Caira, M. R. & Tanaka, K. (2009), Inclusion and Optical Resolution of Guest Molecules by Selected Synthetic Dihydroxy- and Trihydroxy-Host Compounds Containing Heterocyclic Scaffolds, *Top Heterocycl Chem*, Vol. 18:75-102.

[52]Cambridge Structural Database (CSD), Version 5.32 (November 2010), http://ccdc.cam.ac.uk

[53] Novák, T., Ujj, V., Schindler, J., Czugler, M., Kubinyi, M., Mayer Z. A., Fogassy, E. & Keglevish, G. (2007), Resolution of 1-substituted-3-methyl-3-phospholene 1-oxides by Molecular Complex Formation with TADDOL Derivatives, *Tetrahedron: Asymmetry*, Vol. 18: 2965-2972

[54] Toda, F., Tanaka, K., Leung, C. W., Meetsma, A. & Feringa., B. L. (1994),, Preparation of Optically Active 5-Alkoxyfuran-2(5H)-ones and 5-Methoxy-dihydrofuran-2(3H)-one by Chiral Inclusion Complexation, *J. Chem. Soc., Chem. Comm.* 2371- 2372.

[55] Hubel, R., Polborn, K. & Beck, W. (1999), Cinchona Alkaloids as Versatile Ligands- Coordination of Transition Metals to the Four Potential Donor Sites of Quinine, *Eur. J. Inorg. Chem*, 471-482.

[56] Gjerløv, A. B. & Larsen, S. (1997), Quininium (S)-Mandalate, *Acta Crystalographica Section C,* Vol. C53: 1505-1508.

[57] Cambridge Structural Database (CSD), Version 1.13, November 2010, http://ccdc.cam.ac.uk

[58] Ryttersgaard, C. & Larsen, S. (1998), Quininium Hydrogen (*S*,*S*)-Tartrate Hemihydrate, a Salt with a Unique Conformation of the Hydrogen Tartrate Ion, *Acta-Crystallogr., Sect.C: Cryst. Struct. Commun.* Vol. 54:1698-1701.

[59] Oleksyn, B. J. & Serda P. (1993), Salt-bridge formation by *Cinchona* alkaloids: quininium salicylate monohydrate, *Acta Crystallogr., Sect. B: Struct. Sci.* Vol. 49:530-534.

[60] Chang, H. C., Tang, C. P., Popovitz-Biro, R., Lahav, M. & Leiserowitz, L. (1981), *New J.Chem.* Vol: 5,475.

[61] Tang, C. P., Chang, H. C., Popovitz-Biro, R., Frolow, F., Lahav, M., Leiserowitz, L. & McMullan R.K. (1985), Reaction pathways in crystalline host-guest inclusion complexes: rotation by a net 180.degree. of the acetyl group on photo-addition of guest acetophenone and m-chloroacetophenone to the atom C5 of host deoxycholic acid, *J. Am. Chem.Soc.* Vol.107: 4058-4070.

[62] Popovitz-Biro, R., Tang, C. P., Chang, H. C., Lahav, M. & Leiserowitz, L. (1985), Solid-state photochemistry of guest aliphatic ketones inside the channels of host deoxycholic and apocholic acids, *J. Am. Chem. Soc.* Vol. 107: 4043-4058.

[63] Lahav, M., Leiserowitz, L., Popovitz-Biro, R. & Tang C.-P. (1978), Reactions in inclusion molecular complexes. 2. A topochemical solid-state photoaddition of acetone to deoxycholic acid, *J. Am. Chem. Soc.* Vol. 100: 2542-2544.

[64] Nassimbeni, L. R., Niven, M. L., Stuart, D. A. & Zemke, K. J. (1986), 2:1 Complex of desoxycholic acid and ethyl acetate: Disorder in the structure at 298 and 163 K, *J.Crystallogr.Spectrosc.Res. ,*Vol. 16: 557-567.

[65] Miyata, M., Sada, K. & Yoswathananont, N. (2004), Deoxycholic acid, cholic and apocholic acids, *Encyclopedia of Supramolecular Chemistry*, Ed: Atwood, J. L. & Steed, J. W., Vol. 1:441-451

[66] Craven, B. M. and DeTitta, G. T. (1972), Crystal structure determination of the 1:1 complex of deoxycholic acid and acetic acid, *J. Chem. Soc., Chem. Commun.*, 530-531

[67] Jover, A., Meijide, F., Núñez, E. R., Tato, J. V., Castiñeiras, A., Hofmann, A. F. & Ton-nu, H.-T. (2000) Crystal structure of 3β,12α-dihydroxy-5β-cholan-24-oic acid (iso-deoxycholic acid), J*ournal of molecular structure*, Vol. 523:299-307.

[68] Sada, K., Shiomi, N & Miyata M (1998), Nanocavities with fine adjustments in channel-type inclusion crystals of alkylammonium deoxycholates. Control of molecular cavities by partial filling of molecular channels, *Journal of American Chemical Society,* Vol. 120:10543-10544.

[69] Ikonen, S., Kolehmainen, N. & Kolehmainen, E. (2010), Supramolecular architectures formed by co-crystallization of bile acids and melamine, CrystEngComm, Vol. 12:4304-4311.

[70] Tahir, M. I. M., Rees, N. H., Heyes, S.J., Cowley, A. R., & Prout, K. (2008), Discrimination of Chiral Guests by Chiral Channels: Variable temperature studies by SXRD and Solid State 13C NMR of the deoxycholic acid complexes of camphorquinone and endo-3-bromocamphor, *Chirality* Vol. 20:863–870.

CHAPTER 2

EXPERIMENTAL METHODS AND MATERIALS

2.1 Materials

2.1.1 Host compounds

(1*S*,3*R*,4*S*,8*S*,9*R*)-4-(hydroxy(5-vinyl-1-azabicyclo(2.2.2)oct-2-yl)methyl)-6-methoxyquinoline ((-)-quinine), referred to as QUIN in the project, (+)-deoxycholic acid, (DCA) and (+)-cholic acid (CA), (**Figure 2.1.1)** are large rigid molecules that have the functional groups that can hydrogen bond to other donors and acceptors. (-)-Quinine has a nitrogen atom that can accept a proton, forming a salt and result in a charge assisted hydrogen bond. It also has a hydroxyl group that can donate hydrogen in a hydrogen bond. DCA and CA have carboxylic acid groups that can act as both hydrogen bond donor and acceptor. The groups can also lose a proton to a base, forming a salt and result in a charge-assisted hydrogen bond. The hydroxyl group at Carbon 3 of DCA and CA can also be a hydrogen bond donor. (-)-Quinine, DCA and CA were supplied by Sigma Aldrich Chemical Co.

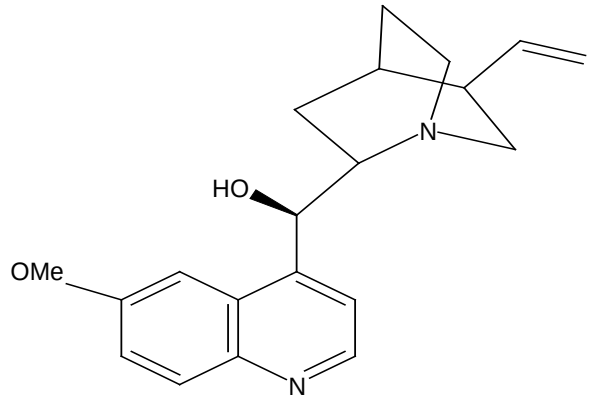

QUIN

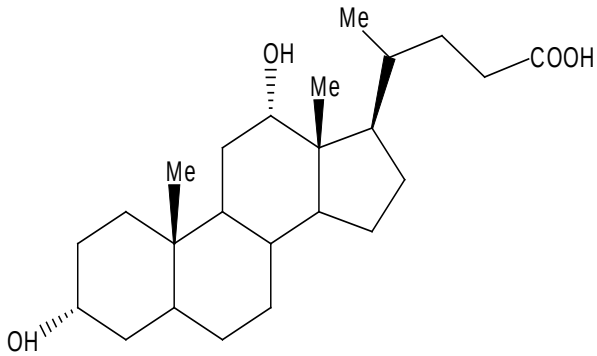

DCA

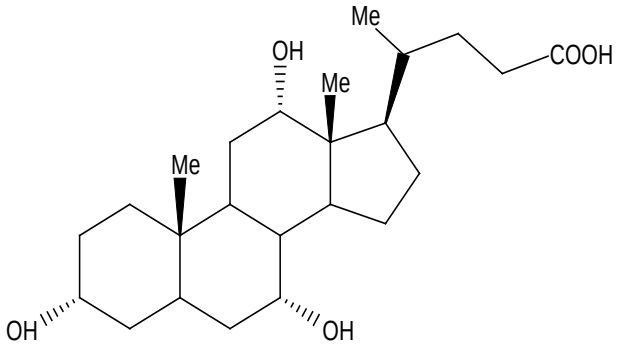

CA

Figure 2.1.1: Illustration of the host compounds investigated

2.1.2 Guest compounds

Small molecules that have the potential to form hydrogen bonds were employed for experimental purposes. **Table 2.1.1** shows the physical properties of the guest compounds used while their structures are illustrated in **Figure 2.1.2**.

D and *L* malic acids (*D*-MA and *L*-MA) were supplied by Fluka Analytical while *DL*-malic acid (*DL*-MA) was supplied by Sigma Aldrich Chemical Co. Di-*n*-butylamine (DI-BUAM) was obtained from Saarchem and diethylamine (DIETAM) was acquired from BDH Chemicals Ltd. Sigma Aldrich Chemical Co. also supplied 1-propylamine (PPA), *n*-butylamine (1-BUAM), (*R,S*)-*sec*-butylamine (2-BUAM) and (*S*)-(+)-*sec*-butylamine (*S*-BUAM). (*R*)-(+)-2-amino-3-methylbutane (*R*-MeBUAM) and (*S*)-(-)-2-amino-3-methylbutane (*S*-MeBUAM) were also obtained from Sigma Aldrich Chemical Co.

Table 2.1.1: Physical properties of the guest compounds studied[1]

Guest	Formula	Mr (g.mol^{-1})	Density	Bp (°C)	Mp (°C)
D-(+)-malic acid	$C_4H_6O_5$	134.09	-	-	98-102
L-(-)-malic acid	$C_4H_6O_5$	134.09	-	-	101-102
DL-Malic acid	$C_4H_6O_5$	134.09	-	-	131-132
1-Propylamine	C_3H_9N	59.11	0.719	48-49	-
n-Butylamine	$C_4H_{11}N$	73.14	0.733	78	-
(*R,S*)-*sec*- Butylamine	$C_4H_{11}N$	73.14	0.724	63	-
(*S*)-(+)-*sec*-butylamine	$C_4H_{11}N$	73.14	0.708	63	-
(*R*)-(+)-2-amino-3-methylbutane	$C_5H_{13}N$	87.16	0.750	85-87	-
(*S*)-(-)-2-amino-3-methylbutane	$C_5H_{13}N$	87.16	0.746	85-87	-
Di-*n*-butylamine	$C_8H_{19}N$	129.24	0.760	159-160	-
Diethylamine	$C_4H_{11}N$	73.14	0.707	55.5	-

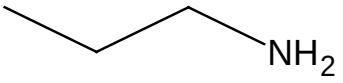

1-Propylamine (PPA)

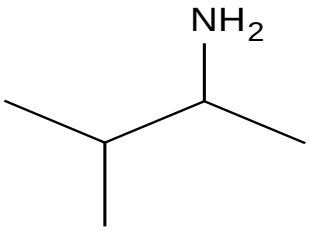

3-methyl-2-butylamine (MeBUAM)

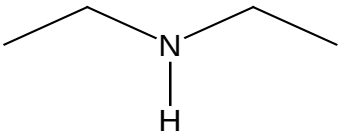

Diethylamine (DIETAM)

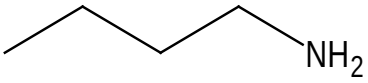

n-Butylamine (1-BUAM),

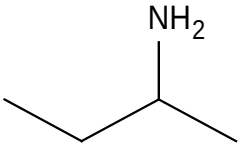

sec-Butylamine (2-BUAM)

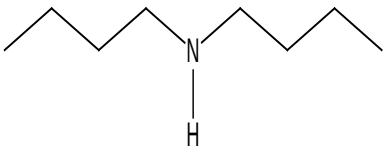

Di-*n*-butylamine (DIBUAM)

Figure 2.1.2: Schematic diagrams of the guest compounds

2.2 Methods

2.2.1 Crystal growth

The host compounds were dissolved in the liquid guests in stoichiometric ratios aided by heating at 333 K and stirring where low solubility was encountered. In cases where the host was insoluble in the liquid guest, a co-solvent was used. Different solvents such as water, ethanol and acetone were used in cases where both the host and guest are solids. The stoichiometric quantities of the guest and host compounds were dissolved in excess solvent separately and then mixed. The solutions were allowed to cool at room temperature, covered with parafilm and left to crystallize.

2.2.2 Thermogravimetric analysis (TGA)

Thermogravimetric analysis (TGA) is the study of chemical changes in a material by measuring the sample weight as a function of temperature or time. The sample is subjected to a temperature programme. Thermogravimetric curves are referred to as mass loss curves, though exceptions occur in cases where the sample reacts with the immediate atmosphere, e.g. oxidation. Thermogravimetric curves can be used to evaluate the number of decomposition stages, temperature ranges and fractional weight loss of each stage.[2]

Mass loss was determined by thermogravimetric analysis (TGA) using the Perkin-Elmer Pyris 6 system. A temperature programme of 303 K to 633 K at 10 K min^{-1} was used and the flow of nitrogen as a purge gas was set at 20 ml min^{-1}.

The samples (resultant crystals) were removed from the mother liquor, carefully dried with filter paper, crushed and analysed at the set programme. A measure of mass loss as a function of temperature (thermogravimetric (TG) curve) was obtained from which the ratio of host: guest was determined.

2.2.3 Differential scanning calorimetry (DSC)

The sample and the reference material are exposed to a temperature programme and the heat flow is recorded as a function of time or temperature. The resultant curve is the DSC curve.

There are two types of DSC; power compensated and heat flux DSC.

1) Power compensated DSC

Separate heaters are used to heat the sample and the reference material whilst the temperature difference (ΔT) is kept as close to zero as possible. The difference in electrical power needed to uphold the temperature of the sample and the reference material is recorded. To obtain a DSC curve, the difference in electrical power required to lower ΔT to zero is recorded as a function of time or temperature.

2) Heat flux DSC

Unlike in power compensated DSC, one heat source is required to heat the sample and the reference material and the temperature difference (ΔT) is measured. A calorimetric sensitivity which is governed by an instrumental constant K is needed to convert the difference in temperature to power difference (ΔP).[1]

Changes that occur in the sample during heating were determined by differential scanning calorimetry (DSC), using a Perkin-Elmer Pyris 6 system. The samples were scooped out of the mother liquor, dried, crushed, weighed and analysed. The temperature programme similar to the one used in TGA was used to analyse the samples. A DSC curve (heat flow vs. temperature) was obtained and the onset temperatures (T_{on}) of various peaks were determined.

2.2.4 Single Crystal X-ray Diffraction

X-ray diffraction is a non-destructive analytical technique for determination of crystal structures and atomic spacing. Information such as unit cell dimensions, bond-lengths, bond-angles, and details of site-ordering of crystalline materials can be obtained through the technique. Data obtained from X-ray analysis is refined and interpreted in order to solve crystal structures.[3]

X-ray crystallography is an experimental technique that exploits the fact that X-rays are diffracted by crystals. The technique relies on the fact that the atoms and their associated electron clouds form a three-dimensional grating whose spacings are comparable to the wavelength of the impinging radiation, which is approximately 1 Å, ($1x10^{-10}$ m).[4] The efficiency of X-ray crystallography has been improved due to the advances in technology. High power radiation sources that emit electromagnetic radiation by passing charged particles via magnetic fields have been used as well as area detector data collection instruments. High speed computers have also contributed vividly in increasing the effectiveness of this technique.[5]

X-ray tubes or synchrotron radiation are used to generate the X-rays. A stationary or rotating solid target is bombarded with a focused electron beam that is accelerated across a high voltage field. A continuous X-ray spectrum is recorded as the electron beam collides with atoms in the target

(crystalline material). The target gets ionized, the inner shell electrons are released and the free electron completes the shell causing an emission of an X-ray photon with energy that can be attributed to the target material. X-ray tubes that are frequently used are Copper (Cu) which emits 8 keV at 1.54 Å and Molybdenum (Mo) emitting 14 keV at 0.8 Å.[6]

Good quality, suitably sized crystals were selected for X-ray photography and data collection. The crystals were coated with Paratone oil and mounted on a glass fibre for data collection. The crystal unit cell parameters were determined from intensity data measured on a Nonius Kappa CCD diffractometer[7] and a Bruker DUO APEX 2 diffractometer. A Bruker K780 generator was sued to produce X-rays at 50kV and 30mA.[8] A 1.2 kW monochromated MoKα radiation of wavelength 0.7107 Å generated by a NONIUS FR590 generator was used. The operating parameters of the generator were 53 kV and 23 mA. Data were collected at room temperature (293-295 K) or at low temperature (113 K).low temperature was achieved with a constant stream of nitrogen gas obtained from a Cryostream cooler (Oxford Cryostream, UK) at a flow rate of 20mL min^{-1}. Intensity data were collected by the standard phi scan and omega scan techniques. The data was scaled and reduced using the Denzo-SMN[9] program for Nonius Kappa CCD. For the Bruker APEX 2, the cell refinement and data reduction was achieved by using program SAINT.[10]

Structures were solved using SHELXS-97[11] which was run on a graphical user interface, X-SEED.[12] The structural refinement was performed by the SHELXL-97[13] program which uses full-matrix least-squares minimisation of the function $\left(\sum w\left(F_0^2 - kF_c^2\right)^2\right)$. The agreement between the observed F_0 and the calculated F_c structure are expressed by the residual R, which is the indirect measure of the accuracy of the structure and should be low if the model is satisfactory. The residual index R_1 is the agreement between the observed and the calculated structure factors based on F (Eq. 1), while the residual index wR_2 is the agreement based on F^2, (Eq. 2).

Equation 1: $$R_1 = \frac{\sum \left\| F_0 \right| - \left| F_c \right\|}{\sum \left| F_0 \right|} \qquad \text{Eq. 1}$$

$$wR = \sqrt{\frac{\sum w\left(F_0^2 - F_c^2\right)^2}{\sum w\left(F_0^2\right)}} \qquad \text{Eq. 2}$$

w is the weighting scheme which was refined for each structure.

$$w = \frac{1}{\sigma^2 F_0^2 + (aP)^2 + bP} \qquad \text{Eq. 3}$$

$$\text{where } P = \frac{\max(0, F_0^2) + 2F_c^2}{3} \qquad \text{Eq. 4}$$

and a and b were also refined for each structure.

The goodness of fit, S, was determined for each structure and is based on F^2, see Eq. 5.

$$S = \left(\frac{\sum w(F_0^2 - F_c^2)^2}{n - P} \right)^{\frac{1}{2}} \qquad \text{Eq.5}$$

where n is the number of reflections and p is the total number of parameters refined.

2.2.5 Computing Components

PovRay renders graphics for structures.[14]

LAYER: displays intensity data as simulated precession photographs of the reciprocal lattice levels and allows for the investigation of the systematic absences which occur.[15]

LAZY PULVERIX: This software calculates the theoretical powder X-ray diffraction pattern from single crystal X-ray diffraction data.[16]

MsRoll: calculates the void spaces in the structure. It can be used to calculate the guest volume.[17]

POVLabel is utilized to edit the atomic labels of POV-Ray images.[18]

Xprep: this is a program that is used to set up SHELX input files and determines the space group.[19]

PLATON: It is used to calculate the molecular parameters of the structures.[20]

ConQuest: This is a search engine used to explore the Cambridge Structural Database for information.[21]

CCDC Mercury: This structural software provides all-purpose and highly developed functionality for inspecting crystal structures. It can import chemical bond types from 2D connection tables and present them in 3D illustration. Most importantly it has the capability to locate, build and display networks of inter- and intramolecular non-covalent bonds. It has options for presenting numerous structures at once and performing least-squares overlay of pairs of structures.[22]

2.2.6 Powder X-ray Diffraction

This is a quick analytical procedure principally employed for phase identification of a crystalline material. This technique can be used to acquire information on unit cell dimensions.[23] This method obtains its name from the fact that the sample is in the form of microcrystalline fine particles. About a century ago, diffraction patterns were recognized as a possible means of phase identification but a systematic means of unravelling the superimposed diffraction patterns was planned only decades later. [24]

A collection of indiscriminately oriented polycrystallites is exposed to the X-ray beam. Each of these polycrystallites causes its own diffraction pattern and individual spots on a film are spread into rings of diffracted intensity. A point or 1-D area detector is scanned across a narrow strip of the rings for measurement. A plot of total diffracted intensity against the diffracted angle, 2θ is used to represent the diffraction data.[25]

Samples were manually ground and placed in a sample holder in the path of the X-ray beam. The intensities were measured on a Hüber Imaging Plate Guinier Camera 670 using nickel-filtered CuKα_1 (1.5409 Å) radiation produced at 40 kV and 20 mA by a Philips PW1120/00 generator fitted with a Hüber long fine-focus tube PW2273/20 and a Hüber Guinier monochromator Series 611/15.

2.2.7 Non-isothermal kinetics

Kinetic studies are performed in order to study the activation energies (E_a) involved when the guest is released from the inclusion compounds.

$$\mathbf{H{\cdot}G_{(s)} \rightarrow H_{(s)} + nG\uparrow}$$

A non-isothermal method was used for the determination of the kinetics of desolvation. The samples were prepared as in thermal analysis; they were crushed to a fine powder to reduce the effect of particle size. TG experiments were conducted at various scan rates.

Flynn and Wall,[26] 1966 developed a method in which the thermogravimetric rate is analysed with respect to temperature. A series of thermogravimetric runs are performed over a selected temperature range at different heating rates.

The equation $dC/dT = A / \beta f(C) e^{-Ea/RT}$ is used to describe the thermogravimetric rate, where C is the mass loss and β is the heating rate.

By reducing the above equation, $d \log \beta / d (1/T) \approx (0.457/ R) E_a$ is obtained. A plot of log β vs. 1/T yields a straight line with slope $- (0.457 E_a)/R$.

2.2.8 Kinetics of absorption

Perfect crystals in reality are not common; most crystal lattices contain imperfections. The imperfection sites have higher free energy therefore are highly reactive.[27] Solid state kinetics occurs in different models such as nucleation, geometrical contraction, reaction order and diffusion. However the most common models are the reaction order and geometrical contraction (contracting volume and contracting area). Reaction-order models derived using concepts applicable to gas and solution reactions. The rate of reaction is assumed to be proportional to a function of the concentration of the reactants. Order based models are from the general formula equation (Eq. 6) below.

$$\frac{d\alpha}{dt} = k(1-\alpha)^n \qquad \text{Eq. 6}$$

where $d\alpha/dt$ is the rate of reaction, k is the rate constant and n is the reaction order. For a first order reaction the integral expression below (Eq. 7) is obtained.

$$-\ln (1-\alpha) = kt \qquad \text{Eq. 7}$$

The integral expressions for contracting area and contracting volume are represented by Eq. 8 and Eq. 9 respectively.[28]

$$\left[1-(1-\alpha)^{\frac{1}{2}}\right] = kt \qquad \text{Eq. 8}$$

$$\left[1-(1-\alpha)^{\frac{1}{3}}\right] = kt \qquad \text{Eq. 9}$$

Solid samples were exposed to vapours of volatile guest compounds. The vapour pressure of the guest was modified by adding different ratios of water. The mass gained by the solid host was monitored with time and ALPHATIME computer software was used to plot alpha vs. time curves. Different solid state reaction models were fitted to the data and the model chosen was most linear over the widest range, ($R^2 \approx 0.99$).

2.2.9 Infrared (IR) spectroscopy

Infrared spectroscopy is one of the most important analytical methods available today. Fourier transform spectrometers have resulted in the improvement of this technique since its introduction in the 1940s. The Fourier Transform infrared spectrometer utilizes an interferometer and the reputable mathematical process of Fourier transform. IR offers an advantage that samples can be analysed in any state.[29]

Infrared spectroscopy relies on the vibrations of the atoms in the molecule. The vibration frequencies are characteristic of the functional groups. The spectrometer consists of a source of infrared that emits radiation which is split into two equal beams. The other beam passes through the sample and if the frequency of the sample molecule falls in the range of the instrument, the molecule absorbs the energy. The intensity of the two beams is then compared in order to obtain the spectrum. The range of the wavelength in which comparison is performed, is spread by a prism or grating. The final spectrum is a plot of absorption against wavelength/ wave number/ frequency.[30]

REFERENCES

[1] Windholz, M. Ed. (1976), The Merck Index: An Encyclopaedia for chemicals and drugs, Merck & Co. Inc., New Jersey.

[2] Haines, P. J. (1995). Thermal Methods of Analysis, Blackie Academic & Professional, London.

[3] Brown P. J. & Forsyth, J. B. (1973), The crystal structure of solids, Edward Arnold Limited, London.

[4] Lambert, J. B., Shurvell, H. F., Verbit, L., Cooks, R. G. & Stout, G. H. (1976), Organic Structural Analysis, Macmillan Publishing Co., New York.

[5] Rissanen, K. (2004), X-Ray Crystallography, *Encyclopedia of Supramolecular Chemistry*, Ed: Atwood, J. L. & Steed, J. W., Vol. 2:1586-1591.

[6] Birkholz, M. (2006) Thin Film Analysis by X-Ray Scattering. WILEY-VCH Verlag GmbH & Co. KGaA, Weinheim.

[7] COLLECT (1998), data collection software, Nonius, Delft, The Netherlands.

[8] APEX 2 (2005), Version 1.0-27 Bruker AXS Inc, Madison, Wisconsin.

[9] Otwinowski, Z. & Minor, W. (1997), Methods in Enzymology, Macromolecular Crystallography Part A, Carter, C. W. and Sweet, R. M., (Eds), Academic Press, New York, 276:307-326.

[10] Program SAINT, (2006), Version 7,60a, Bruker AXS Inc., Madison, WI, USA.

[11] Sheldrick, G. M. (2008), A short history of SHELX, *Acta Crystallographica* Section *A*:112-122.

[12] Barbour, L. J. (2003), X-Seed, Graphical interface for SHELX program, *Journal of Supramol. Chem*., Vol. 1:189.

[13]Sheldrick, G. M. (1997), Program for Crystal Structure Determination, University of Göttingen, Germany.

[14] Pov-Ray for windows, (1991-1999), Version 3.1e.watcom.win32, The persistence of vision development team.

[15] Barbour, L. J. (1999), LAYER, A computer program for the graphic display of intensity as simulated precession photographs, *J. Appl. Cryst.* Vol.32:351.

[16] Yvon, K., Jeitschko, W. & Parthé, E. (1977), *LAZY PULVERIX*, a computer program, for calculating X-ray and neutron diffraction powder patterns, *J. Appl. Cystallogr.* Vol.10: 73-74

[17] Connolly, M. L. (1993), The molecular surface package , *J. Mol. Graphics*, Vol. 11: 139–141.

[18] Barbour L. J. (2001), X-Seed - A Software Tool for Supramolecular Crystallography, *Journal of Supramolecular Chemistry,* Vol. 1:189-191.

[19] XPREP, (1997), Data Preparation and reciprocal space group exploration, Version 5.1/NT, Bruker Analytical X-ray systems.

[20] Spek, A. L. PLATON, (1980-2000), A multi-purpose crystallographic tool, Version 10500.

[21] ConQuest, (2001), A program for the search of the CSD, Version 1.7.

[22] Allen, F. H. & Lipscomb, K. J. (2004), The Cambridge Structural Database, *Encyclopaedia of Supramolecular Chemistry*, Ed: Atwood, J. L. & Steed, J. W., Vol. 1:161-168.

[23] Karki, S., Fábián, L., Friščić, T. and Jones, W. (2007), Powder X-ray Diffraction as an Emerging Method to Structurally Characterize Organic Solids, *Organic Letters,* Vol. 9:3133-3136

[24]Jenkin, R. (2000), X-ray Techniques: Overview, *Encyclopedia of Analytical Chemistry,* pg. 13269–13288, R.A. Meyers (Ed.), John Wiley & Sons Ltd, Chichester.

[25] Evans, J. S. O. (2004) X-ray and Neutron powder diffraction, *Encyclopedia of Supramolecular Chemistry*, Ed: Atwood, J. L. & Steed, J. W., Vol. 2:1592-1598.

[26] Flynn, J. H. & Wall, L. A. (1966), A Quick, Direct Method for the Determination of Activation Energy from Thermogravimetric Data, *Journal of Polymer Science, Polymer Letters*, 4: 323-328.

[27] Khawam, A. & Flanagan D. R., (2006) Basics and Application of Solid-State Kinetics: A Pharmaceutical Perspective, *Journal of Pharmaceutical Science*, Vol. 95:472-498.

[28] Khawam, A. & Flanagan D. R., (2006) Solid-State Kinetics: Basics and Mathematical Fundamentals, *Journal of Physical Chemistry B*, Vol. 110:17315-17328.

[29] Stuart, B., George, B. & McIntyre, P. (1996), Modern Infrared Spectroscopy, John Wiley & Sons, NewYork, USA.

[30] Williams, D. H. & Fleming, I. (1995), Spectroscopic methods in organic chemistry, 5th Edition, McGraw-Hill, UK.

CHAPTER 3

QUININE INCLUSION COMPOUNDS

The crystals of (-)-quinine and malic acid were obtained by dissolving stoichiometric quantities of the host and guest in excess ethanol and allowing them to crystallize by slow evaporation at room temperature. The crystal of **(QUIN$^+$)(*D*-MA$^-$) •H_2O** were obtained by dissolving *D*-(+)-malic acid in water then added the solution to solid quinine. Thermal analysis and X-ray diffraction were performed on the resultant crystals.

3.1 Thermal analysis

Thermal analysis results of the starting material are reported in **Table 3.1.1**.

Table 3.1.1: DSC analysis of starting compounds

	QUININE	*L-(-)*-MALIC ACID	*D-(+)*-MALIC ACID	*DL*-MALIC ACID
Literature Melting point (K)	446-448	374-375	371-375	404-405
Endotherm (T_{on}, K)	441.5	375.4	375.4	402.5

The onset temperatures for the endotherms of the solids are close to that reported by the Merck index[1] and those reported by the suppliers. These results substantiate the purity of the compounds used.

On exposing the crystals obtained to a temperature programme, a two step decomposition was observed on the thermogravimetric curves. The results obtained are summarised in **Table 3.1.2**.

Table 3.1.2: DSC and TG results for inclusion compounds of QUIN with malic acid

Compound	**(2QUIN$^+$)(*L*-MA^{2-}) •2H_2O**	**(2QUIN$^+$)(*D*-MA^{2-}) •2H_2O**	**(QUIN$^+$)(*D*-MA$^-$) •H_2O**	**(2QUIN$^+$)(*DL*-MA^{2-}) •2H_2O**
H·G·W ratio	1:½:1	1:½:1	1:1:1	1:½:1
$Endo_1$ (T_{on}, K)	333.3	384.5	375.9	343.2
$Endo_2$ (T_{on}, K)	457.7	448.5	452.3	451.1
% mass loss	3.8	4.3	4.5	4.4
Theoretical mass loss	4.4	4.3	3.8	4.4

The first mass loss step was assigned to the loss of water. The second step was attributed to the decomposition of the compound. The DSC analysis of the quininium salts each gave rise to 3 peaks, the first endotherm being due to loss of water, the second one assigned to the melt of the salt and the third broad endotherm is due to decomposition. The appearance of endotherms for the decomposition of the salts at temperatures above the melting points of the starting materials

demonstrates the formation of new and more stable inclusion compounds. **Figure 3.1.1 a-d** illustrates the different curves obtained for each salt formed. The greater mass loss of 4,5% on the thermogravimetric curve of **(QUIN^{+})(*D*-MA^{-}) •H_2O** could be because of the loss of surface solvent.

The two salts of quinine and *D-(+)*-malic acid were obtained from different solvents. The crystals of **(2QUIN^{+})(*D*-MA^{2-})•2H_2O,** **(2QUIN^{+})(*L*-MA^{2-})•2H_2O** and **(2QUIN^{+})(*DL*-MA^{2-})•2H_2O** were obtained by slow evaporation of mixtures of quinine and relevant malic acid in ethanol whereas the crystals of **(QUIN^{+})(*D*-MA^{-})•H_2O** were obtained from water.

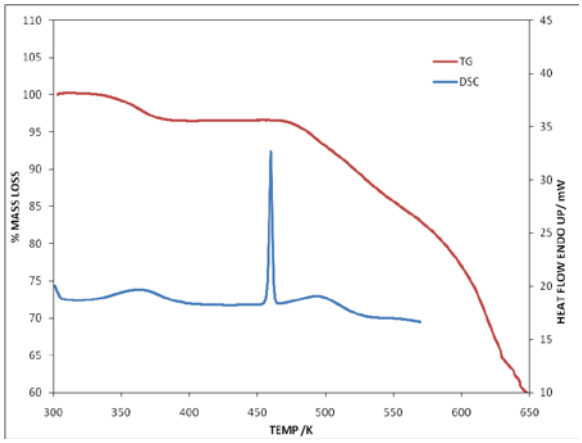

a. **(2QUIN^{+})(*L*-MA^{2-})•2H_2O**

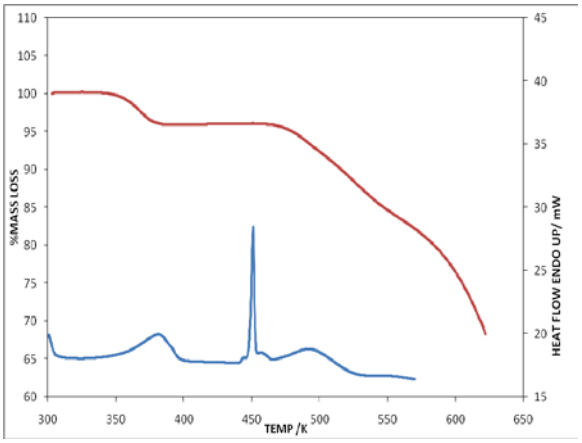

b. **(2QUIN^{+})(*D*-MA^{2-})•2H_2O**

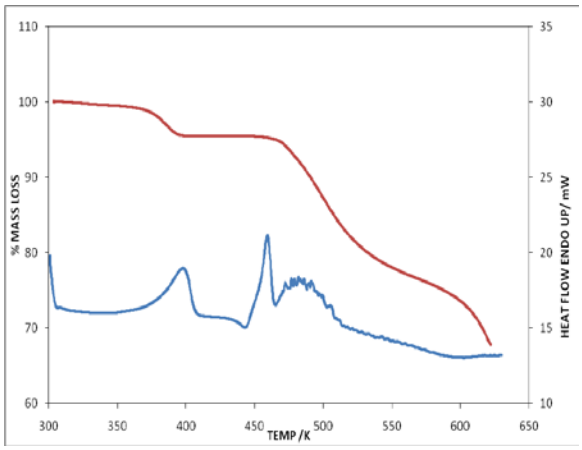

c. **(QUIN^{+})(*D*-MA^{-})•H_2O**

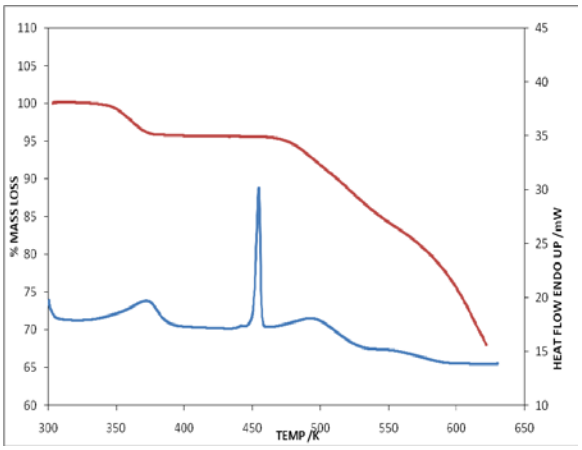

d. **(2QUIN^{+})(*DL*-MA^{2-})•2H_2O**

Figure 3.1.1: Thermal analysis results for inclusion compounds of quinine and malic acid

3.2 Structural analysis

3.2.1 Di-quininium *D-(+)*-malate and *L-(-)*-malate in Ethanol

Table 3.2.1: Crystal data table of QUIN with *D-(+)*-malic acid and *L-(-)*-malic acid (grown from ethanol)

Compound	**$(2QUIN^+)(L\text{-}MA^{2-})\bullet 2H_2O$**	**$(2QUIN^+)(D\text{-}MA^{2-})\bullet 2H_2O$**
Molecular Formula	$(2C_{20}H_{25}O_2N_2^+)(C_4H_4O_5^{2-})\bullet 2H_2O$	$(2C_{20}H_{25}O_2N_2^+)(C_4H_4O_5^{2-})\bullet 2H_2O$
Molecular Mass (g mol^{-1})	819.1	819.1
Data collection temperature (K)	173(2)	173(2)
Crystal system	Monoclinic	Monoclinic
Space group	*C*2	*C*2
a (Å)	20.5669 (18)	20.5373 (18)
b (Å)	6.6376 (6)	6.7424 (6)
c (Å)	15.5538 (15)	15.5061 (14)
α (°)	90.00	90.00
β (°)	103.906 (2)	105.843 (2)
γ (°)	90.00	90.00
Volume ($Å^3$)	2061.1 (3)	2065.6 (3)
Z	2	2
D_c, Calculated density (g cm^{-3})	1.365	1.310
Final R indices [I>2sigma(I)]	R_1= 0.0349 wR_2 = 0.0951	R_1 = 0.0676 wR_2 = 0.1897
R indices (all data)	R_1 = 0.0385 wR_2 = 0.0979	R_1= 0.0759 wR_2= 0.1985
Largest diff. peak and hole (e$Å^{-3}$)	-0.183; 0.565	-0.337; 0.755

Small needle-like crystals of **$(2QUIN^+)(L\text{-}MA^{2-})\bullet 2H_2O$** and **$(2QUIN^+)(D\text{-}MA^{2-})\bullet 2H_2O$** obtained by slow evaporation of quinine with D and *L-(-)*-Malic acid mixtures in ethanol were analysed. The inclusion compounds crystallised the monoclinic crystal system, space group of *C*2 and the Z value for the two compounds was found to be 2. There is a proton transfer from the carboxylic acid moiety of the malic acid to the nitrogen atom on the quinine resulting in a salt. The formula unit is composed of two quininium cations, one malate anion and two water molecules giving a molecular representation of $(2C_{20}H_{25}O_2N_2^+)(C_4H_4O_5^{2-})\bullet 2H_2O$ for each inclusion compound. The ratio of the water molecules were calculated from TGA results and the site occupancy factors were corrected to these ratios. All non-hydrogen atoms were refined anisotropically. The malate ion is disordered on a two-fold axis and lies at the centre of symmetry at Wyckoff position *b* on a diad. The formula units for both structures are shown in **Figure 3.2.1**. The water molecules on both structures are disordered over two positions.

A

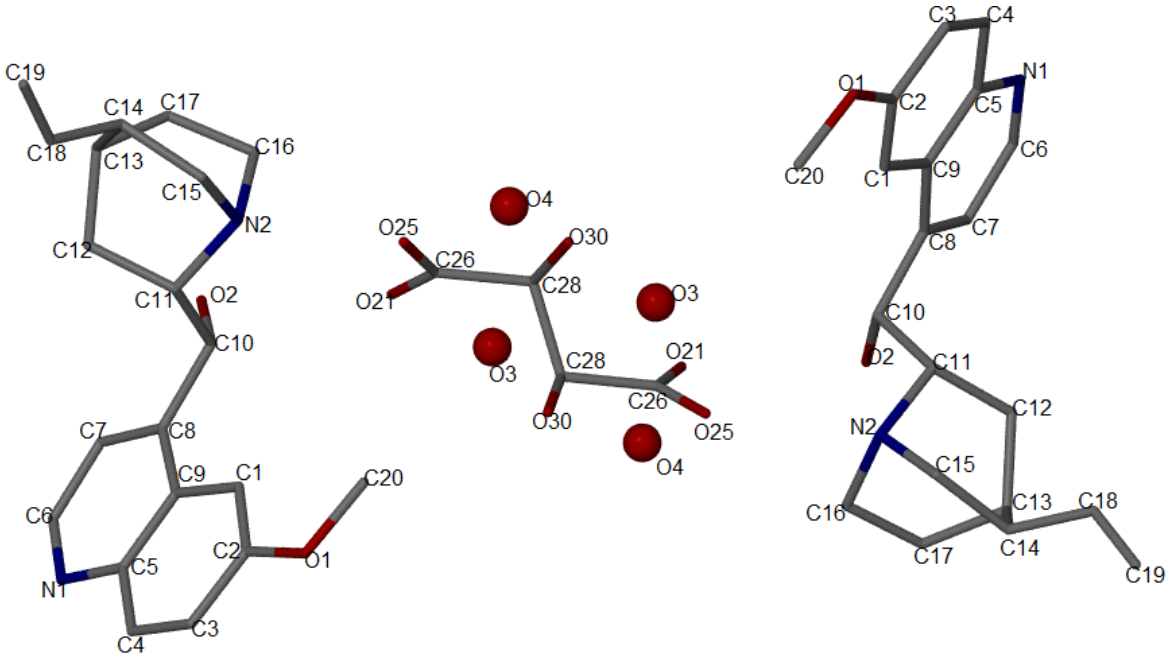

B

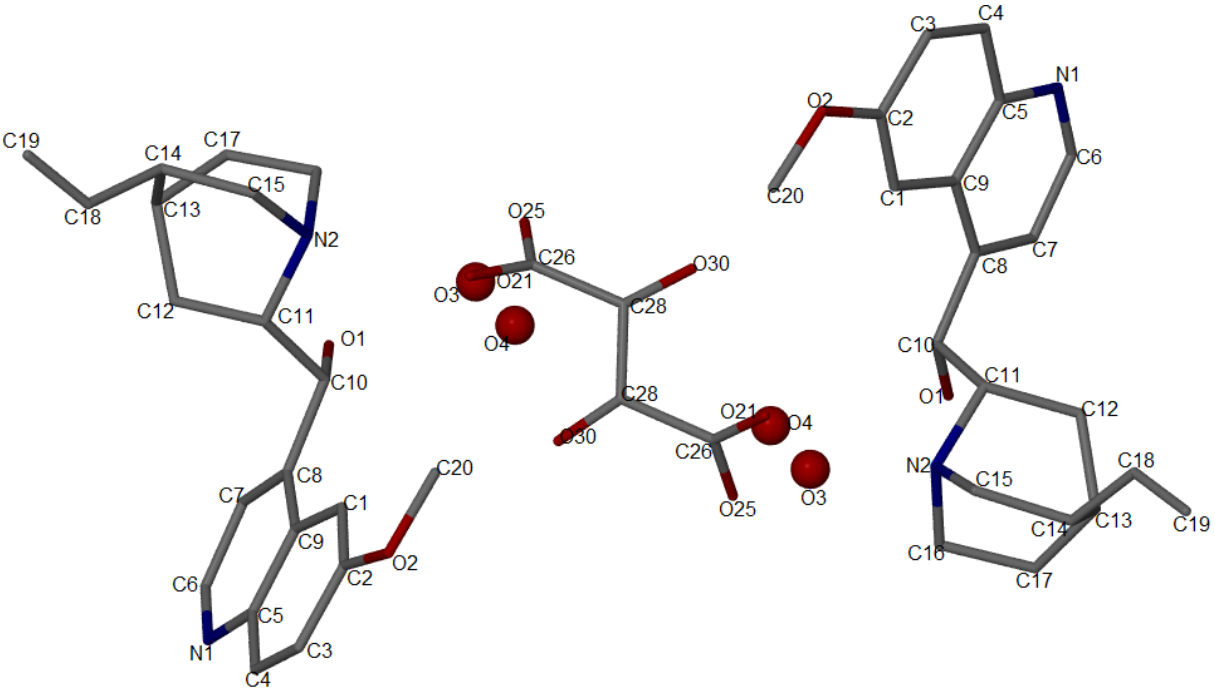

Figure 3.2.1: **(2QUIN^{+})(*L*-MA^{2-})•2H$_2$O** (A) and **(2QUIN^{+})(*D*-MA^{2-})•2H$_2$O** (B) with the hydrogen atoms removed for clarity

Hydrogen bonding patterns in both structures are shown in **Figure 3.2.2**.

A

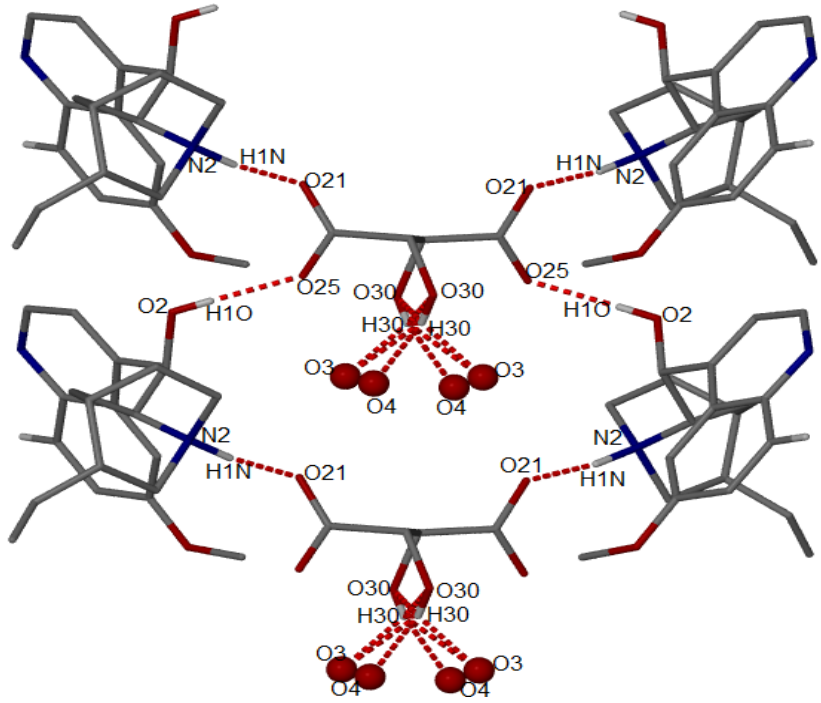

B

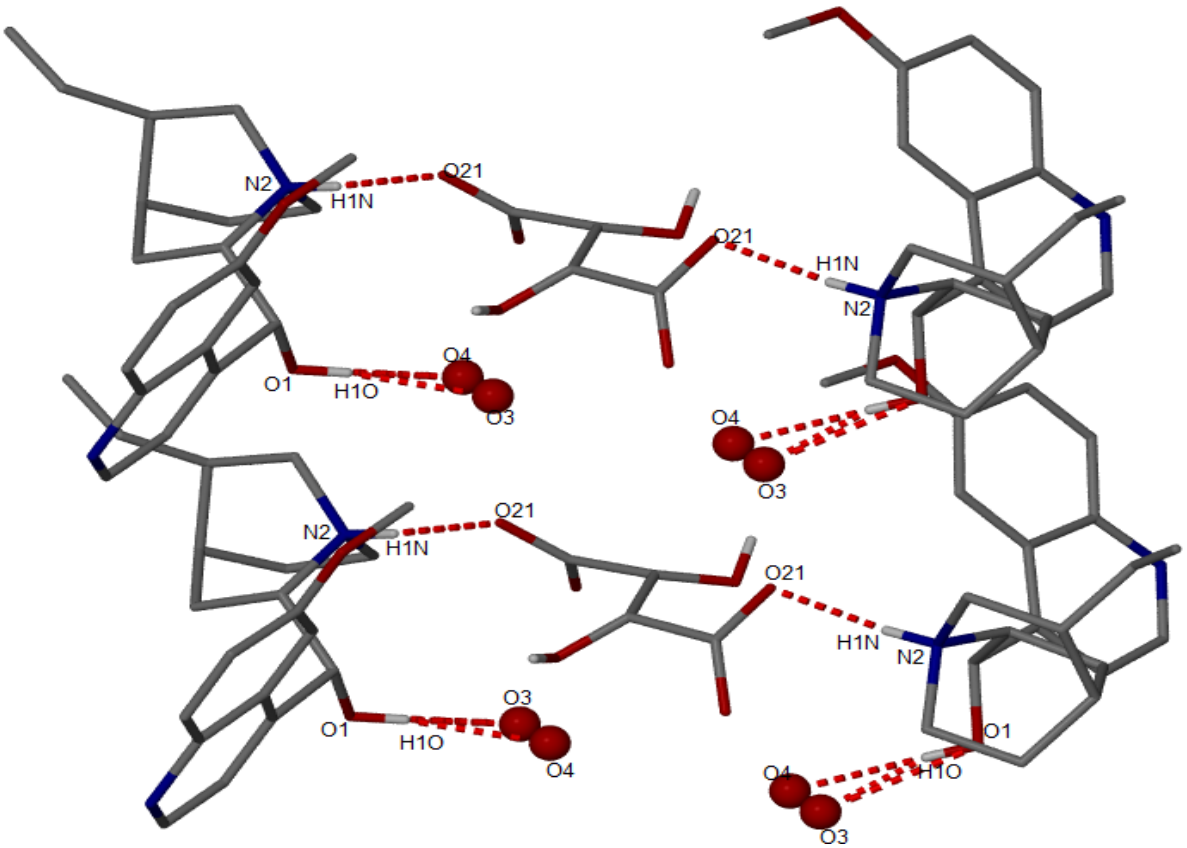

Figure 3.2.2: Hydrogen bonding in **(2QUIN^{+})(*L*-MA^{2-})•2H$_2$O** (A) and **(2QUIN^{+})(*D*-MA^{2-})•2H$_2$O** (B) Different hydrogen bonding patterns are observed in the two structures. The structure of **(2QUIN^{+})(*L*-MA^{2-})•2H$_2$O** is characterised by pairs of hydrogen bonded chains that are crystallographically related by diads. Both oxygen atoms at the carboxylate (O25 and O21) are

hydrogen bonded. O21 is bonded to N2, the protonated nitrogen atom of the quininium ion while O25 is hydrogen bonded to the hydroxyl group of the neighbouring quininium ion. In addition there are discrete hydrogen bonds observed between the disordered oxygen atoms of the water molecules (O3 and O4) and the hydroxyl group of the malate ion. One such chain may be described in graph set notation as $C_2^2(9)D_1^1(2)$. Letters C, R and D on the graph set notation denotes chain, ring and dimer or finite set generated by hydrogen bonding and S is for intramolecular hydrogen bonding. The subscript and superscript give the number of donors and acceptors respectively. The corresponding number of atoms in the repeat unit is written in parentheses.[2]

For the structure of **(2QUIN$^+$)(*D*-MA^{2-})•2H$_2$O**, discrete hydrogen bonds related by a two fold axis are formed at the N atom and the hydroxyl moiety of the cation. Hydrogen bonding is observed between the protonated nitrogen atom of QUIN$^+$ and O21 of the carboxylate. The -OH group of the cation formed a hydrogen bond with the disordered oxygen atoms of the water (O3 and O4). The graph set for such an interaction is $D_2^2(8)D_1^1(2)$. **Table 3.2.2** shows the metrics of the observed hydrogen bonds.

Table 3.2.2: Hydrogen bond parameters

COMPOUND	D-H···A	D···A (Å)	D-H (Å)	H···A (Å)	D-H···A (º)
(2QUIN$^+$)(*L*-MA^{2-})•2H$_2$O	O30-H30···O3	2.356 (6)	0.84 (1)	1.77 (1)	125 (1)
	O30-H30···O3[a]	2.860 (6)	0.84 (1)	2.12 (1)	146 (1)
	O30-H30···O30[a]	2.662 (6)	0.84 (1)	2.16 (1)	118 (1)
	N2-H1N···O21	2.706 (2)	0.90 (1)	1.82 (1)	170 (3)
	O2-H1O···O25[b]	2.667 (2)	0.77 (3)	1.89 (3)	175 (3)
	O30-H30···O4	2.408 (6)	0.84 (1)	2.10 (1)	101 (1)
a = 1-x, y, 2-z; *b* = x,-1+y,z					
(**2QUIN$^+$)(*D*-MA^{2-})•2H$_2$O**	N2-H1N···O21	2.725 (4)	0.82 (1)	1.91 (1)	174 (6)
	O2-H1O ···O3	2.511 (1)	0.78 (5)	1.77 (5)	159 (5)
	O2-H1O ···O4	2.886 (1)	0.78 (5)	2.12 (5)	172 (5)

The packing diagrams of the quininium salts are shown in **Figure 3.2.3**.

A

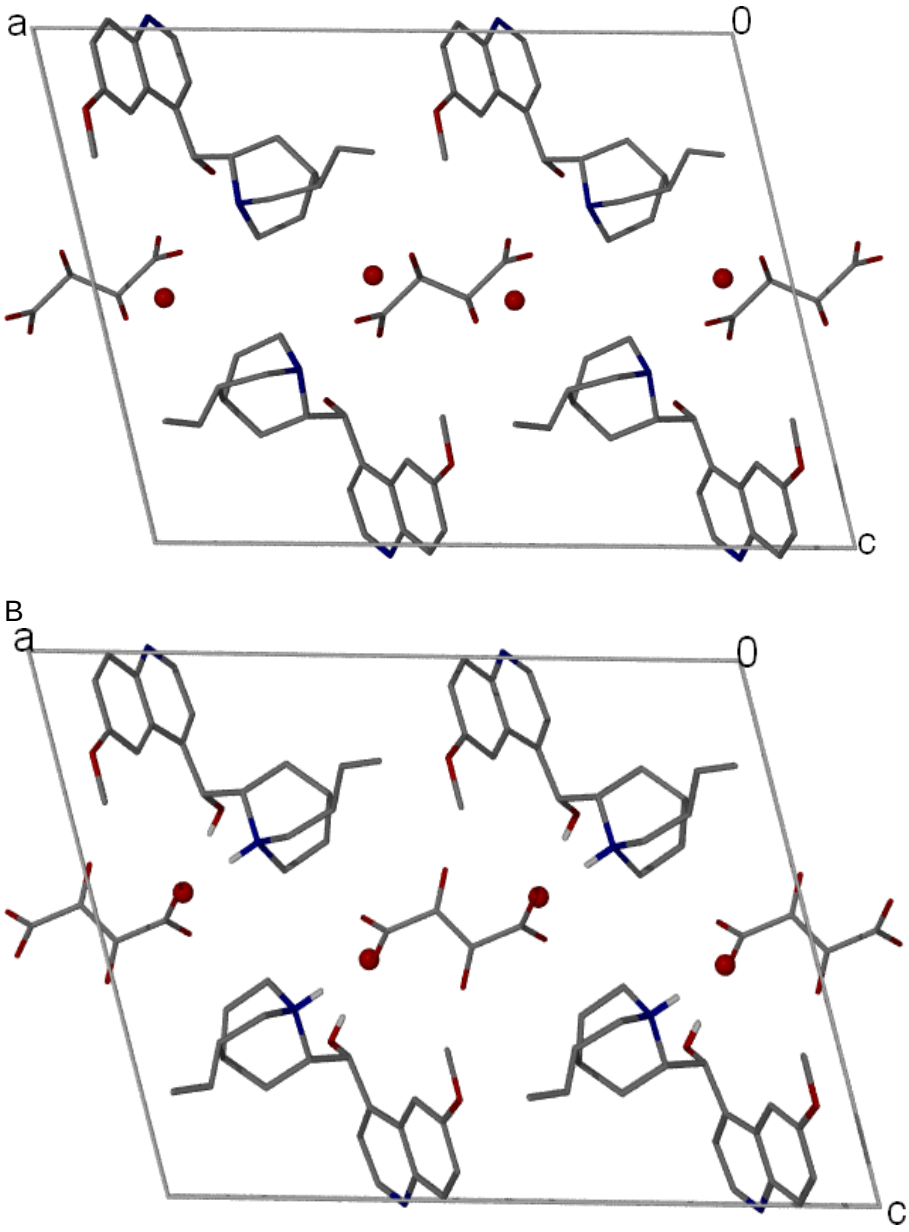

Figure 3.2.3: Packing diagrams of **(2QUIN^{+})(*L*-MA^{2-})•2H$_2$O** (A) and **(2QUIN^{+})(*D*-MA^{2-})•2H$_2$O** (B) viewed down [010]

The two structures were found to pack in a similar manner. QUIN^{+} is located in general positions. The quininium cations form a network that is isostructural, forming voids in which the malate ions and water molecule reside. **Figure 3.2.4** shows van der Waals radii representation of the channels formed by the cations viewed down [010]. A slight difference was observed in the size and the shape of the cavities formed.

A

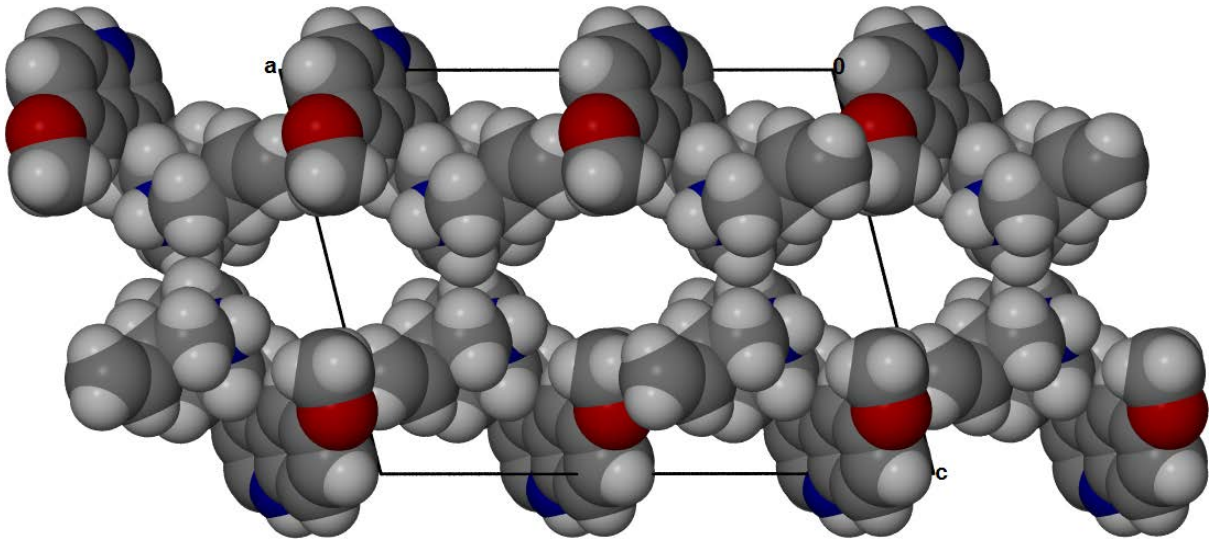

B

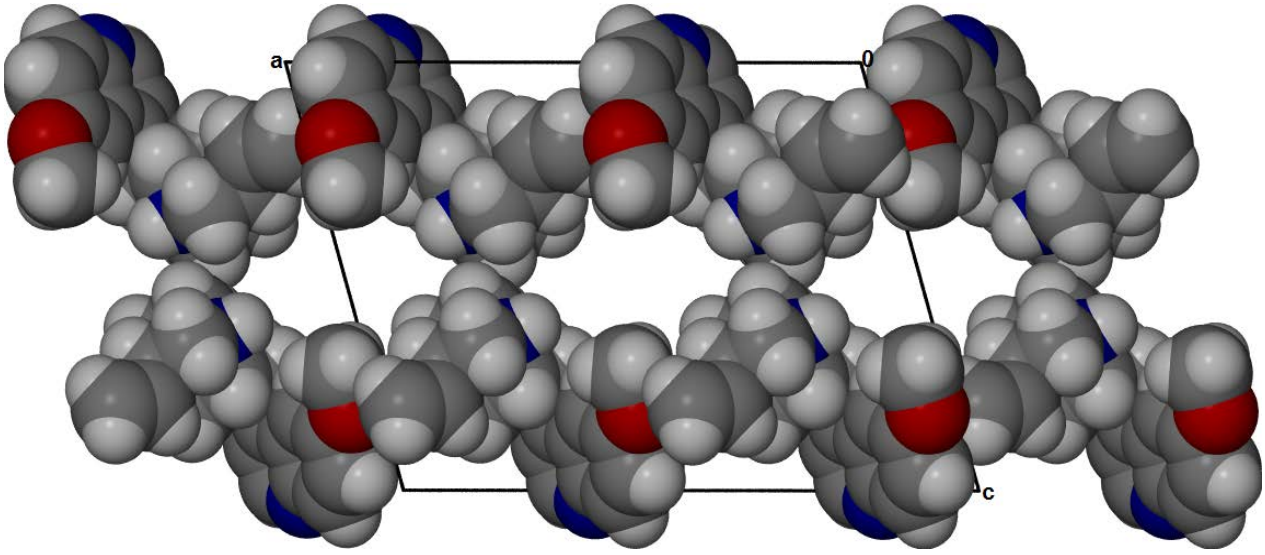

Figure 3.2.4: The packing diagrams of the cations in **(2QUIN^{+})(*L*-MA^{2-})•2H$_2$O** (A) and **(2QUIN^{+})(*D*-MA^{2-})•2H$_2$O** (B) viewed down [010], showing the channels which accommodate the anion and the water molecules in the crystal structure

The packing factors for guest sites in the two structures were determined using the MSRoll[3] program. The volumes of the guest and water molecules were determined and compared to the voids they occupy. The packing factor (PF, %) was calculated by combining the volumes of the guest and water molecules and dividing it by the volume of the voids they occupy. The volumes of the voids were calculated using a probe of radius 1.2 Å. **Table 3.2.3** shows data for calculation of packing factors for **(2QUIN^{+})(*L*-MA^{2-})•2H$_2$O** and **(2QUIN^{+})(*D*-MA^{2-})•2H$_2$O**. Each structure contains two water molecules therefore its volume was doubled.

Table 3.2.3: Packing factors (PFs) for **(2QUIN$^+$)(*L*-MA^{2-})•2H$_2$O** and **(2QUIN$^+$)(*D*-MA^{2-})•2H$_2$O**

	(2QUIN$^+$)(*L*-MA^{2-})•2H$_2$O	**(2QUIN$^+$)(*D*-MA^{2-})•2H$_2$O**
$V_{guest\ mol}$ (Å^3)	100.2	97.9
V_{water} (Å^3)	38.6	42.0
V_{total} (Å^3)	138.8	139.9
V_{void} (Å^3)	189.6	196.7
V_{mol}/V_{void} = PF%	73.3	71.1

$V_{guest\ mol}$ - guest volume, V_{void} - void volume and V_{water} - 2H$_2$O Volume

Packing factor calculations for guest site (green dot on **Figure 3.2.5)** gave 73.3% and 71.1% for **(2QUIN$^+$)(*L*-MA^{2-})•2H$_2$O** and **(2QUIN$^+$)(*D*-MA^{2-})•2H$_2$O** respectively. This means that the *L-(-)*-malate structure is more tightly packed at the guest site than the *D-(+)*-malate.

The overall packing factor for the unit cell was calculated by measuring volumes of molecules in the unit cell (4 hosts, 2 guests and 4 water molecules) and dividing them by the volume of unit cell. This gave a packing factor of 71% for both structures.

There are small unoccupied voids between the host molecules (red dot on **Figure 3.2.5**) in both structures. These voids have volumes of 33.6 Å^3 in the *L-(-)*-malate structure and 28.9 Å^3 for the *D-(+)*-malate structure.

Differences in the guest site packing factors compensated for the small unoccupied voids between host molecules, giving the same overall packing factors for the unit cell.

CCDC Mercury[4] software was used to calculate isostructurality. It was determined by overlaying the cation network as shown in **Figure 3.2.5**, with the *D-(+)*-malate structure in red and the *L-(-)*-malate structure in blue. The divergence of the motifs is expressed as a root mean square (RMS), with a value of 0.287 obtained for the compared networks.

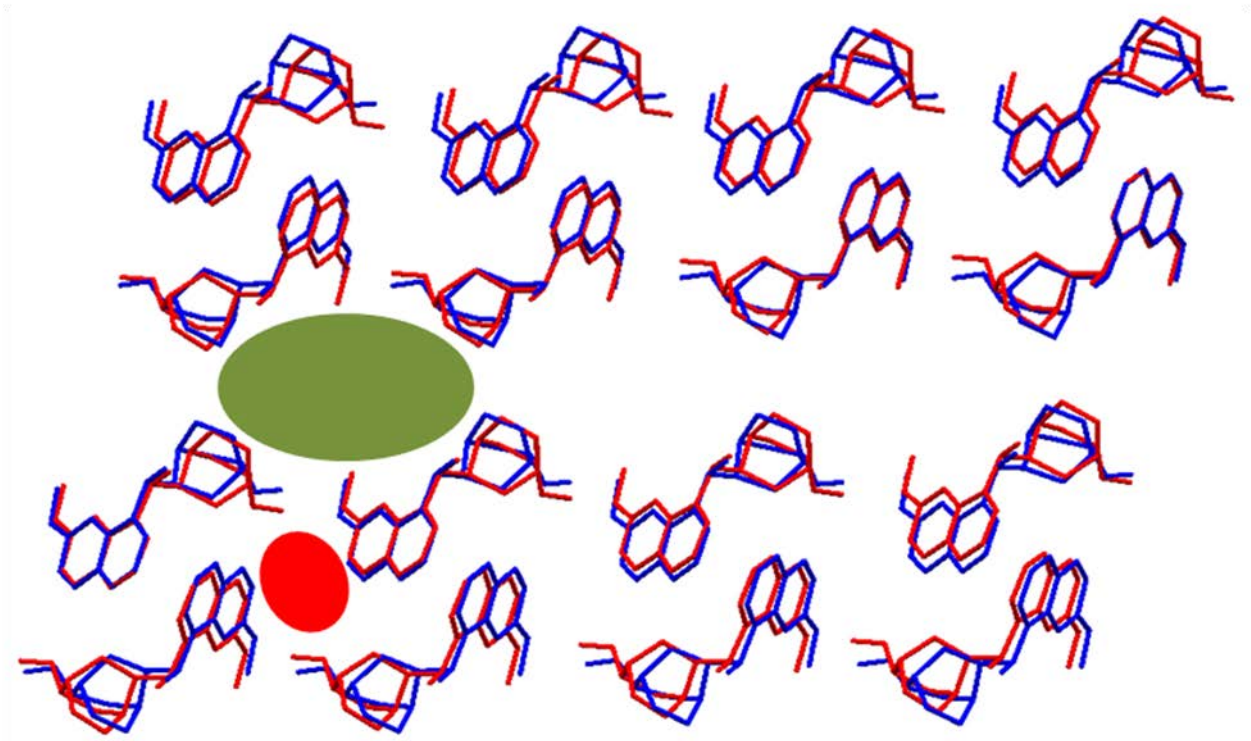

Figure 3.2.5: The overlay of the cations from both structures shows isostructurality and the guest site (green) and smaller unoccupied voids (red)

3.2.2 Di-quininium *DL*-malate

On trying to resolve the racemic mixture of malic acid, (*DL*-malic), a mixture of quinine and *DL*-malic acid was dissolved in ethanol and needle like crystals were obtained. **Table 3.2.4** shows the crystal data for the obtained structure and the formula unit is displayed in **Figure 3.2.6** (A). Figure 3.2.6 (C) shows the disorder of the *DL*-malate ion with the *D* enantiomer shown in green and the *L*-malate in green.

Table 3.2.4: The crystal data for **$(2QUIN^{+})(DL\text{-}MA^{2-})\bullet 2H_2O$**

Compound	**$(2QUIN^{+})(DL\text{-}MA^{2-})\bullet 2H_2O$**
Molecular Formula	$(2C_{20}H_{25}O_2N_2^{+})(C_4H_4O_5^{2-})\bullet 2H_2O$
Molecular Mass (g mol^{-1})	819.1
Data collection temp. (K)	173(2)
Crystal system	Monoclinic
Space group	*C*2
a (Å)	20.513 (3)
b (Å)	6.6802 (8)
c (Å)	15.5242 (15)
α (°)	90.00
β (°)	104.991(2)
γ (°)	90.00
Volume ($Å^3$)	2054.9 (3)
Z	2
D_c, Calculated density (g cm^{-3})	1.311
Final R indices [I>2sigma(I)]	R_1 = 0.0994 wR_2 = 0.2993
R indices (all data)	R_1= 0.1187 wR_2 = 0.3272
Largest diff. peak and hole ($eÅ^{-3}$)	-0.809; 1.289

A

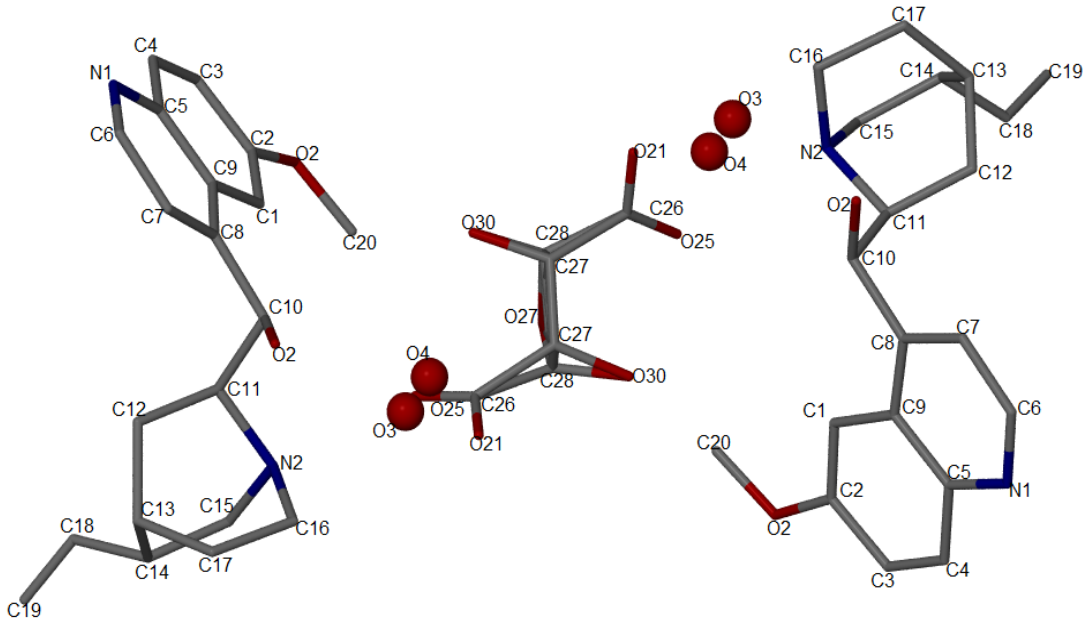

B

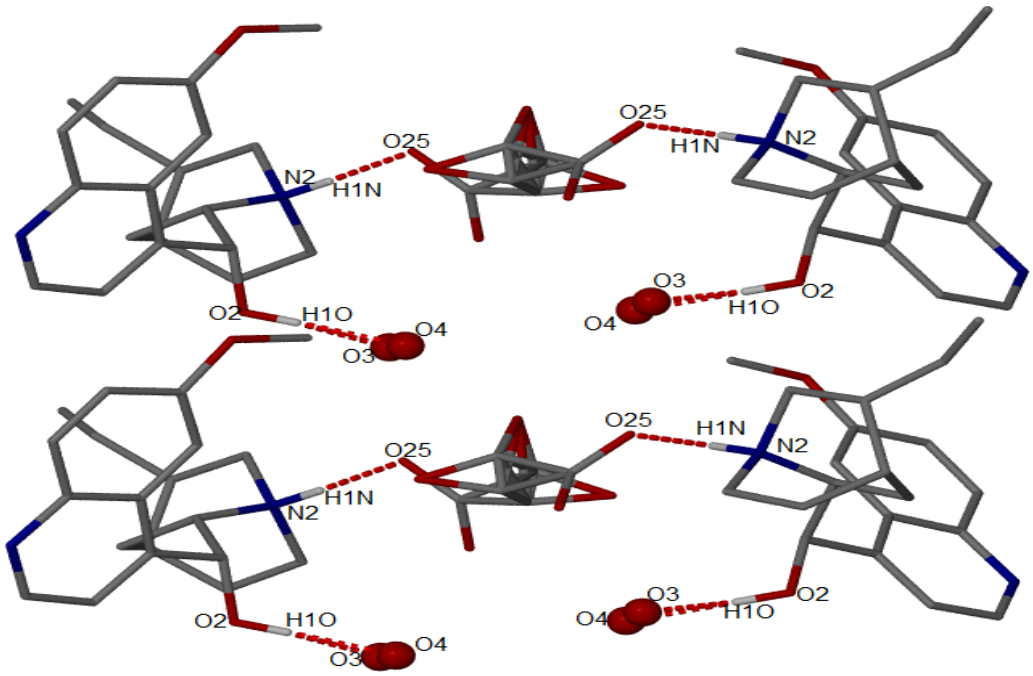

C

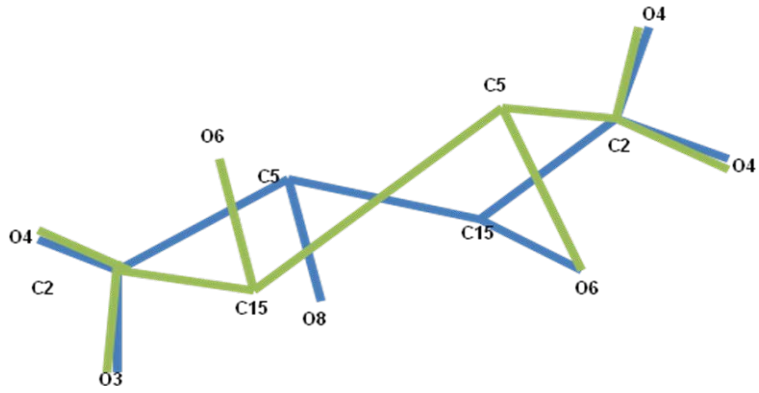

Figure 3.2.6: Formula unit (A), hydrogen bonding (B) in **(2QUIN^{+})(*DL*-MA^{2-})•2H$_2$O** and clarification of the *DL*-malate ion disorder (C)

A structure that resembles that of the two previous structures was obtained. The carboxylic acid group of the guest transferred a proton to the nitrogen atom of the QUIN molecule forming a salt. The guest (*DL*-malate) is also disordered on a two-fold axis at Wyckoff position *b*. The water molecule is disordered over two positions. The compound crystallized in the monoclinic crystal system, space group *C*2 and. The Z value was found to be 2.

The hydrogen bonding network, which is the main bonding in the structure is represented in **Figure 3.2.6** (B). The interaction observed in the structure is similar to that of **(2QUIN^{+})(*D*-MA^{2-})•2H$_2$O**. A hydrogen bond is formed between the protonated N atom and one of the oxygen atoms on the carboxylate. The hydroxyl group of QUIN is hydrogen bonded to the water molecules. **Table 3.2.5** shows the hydrogen bond parameters.

Table 3.2.5: Hydrogen bond parameters in **(2QUIN^{+})(*D*-MA^{2-})•2H$_2$O**

Compound	D-H···A	D···A (Å)	D-H (Å)	H···A (Å)	D-H···A (º)
(2QUIN^{+})(*DL*-MA^{2-})•H$_2$O	N2-H1N···O25	2.76 (1)	0.93 (1)	1.83 (1)	174.1 (1)
	O2-H1O···O3	2.41 (1)	0.84 (1)	1.63 (1)	152.1 (1)
	O2-H1O···O4	2.58 (1)	0.84 (1)	1.74 (1)	174.3 (1)

The packing diagram of **(2QUIN^{+})(*DL*-MA^{2-})•2H$_2$O**is shown in **Figure 3.2.7** (A). The host arranges such that channels are formed down [010] and the guests as well as the water molecules resides in these channels. **Figure 3.2.7** (B) shows the channels in which the guest and water molecules reside.

A

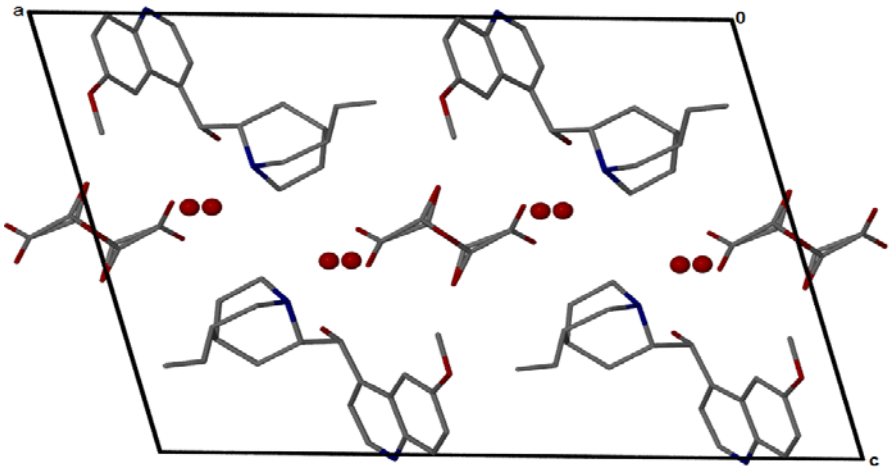

B

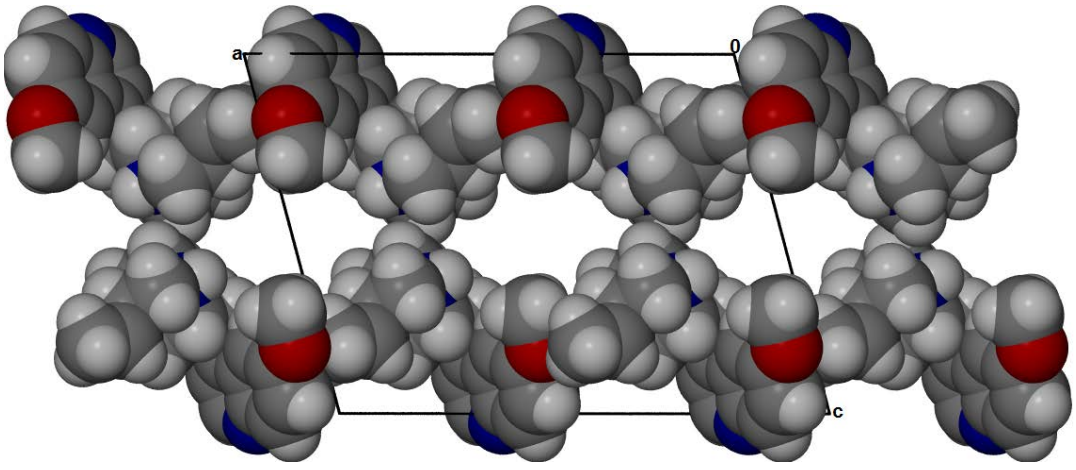

Figure 3.2.7: Unit cell down [010] (A) and packing diagram of **(2QUIN^{+})(*DL*-MA^{2-})•2H$_2$O** viewed down [010] with the guest molecules omitted, host molecules represented in van der Waals radii (B)

The efforts to resolve *DL*-malic were not successful because the two enantiomers were trapped in the host in a 50:50 ratios. The disorder of the guest and the water molecule is responsible for the high R-factor.

3.2.3 Quininium *D-(+)*-malate in water

Upon changing the solvent to water, a new compound of quinine and *D-(+)*-malic acid was obtained, **(QUIN$^+$)(*D*-MA$^-$)•H_2O**). It has the same crystal system and space group as the previously reported salts. The crystal data for the structure is represented in **Table 3.2.6**. The *D-(+)*-malic acid guest donated a single proton to the host and a water molecule is also trapped in the molecular structure. This gave a salt with molecular representation of $(C_{20}H_{25}O_2N_2^+)(C_4H_5O_5^-)•H_2O$ as illustrated by **Figure 3.2.8** (A).

Table 3.2.6: The crystal data table for **(QUIN$^+$)(*D*-MA$^-$)•H_2O**

Compound	**(QUIN$^+$)(*D*-MA$^-$)•H_2O**
Molecular Formula	$(C_{20}H_{25}O_2N_2^+)(C_4H_5O_5^-)•H_2O$
Molecular Mass (g mol^{-1})	476.6
Data collection temp. (K)	173(2)
Crystal system	Monoclinic
Space group	*C*2
a (Å)	20.3950 (3)
b (Å)	6.8096 (9)
c (Å)	19.4300 (4)
α (°)	90.00
β (°)	120.086 (2)
γ (°)	90.00
Volume (Å^3)	2334.9 (6)
Z	4
D_c, Calculated density (g cm^{-3})	1.356
Final R indices [I>2sigma(I)]	R_1 = 0.0365
	wR_2 = 0.0898
R indices (all data)	R_1 = 0.0421
	wR_2 = 0.0928
Largest diff. peak and hole (eÅ^{-3})	-0.187; 0.260

A

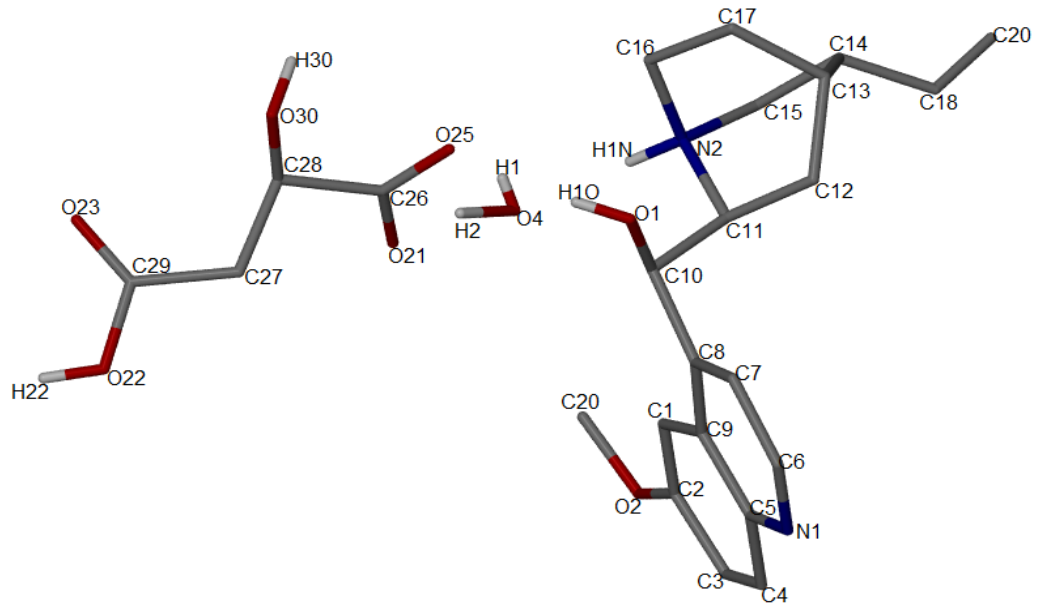

B

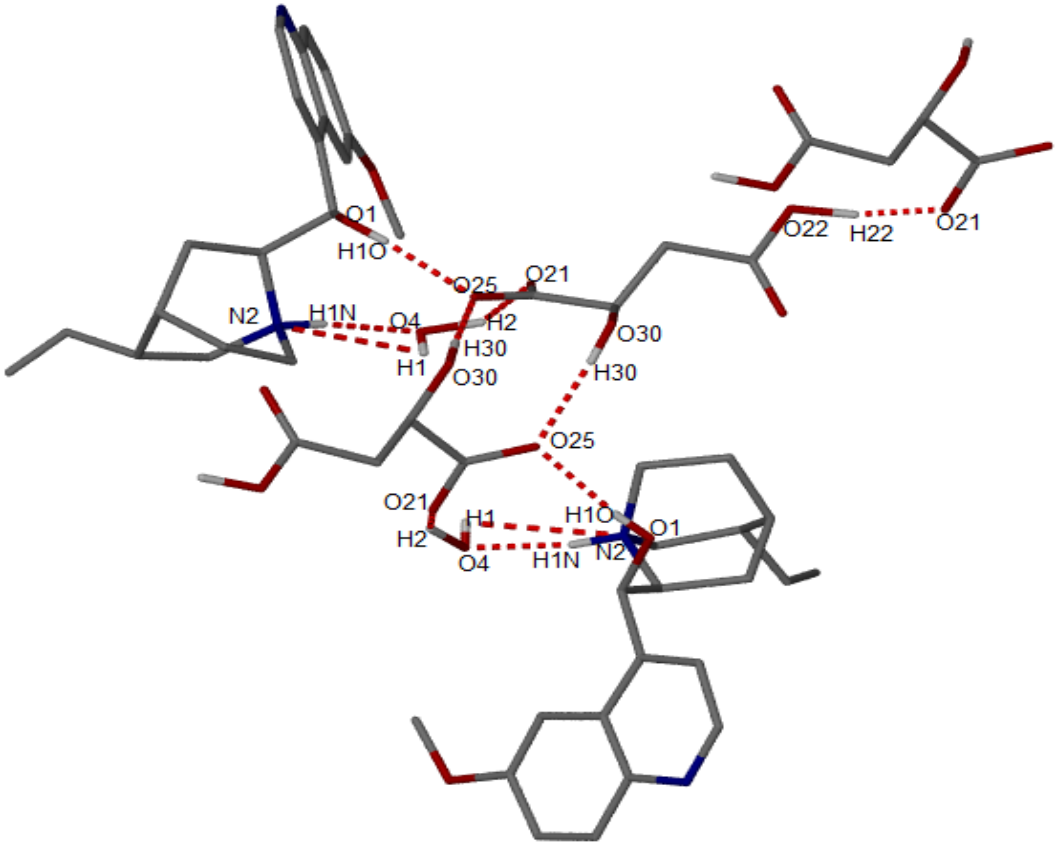

Figure 3.2.8: Formula unit (A) and hydrogen bonding in **(QUIN$^+$)(*D*-MA$^-$)•H$_2$O** (B)

Hydrogen bonding is the main interaction observed in **(QUIN$^+$)(*D*-MA$^-$)•H$_2$O** and it is shown in **Figure 3.2.8** (B). The protonated N2 atom forms a hydrogen bond with the O4 atom of the water molecule. The same water molecule is also involved in hydrogen bonding to the carboxylate moiety of the *D-(+)*-malate. Bifurcated hydrogen bonds are observed at both oxygen atoms of the carboxylate moiety (O21 and O25); O25 forms hydrogen bonds with the OH groups on the

quininium cation and another anion, while O21 hydrogen bonds to the water molecule and the OH of the carboxylic acid of the next anion. These hydrogen bonds form a 10 atom long chain from O21 to O25, **Figure 3.2.8** (B). Along the chain are rings, formed by the malate ions as shown in **Figure 3.2.9** (A) and another one formed by water, quininium and the carboxylate moiety of the malate ion, **Figure 3.2.9** (B). The hydrogen bonding maybe expressed in graph theory as $C_2^2(10)\,R_2^2(10)\,R_3^3(11)$.

A

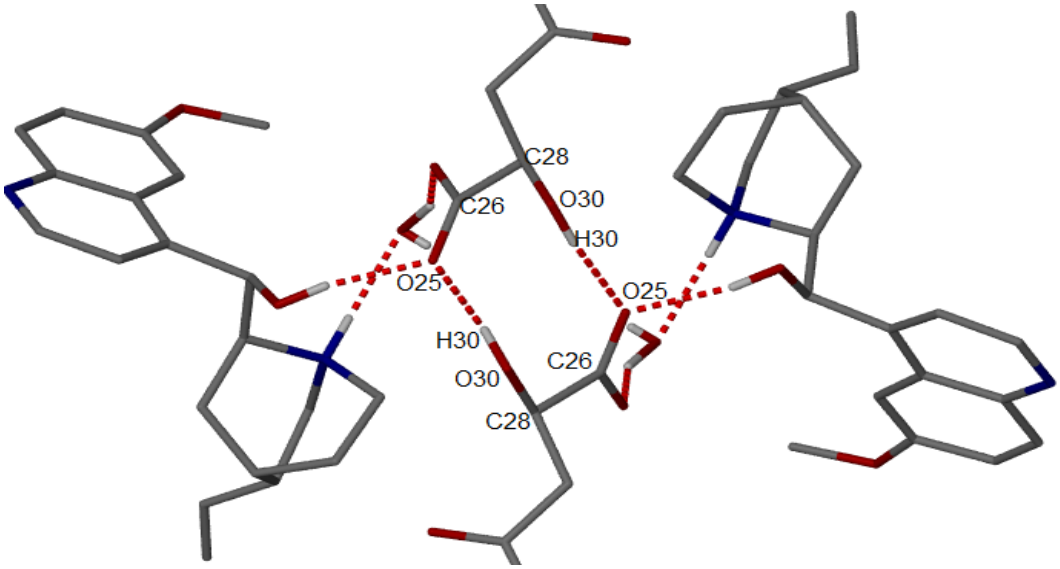

B

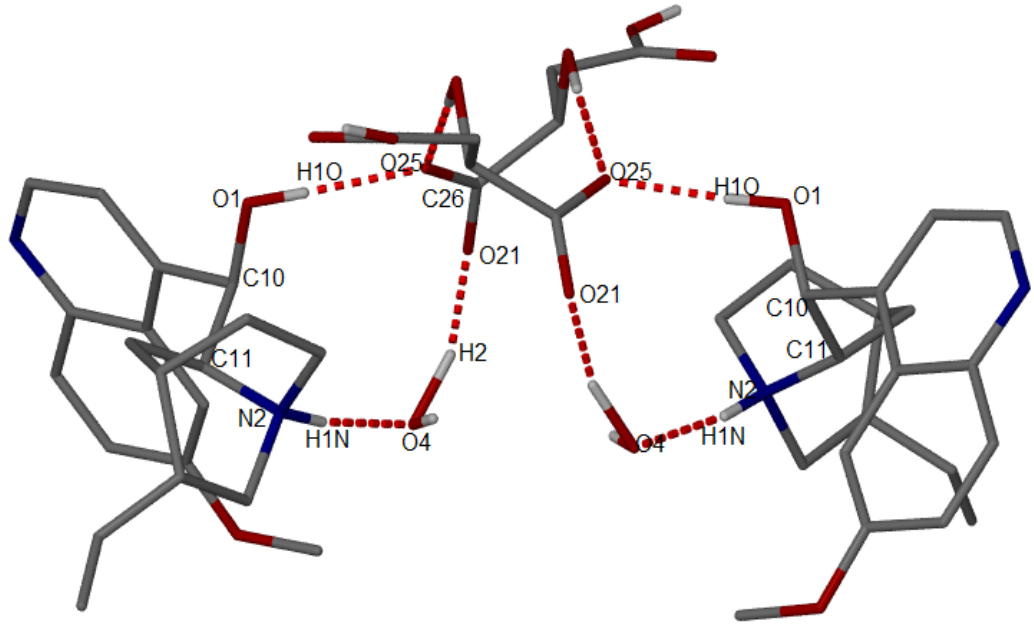

Figure 3.2.9: Hydrogen bond ring formed by two malate ions (A) and by water, quininium and malate ions (B) in the structure of **(QUIN$^+$)(*D*-MA$^-$)•H_2O**

The hydrogen bond distances and angles are summarized in **Table 3.2.7**. The C-H···π interactions were also observed between the quininium ions.

Table 3.2.7: Hydrogen bond parameters in **(QUIN$^+$)(*D*-MA$^-$)•H$_2$O**

Compound	D-H···A	D···A (Å)	D-H (Å)	H···A (Å)	D-H···A (º)
(QUIN$^+$)(*D*-MA$^-$)•H$_2$O	O30-H30···O25 *a*	2.811 (2)	0.84 (1)	2.00 (1)	162 (1)
	O30-H30···O30 *a*	3.130 (2)	0.84 (1)	2.61 (1)	122 (1)
	O22-H22···O21 *b*	2.640 (2)	0.84 (1)	1.85 (1)	164 (1)
	N2-H1N···O4	2.741 (2)	0.89 (1)	1.85 (1)	172 (2)
	O1-H1O···O25	2.716 (2)	0.89 (3)	1.83 (3)	170 (2)
	O4-H1···O30 *c*	2.902 (2)	0.79 (4)	2.13 (4)	163 (4)
	O4-H1···O25 *c*	3.094 (2)	0.79 (4)	2.55 (4)	127 (3)
	O4-H2···O21	2.719 (2)	0.87 (4)	1.86 (4)	172 (3)

a = 1-x,y,1-z ; *b* = ½-x,-½+y,1-z; *c* = x, y+1, z

The unit cell of **(QUIN$^+$)(*D*-MA$^-$)•H$_2$O** viewed down [010] with the hydrogen atoms omitted for clarity is represented by **Figure 3.2.10** (A). QUIN cations arrange in bilayers with the malate ions and water molecules occupying the (002) plane. The voids occupied by the guests are shown in **Figure 3.2.10** (B).

A

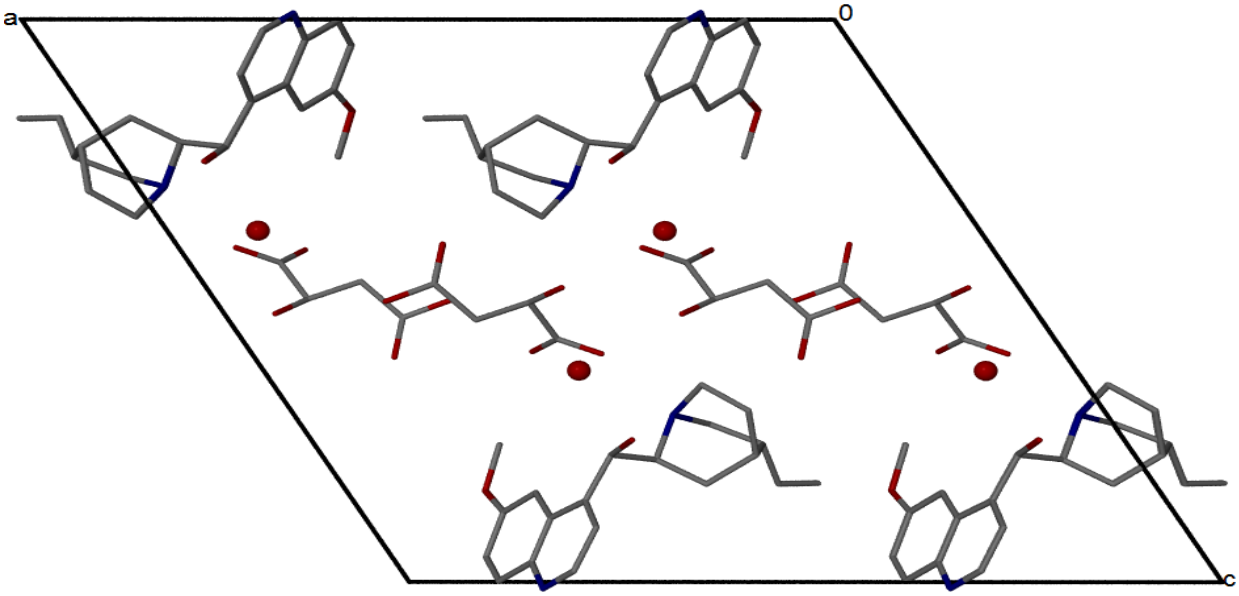

B

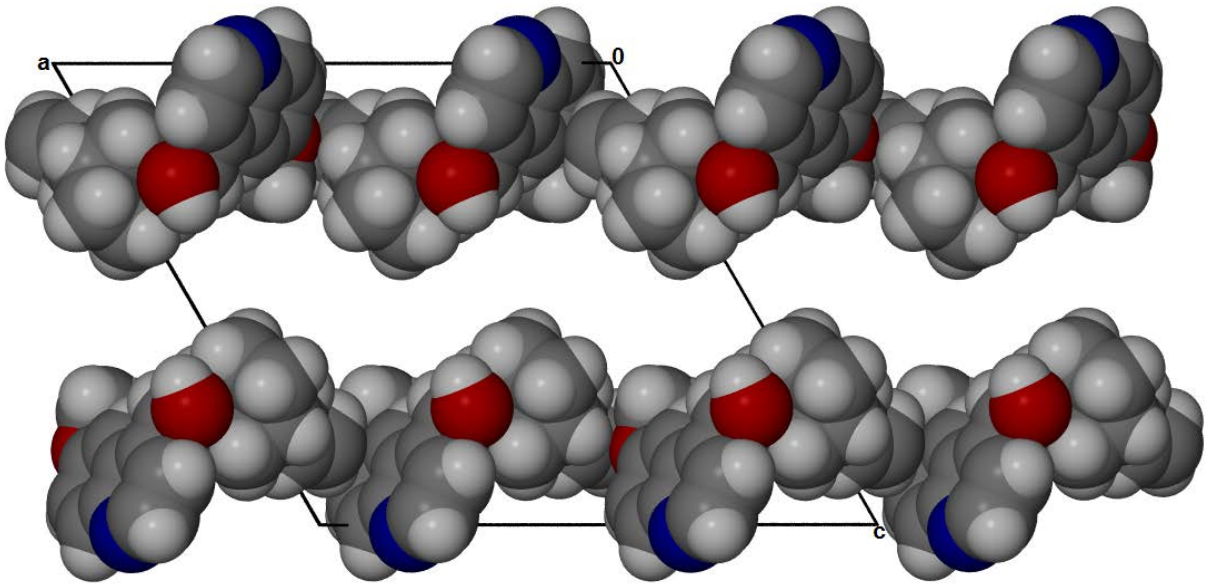

Figure 3.2.10: Unit cell down [010] (A) and the packing diagram of **(QUIN^{+})(*D*-MA^{-})•H_2O** down [010] with the guest molecules omitted, represented as van der Waals radii (B)

3.3 SALT vs. CO-CRYSTAL

Crystallographically the difference between a co-crystal and a salt is subtle, as it depends on the location of a single hydrogen atom. This is illustrated by the formation of a compound between a carboxylic RCOOH and pyridine. Two possibilities are shown in **Figure 3.3.1**.

A

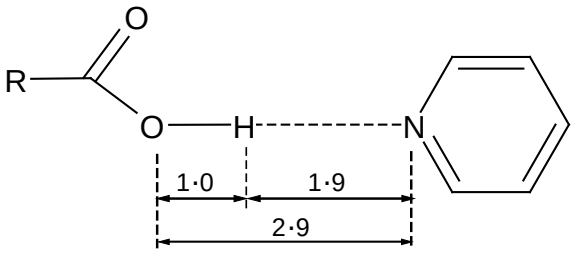

B

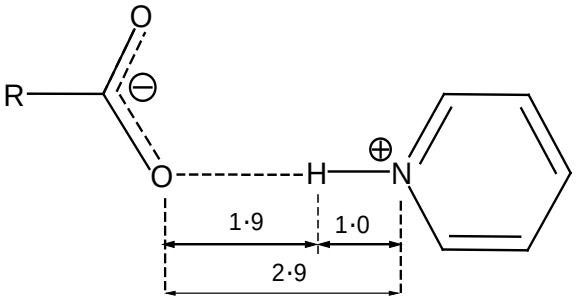

Figure 3.3.1: Illustration of a co-crystal (A) and salt (B), all distances are in Å

From the diagram we can see that the difference between a co-crystal and a salt is the movement of the carboxyl hydrogen by 0.9 Å along the O···N vector. The location of H atoms by X-ray diffraction is not straight forward as the X-ray scattering power of an atom is dependent on its number of electrons. One is dependent on excellent intensity data at high θ, usually at low temperatures. If the quality of the crystal is poor, the H atoms may not show on the difference electron density maps, or their positions are uncertain. Fortunately we can monitor the geometry of the carbonyl groups.

In the co-crystal the C=O and the C-O in C-O-H are distinct, typically 1.20 Å for C=O and 1.33 Å for C-O. By contrast, if a salt is formed, the COO^- moiety displays equal or near equal C-O^- bond lengths of approximately 1.27 Å. This has been discussed in detail by Childs *et al*[5] who have mapped the geometry of carboxyl groups as a function of ΔpKa, the difference in the pKa values of the acid and conjugate acids of the bases involved in the reaction.

In our structures of various forms of malic acid with quinine we obtained results showing salt formation. However, the result of D-(+)-malic acid with quinine in water shows both salt and co-crystal formation. We located the relevant hydrogen atoms in all of the structures and the ensuing C-O bond lengths of the carboxyl moieties clearly indicated either a co-crystal or a salt.

Diagrams adopted from Childs[4] were used to correlate the two parameters. **Figure 3.3.2** shows the relationship between the C-O bond distances and the difference in pKa values of the acid and the base.

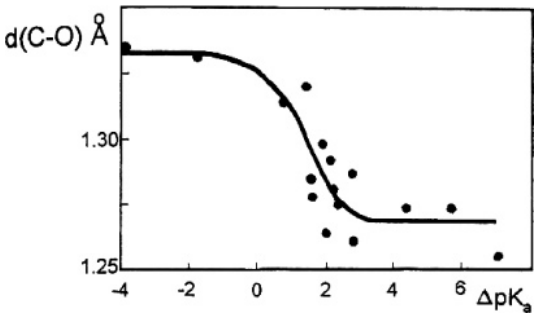

Figure 3.3.2: The correlation between the C-O bond lengths, d(C-O) and ΔpKa values

The C-O bond lengths of the carboxylate were correlated to the pKa values of the malic acid and $QUINH^+$. Malic acid has $pKa_1 = 3.4$ and $pKa_2 = 5.1$ and quinine has a pKa value of 5.1. The ΔpKa values are $pKa_1 = 1.7$ and $pKa_2 = 0.0$.

In the structures of **(2QUIN$^+$)(*L*-MA^{2-})•2H_2O**, **(2QUIN$^+$)(*D*-MA^{2-})•2H_2O** and **(2QUIN$^+$)(*DL*-MA^{2-}) •2H_2O**, the COO^- moieties are related by a two fold axis therefore the C-O bond lengths are equal on both moieties. The bond lengths of these hydrates were compared to ΔpKa and the results were in correspondence with **Figure 3.3.2**. According to this diagram, the shorter C-O bond

lengths, d(C-O), at larger ΔpKa values indicate salt formation while longer C-O distances at small or negative ΔpKa values indicate co-crystal formation. The bonds lengths range from 1.20 Å to 1.26 Å and these results correspond to the ΔpKa values. At the ΔpKa = 1.7, the bond lengths must be approximately 1.26 Å, and this matches with the results obtained.

In **Figure 3.3.2**, there is a transition at ΔpKa values ranging from -1 to 1 and the possible outcomes in that range are elaborated clearly in **Figure 3.3.3** which is the plot of ΔpKa against (ΔD_{C-O}), the difference between C-O distances within the carboxylic or carboxylate moieties.

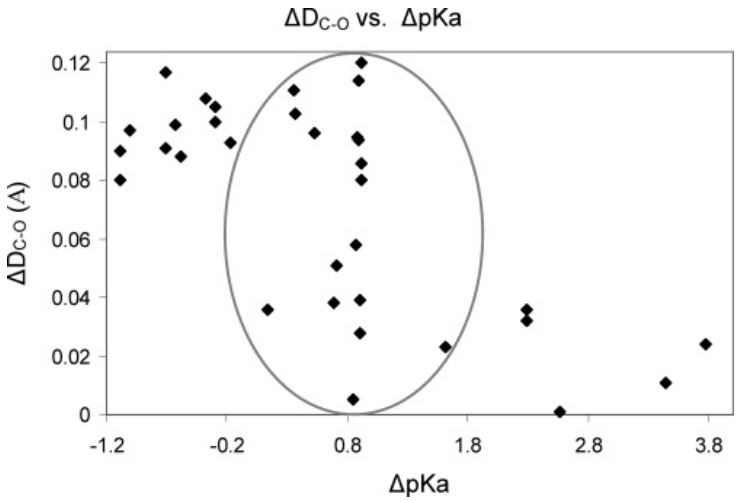

Figure 3.3.3: A plot of ΔpKa vs. ΔD_{C-O} values

The diagram shows that salts are formed at larger ΔpKa values and this is indicated by smaller ΔD_{C-O} while co-crystals form at smaller ΔpKa values and it is shown by larger ΔD_{C-O}. However, at ΔpKa values ranging from -0.2 to 2.0 (circle) either a salt or a co-crystal can be formed. In our results, a salt was obtained for ΔpKa values 0.0 and 1.7.

For the structure of **(QUIN$^+$)(*D*-MA$^-$)•H_2O**, only one carboxylic moiety donated a hydrogen bond to QUIN therefore a combination of a co-crystal and salt is obtained in the structure. This was confirmed by fitting measured d(C-O) and calculated ΔD_{C-O} to plots in **Figure 3.3.2** and **Figure 3.3.3**. The calculated C-O bond parameters are shown in **Table 3.3.1**.

Table 3.3.1: C-O bond lengths parameters in **(QUIN$^+$)(*D*-MA$^-$)•H_2O**

C-O bond	d(C-O) (Å)	ΔD_{C-O}(Å)
C26-O21	1.27	0.02
C26-O25	1.25	
C29-O22	1.33	0.13
C29-O23	1.20	

The bond lengths are well within the expected distances for ΔpKa_1 and this confirms the formation of a salt at C26. This is further substantiated by the plot of ΔpKa vs. ΔD_{C-O} values. The ΔD_{C-O} at C29 lies inside the circle in **Figure 3.3.3** and this is the region where either a salt or a co-crystal

can be formed. The formation of a co-crystal at C29 is confirmed by longer bond length at C29-O22.

QUIN formed stable inclusion compounds with both *D-(+)*-malic and *L-(-)*-malic acid and subtle differences are observed in the two structures hence resolution is almost impossible. Different solvents have shown to have impact on the proton transfer ability from the acid to the base. This is demonstrated by the structures **(QUIN^{+})(*D*-MA^{-})•H_2O** which was obtained from water and **(2QUIN^{+})(*D*-MA^{2-})•2H_2O** obtained from ethanol. Only one proton was transferred when water was used and two protons were transferred in the ethanol structure. The structures obtained from ethanol have water molecules in them, this is the water absorbed from the environment during slow evaporation since the ethanol used was dried with molecular sieve.

REFERENCES

[1] Windholz, M. (Ed.) (1976), The Merck Index: An encyclopedia for chemicals and drugs, Merck & Co., Inc., New Jersey, 1976.

[2] Etter, M. (1990), Encoding and decoding hydrogen-bond patterns of organic compounds, *American Chemical Society*, Vol.23: 120-126.

[3] Connolly, M. L. (1993), The molecular surface package, *J. Mol. Graphics*, Vol. 11: 139–141.

[4] Allen, F. H. and Lipscomb, K. J. (2004), The Cambridge Structural Database, *Encyclopedia of Supramolecular Chemistry*, Ed: Atwood, J. L. & Steed, J. W., Vol. 1:161-168.

[5] Childs, S. L., Stahly, G. P., and Park, A. (2007), The salt-cocrystal continuum: the influence of crystal structure on ionization state, *Molecular Pharmaceutics* Vol. 4: 323-338.

CHAPTER 4

(+)-DEOXYCHOLIC ACID AND CHOLIC ACID

The ability of the bile acids to form salts with a series of amines was determined using Fourier transform infra red spectroscopy. Kinetics of absorption was performed on the combinations of (+)-deoxycholic acid (DCA) with 1-propylamine and DCA with racemic *sec*-butylamine to determine the rate constants of the acid-base reactions. Kinetics of desolvation was also done on the powders of DCA with racemic *sec*-butylamine and DCA with di-*n*-butylamine. Thermal analyses of the DCA-amine combinations were done before crystallisation. The crystals were obtained by dissolving the salts in acetone and allowing them to evaporate slowly at room temperature. The structures of the resultant crystals are discussed.

4.1 IR Spectroscopy & Powder X-Ray Diffraction

According to the CSD[1], very few structures of the bile acids, (+)-deoxycholic acid (DCA) and (+)-cholic acid (CA) with the amines have been reported. The aim of this project is to characterise these inclusion compounds. A preliminary screening of the compounds was carried out using Fourier transform infra red spectroscopy (FT-IR), powder X-ray diffraction (PXRD) and thermal analysis. The purpose of this was to find out if exposing the bile acids to selected alkyl amines would yield a co-crystal or a salt.

Samples were prepared by exposing bile acids to the vapours of the amines and by grinding them in the presence of a few drops of the amines. Some of the ground samples of DCA that yielded promising resulted as indicated by IR and thermal analyses, were further analysed by PXRD.

In the formation of a salt, the carbonyl peak of the carboxylic acid is converted to a carboxylate (COO^-) and it appears in the IR spectrum below 1675 cm^{-1}. Other expected peaks are the two broad stretches at 1900 cm^{-1} and 2500 cm^{-1} for the protonated nitrogen, N^+-H···O, similar peaks are also expected for co-crystals (from O-H···N) and accompanied by a small shift in the carbonyl peak. A typical IR spectrum is shown in **Figure 4.1.1** and IR results obtained are summarised in **Table 4.1.1**.

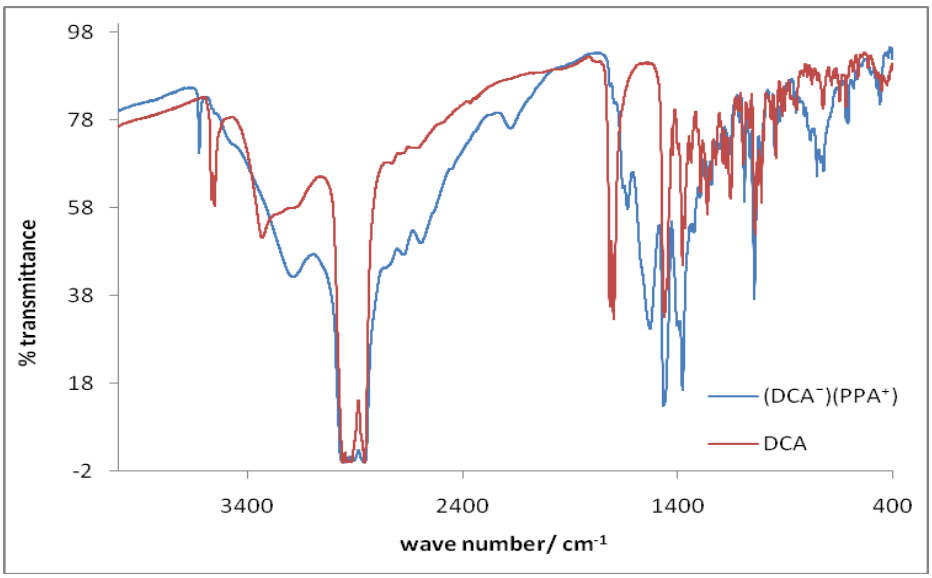

Figure 4.1.1: Typical IR spectra of DCA against a resultant salt (DCA^-)(PPA^+)

Table 4.1.1: IR results of DCA with different amines

		(+)-deoxycholic acid		(+)-cholic acid	
Amine	Peak (cm^{-1})	Grinding	Vapour	Grinding	Vapour
1-Propylamine (PPA)	1600-1675	+	+	+	+
	1850-2100	+	+	-	+
	2450-2600	+	+	-	+
n-butylamine (1-BUAM)	1600-1675	+	+	+	+
	1850-2100	+	+	+	+
	2450-2600	+	+	-	+
(*R,S*)-*sec*-butylamine (2-BUAM)	1600-1675	+	+	+	-
	1850-2100	+	+	+	+
	2450-2600	+	+	-	+
Diethylamine (DIETAM)	1600-1675	+	+	+	-
	1850-2100	+	+	-	-
	2450-2600	+	+	-	-
Di-*n*-butylamine (DIBUAM)	1600-1675	+	+	+	-
	1850-2100	-	-	-	-
	2450-2600	+	-	-	-

In all the experiments of (+)-deoxycholic acid with amines, salts were obtained, confirmed by the presence of the COO^- peak at wave number below 1675 cm^{-1} in all the spectra. A combination of salts and co-crystals was obtained from (+)-cholic acid experiments. Salts of (+)-cholic acid with 2-BUAM, DIETAM and DIBUAM were obtained from grinding experiments, the vapour experiments were unsuccessful. Based on these outcomes, a decision to grow crystals of (+)-deoxycholic acid only was taken.

The resultant salts of PPA, 1-BUAM and 2-BUAM were analysed by PXRD and the powder patterns obtained are illustrated in **Figure 4.1.2**. The patterns were compared to that of the starting

material (DCA). Completely different PXRD patterns were obtained for each sample and this confirms the IR results obtained.

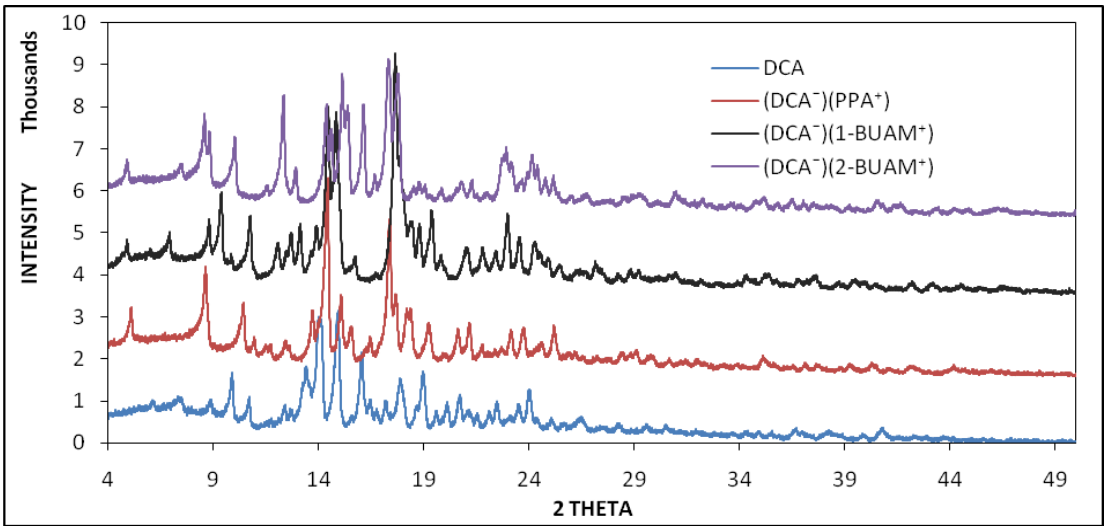

Figure 4.1.2: Powder pattern of DCA vs. salts

4.2 Thermal analysis

The powders were further analysed by DSC and TGA in order to determine the host-guest ratios. The results obtained are reported in **Table 4.2.1**.

Table 4.2.1: DSC and TG results of powders

Compound	**(DCA^-) (PPA^+)**	**(DCA^-) (1-$BUAM^+$)**	**(DCA^-) (2-$BUAM^+$)**	**(DCA^-) ($DIETAM^+$)**	**(DCA^-) ($DIBUAM^+$)**
H·G ratio	1:1	1:1	1:1	1:1	1:1
$Endo_1$ (T_{on}, K)	422.8	313.5	431.0	316.4	412.6
$Endo_2$ (T_{on}, K)	450.4	417.1	458.3	–	–
Experimental % mass loss	10.6*	15.2	15.4	13.4*	24.6
Theoretical % mass loss	13.1	15.7	15.7	15.7	24.8

* It was difficult to determine the experimental mass loss because the host compound decomposes before the guest is completely released. The host compound starts decomposing at 473 K.

The experimental mass losses obtained correspond to the theoretical mass losses with a host-guest ratio of 1:1 for all the compounds. However the stability of the compounds obtained differed. The TGA curves of **(DCA^-)($DIETAM^+$)** and **(DCA^-)(1-$BUAM^+$)** showed a gentle mass loss from 303 K whereas the other compounds were stable up to 373 K. DSC traces obtained are shown in **Figure 4.2.1**. **(DCA^-)(PPA^+)** and **(DCA^-)(2-$BUAM^+$)** curves show two endotherms that are very close and they can be assigned to the loss of the amines. A single endotherm at 412.6 K on the **(DCA^-)($DIBUAM^+$)** curve is assigned to the loss of the DIBUAM. The broad endotherm observed

on the **(DCA$^-$)(1-BUAM$^+$)** curve at 417.1 K was assigned to the loss of the amine. After 600 K the decomposition of the host was observed.

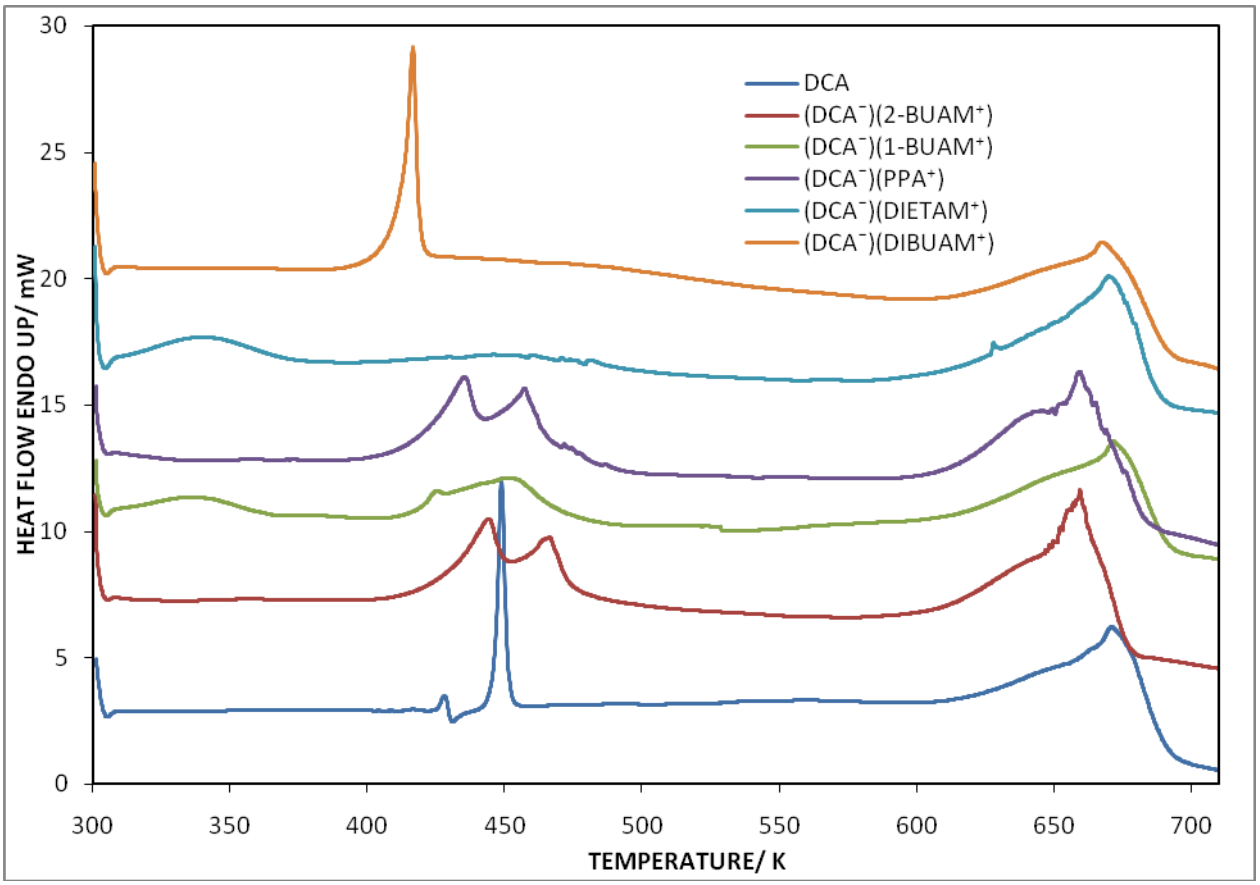

Figure 4.2.1: DSC results of DCA compared to resultant salts

4.3 Kinetics of absorption

Kinetics of absorption was performed on a simple analytical balance connected to a computer system with software that records mass gained as a function of time at 25°C. Weighed amounts of DCA were exposed to the vapours of *n*-propylamine and (*R,S*)-*sec*-butylamine. The vapour pressure of the amines was modified by addition of different quantities of water. DCA was found to be able to absorb a greater percentage of amines than expected stoichiometrically. We noted that the sample resulting from the exposure to the amine vapours was not a dry solid, but was wet. We surmised that the salt formed acted hygroscopically and kept on absorbing excess amine vapour. This was confirmed by the fact that the absorption curves were linear after the stoichiometric quantity of the amine had been absorbed to form the salt. Linear absorption curves are a character of zero order reactions, which, in our case depends on the surface area of the salt exposed to the amine vapours. The curves were therefore analysed up to the expected mass absorbed, in the molar ratio 1:1 (DCA: amine). The curves obtained for DCA and *n*-propylamine (PPA) are shown in **Figure 4.3.1**. The contracting area (R2) and contracting volume (R3) models were fitted to the

data; slopes and the correlation coefficients are reported in **Table 4.3.1**. A similar experiment was performed with DCA exposed to water only, and no absorption was recorded.

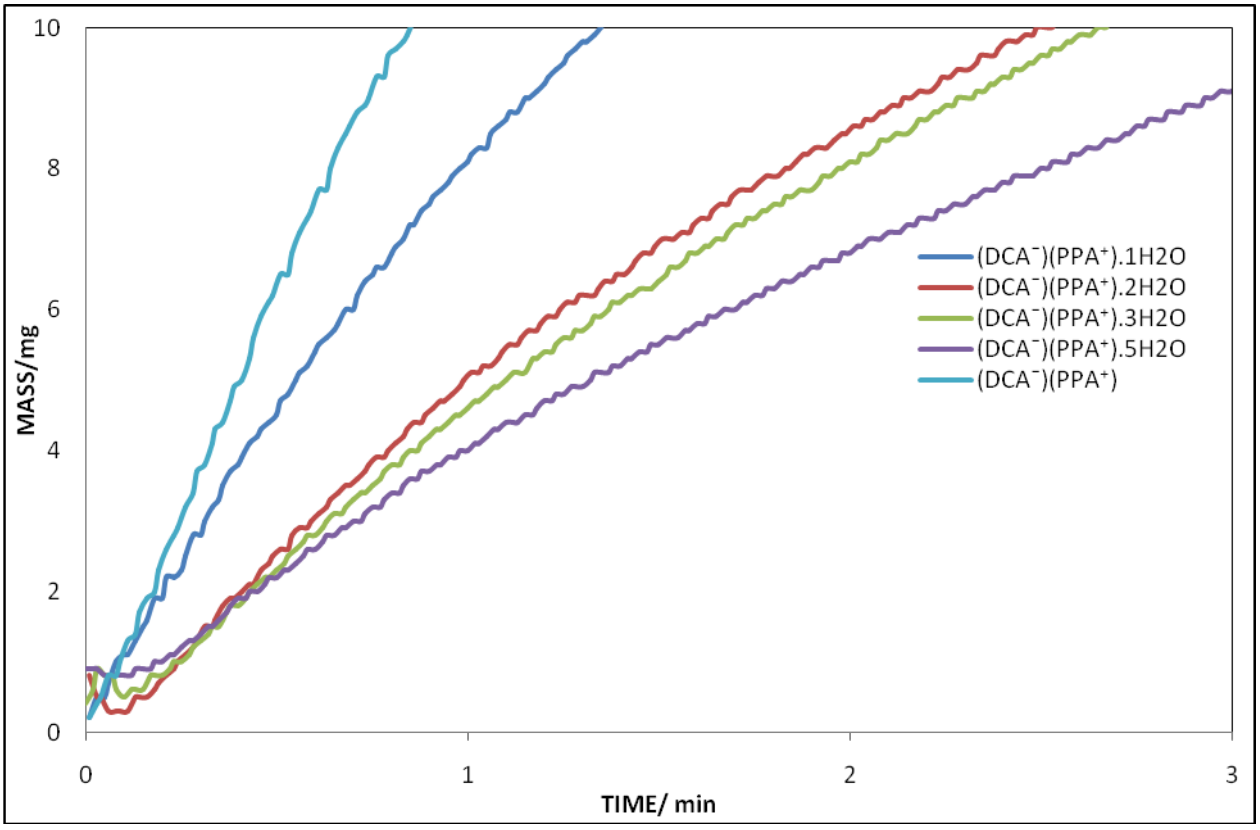

Figure 4.3.1: Kinetics of absorption curves for DCA and 1-propylamine (PPA)

Table 4.3.1: Kinetics of absorption results for DCA with PPA and DCA with 2-BUAM

	H_2O : amine	P_{AMINE} (mmHg)	Slope (R2)	R	Slope (R3)	R
DCA and PPA	0 :1	310.0	1.460	0.9914	1.153	0.9827
	1 :1	155.0	0.750	0.9984	0.479	0.9949
	2 :1	93.9	0.504	0.9966	0.485	0.9867
	3 :1	77.5	0.436	0.9904	0.464	0.9764
	5 :1	51.6	0.327	0.9979	0.259	0.9934
DCA and 2-BUAM	0 :1	178	0.519	0.9953	0.483	0.9847
	1 :1	89.0	0.217	0.9920	0.176	0.9790
	2 :1	53.4	0.183	0.9951	0.165	0.9881
	3 :1	44.5	0.164	0.9970	0.132	0.9884
	5 :1	29.7	0.086	0.9992	0.057	0.9977

The results obtained showed that the absorption mechanism fits a contracting area model rather than the contracting volume model. The vapour pressures of the mixtures were calculated according to **Figure 4.3.2**, assuming that the amine vapours behaves ideally. The vapour pressures (P_0) of 1-propylamine and (*R,S*)-*sec*-butylamine are 310 mmHg and 178 mmHg respectively at 298 K.

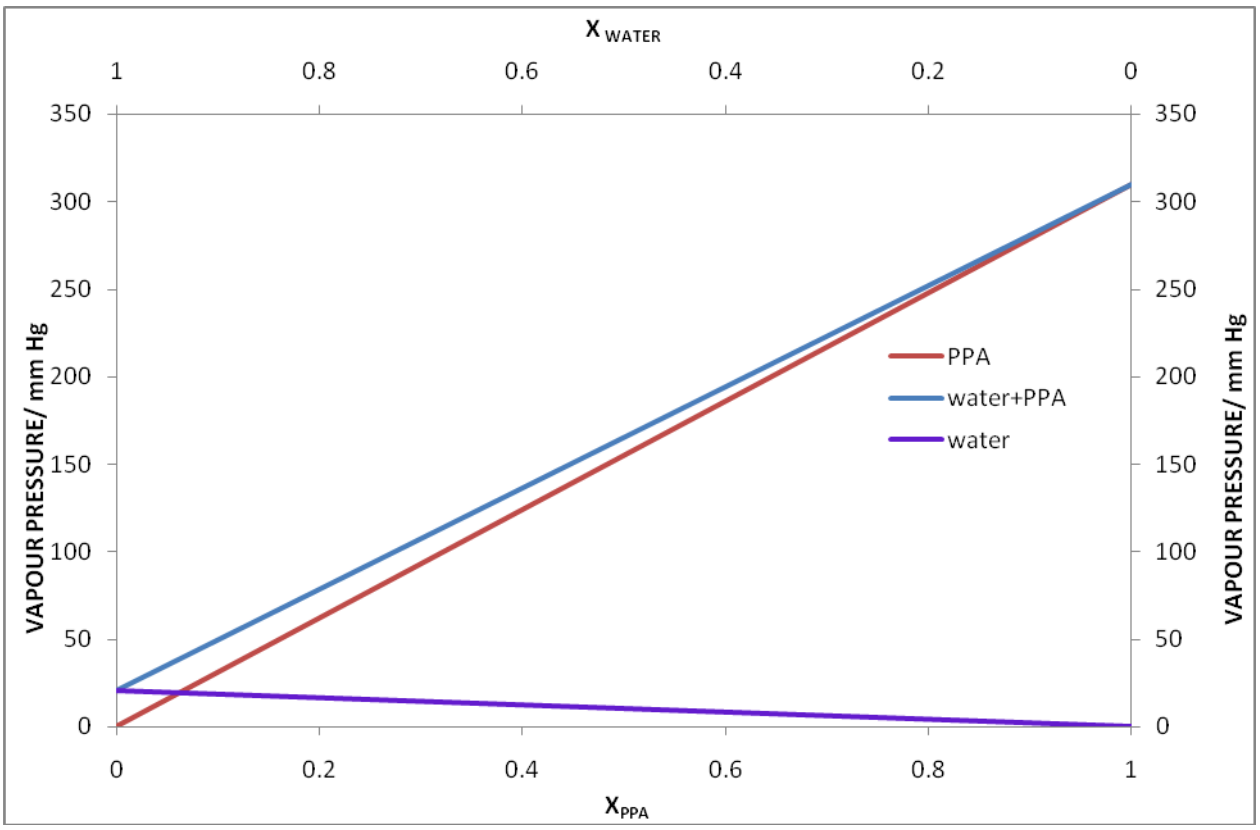

Figure 4.3.2: Vapour pressures of propylamine, water and mixtures, where X= mole fraction

The slopes of the curves obtained give k_{obs} at different partial pressures of the 1-propylamine and (*R,S*)-*sec*-butylamine. Therefore the rate of the reaction can be written as follows (Eq. 10)

$$\frac{d\alpha}{dt} = kP_{AMINE} f(\alpha) \qquad \text{(Eq. 10)}$$

where $kP_{AMINE} = k_{obs}$, (*k* is the rate constant in min^{-1}) and $f(\alpha) = \left[2(1-\alpha)^{1/2}\right]$ for contracting area (R2), $f(\alpha) = \left[3(1-\alpha)^{2/3}\right]$ for contracting volume (R3) and P_{AMINE} is the vapour pressure of the amine.

$P_{AMINE} = P_0 \times X_{AMINE}$ (Eq. 11)

The integral forms of f(α) are $\left[1-(1-\alpha)^{1/2}\right]$ for contracting area (R2) and $\left[1-(1-\alpha)^{1/3}\right]$ for contracting volume (R3).

k_{obs} decreases with the decreasing partial vapour pressures of the amines. The highest k_{obs} recorded for the absorption of 1-propylamine was 1.460 with a correlation coefficient (R) of 0.9914, α range 0.05 to 0.75 for R2. A minimum of 0.327 with R equals 0.9979 was reported in the α range 0.05 to 0.75.

In the experiment of *sec*-butylamine, k_{obs} values ranging from 0.519 to 0.086 were recorded for R2. The maximum and minimum have correlation coefficients of 0.9920 and 0.9992 respectively in the α range 0.05 to 0.90. The rate constant, *k,* is determined from a plot of vapour pressure vs. k_{obs} as shown in **Figure 4.3.3**.

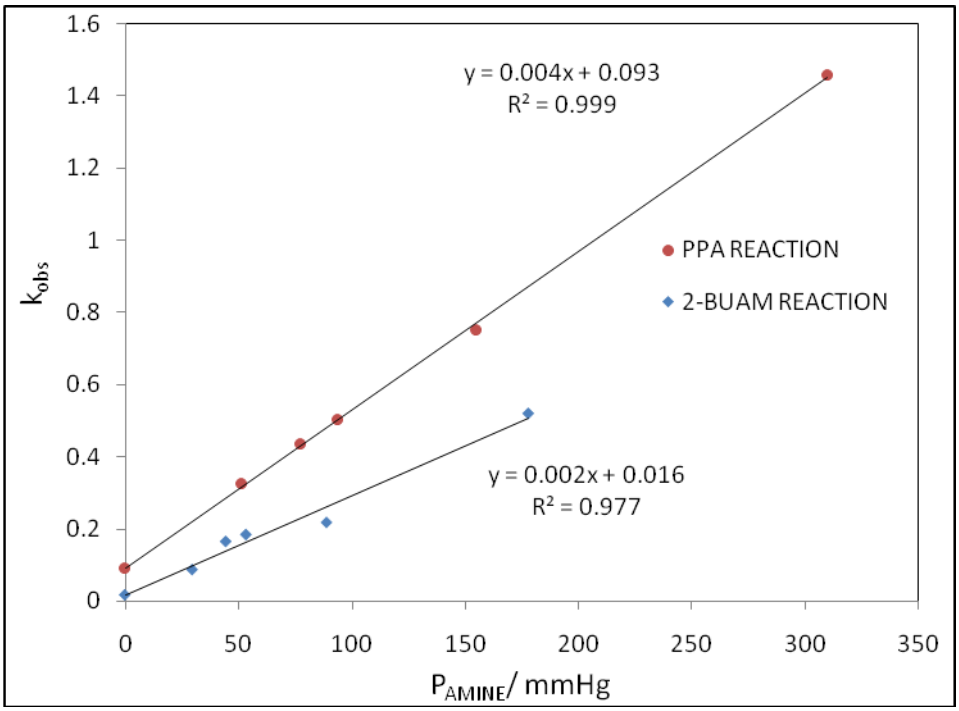

Figure 4.3.3: Plot of vapour pressure vs. k_{obs} for the reaction of DCA with 1-propylamine (PPA) and racemic *sec*-butylamine (2-BUAM)

The slope of the plot in **Figure 4.3.3** gives the rate constant (*k*) of the respective reactions. The rate constant for the reaction of DCA with PPA was found to 4.0×10^{-3} min^{-1} and 2.0×10^{-3} min^{-1} for DCA with 2-BUAM. The higher rate constant values obtained for the absorption of PPA can be explained by its higher vapour pressure.

4.4 Kinetics of desolvation

Kinetics of desolvation was performed on powders of mixtures of DCA and racemic *sec*-butylamine and DCA with di-*n*-butylamine. Non-isothermal methods were used where a series of TG analyses was carried out at different heating rates (2, 4, 10, 32 K min^{-1}). The resultant percentage mass loss vs. temperature curves were converted to the alpha (α) vs. time curves. Eq. 12 is used to calculate α.

$$\alpha = \frac{m_o - m_t}{m_o - m_f} \qquad \text{(Eq. 12)}$$

where m_o is the initial mass, m_t is the mass at time t and m_f is the final mass

The different decomposition stages were analyzed for each heating rate and plots of log heating rate vs. reciprocal temperature (1/T) were constructed for each decomposition stage. The activation energy was calculated from the slopes of these graphs. The results obtained are shown in **Figure 4.4.1** and **Figure 4.4.2** and in **Table 4.4.1**.

A B

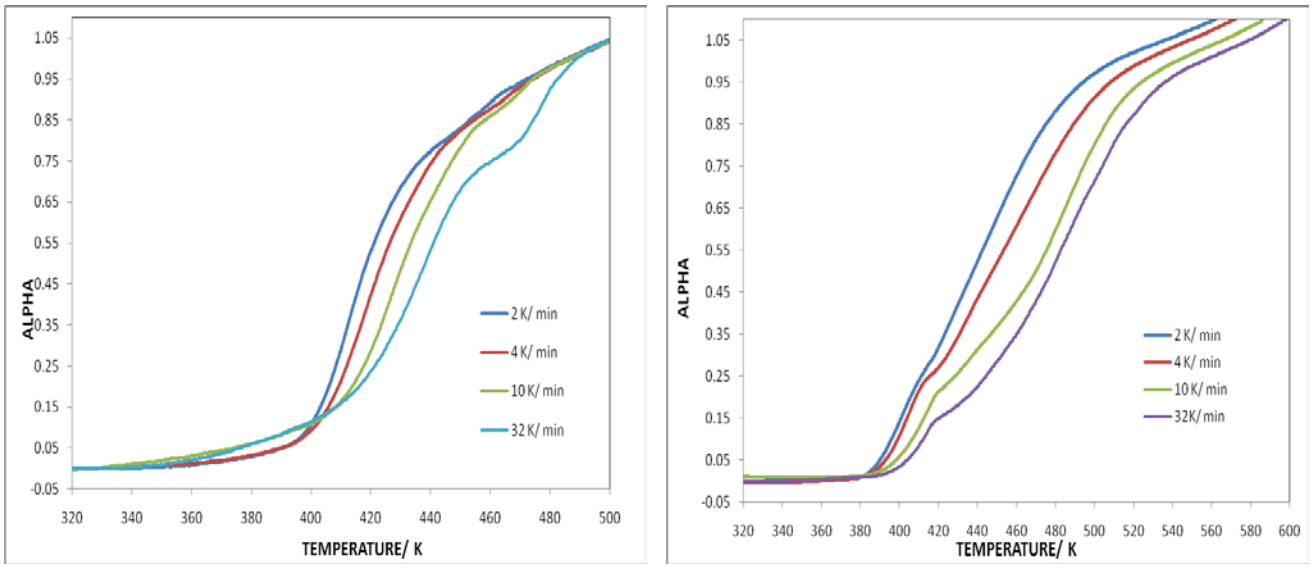

Figure 4.4.1: Alpha-time plots of **(DCA^-)($2\text{-}BUAM^+$)** (A) **and (DCA^-)($DIBUAM^+$)** (B)

A B

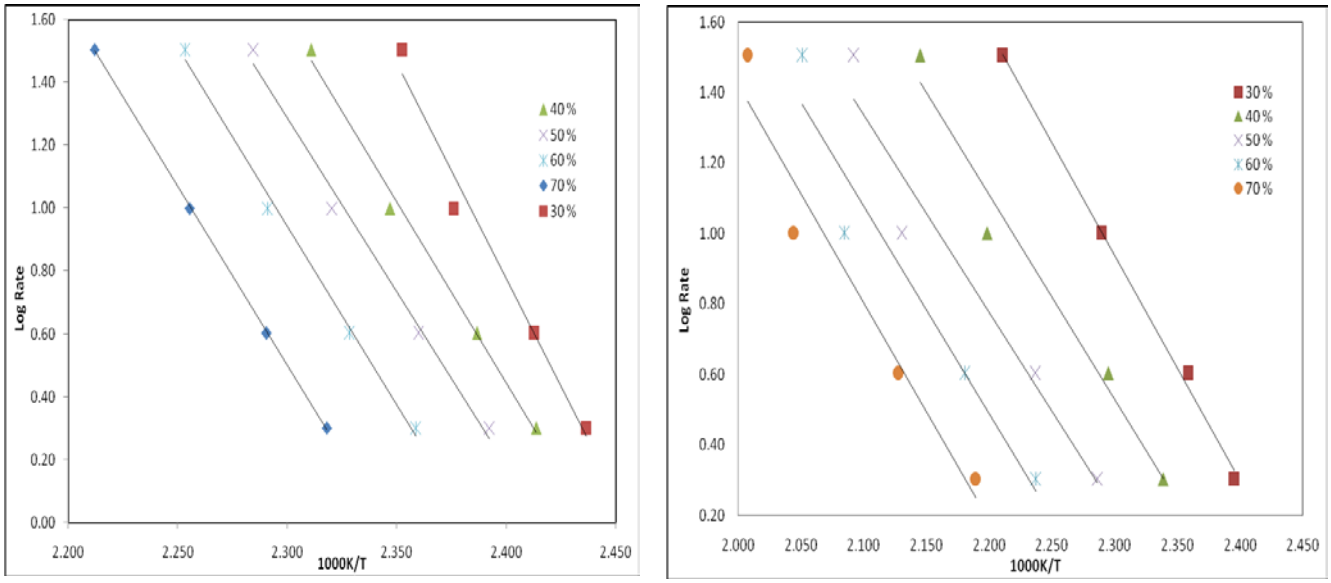

Figure 4.4.2: Kinetic plots for the decomposition of **(DCA^-)($2\text{-}BUAM^+$)** (A) and **(DCA^-)($DIBUAM^+$)** (B)

Activation energy (E_a) is calculated from the equation below, Eq. 13[2&3] in the α range 0.3 to 0.7.

$$\text{slope} = -0.457\frac{E_a}{R} \qquad \text{(Eq. 13)}$$

where *R* is the universal gas constant with value 8.314 J mol^{-1} K^{-1}.

Table 4.4.1: Kinetic data for **(DCA^-)(2-$BUAM^+$)** and **(DCA^-)($DIBUAM^+$)**

Compound	Reaction stage (%)	Slope	Ea (kJ mol^{-1})
(DCA^-)(2-$BUAM^+$)	30	-13.8	250.1
	40	-11.5	209.4
	50	-11.1	201.6
	60	-11.4	206.8
	70	-11.4	206.7
(DCA^-)($DIBUAM^+$)	30	-6.4	116.4
	40	-5.8	105.7
	50	-5.6	101.9
	60	-5.9	107.2
	70	-6.2	112.4

According to Coleman[4], E_a of desolvation for the guests that reside in channels is ~ 60 kJ mol^{-1} and ~ 150 kJ mol^{-1} for guest ions trapped in cavities. The activation energy for **(DCA^-)(2-$BUAM^+$)** is slightly higher than the reported E_a value ~ 150 kJ mol^{-1} and E_a for **(DCA^-)($DIBUAM^+$)** falls in the range of the expected values for inclusion compounds. The crystal structure analyses are summarised in the latter section.

4.5 Thermal analysis of crystals

Crystals were obtained by dissolving salts obtained in the previous experiments in acetone. The solutions were allowed to evaporate slowly at room temperature. Crystals of **(2DCA^-)(2PPA^+)•5H_2O** were obtained from undried acetone. In another experiment, acetone was dried overnight using molecular sieves and used to grow crystals of **(DCA^-)(PPA^+)•ACE**. Thermal analysis results obtained are reported in **Table 4.5.1**.

Table 4.5.1: The thermal analysis results of DCA & PPA and DCA & DIBUAM

Compound	**$(DCA^-)(PPA^+)$•ACE**	**$(2DCA^-)(2PPA^+)$•$5H_2O$**	**$(DCA^-)(DIBUAM^+)$**
H·G ratio	1:1:1	2:2:5	1:1
$Endo_1$ (T_{on}, K)	–	343.3	–
$Endo_2$ (T_{on}, K)	–	381.8	–
$Endo_3$ (T_{on}, K)	413.2	416.9	401.5
1st Exp. % mass loss	11.9	7.6	25.7
Theoretical % mass loss	13.1	9.1	24.8
2nd Exp. % mass loss	–	11.2	–
Theoretical % mass loss	–	13.1	–

Exp. = experimental

The mass loss obtained for **$(DCA^-)(PPA^+)$•ACE** correspond to the loss of propylamine only, this could be because acetone evaporated during sample preparation. Nuclear magnetic resonance (NMR) analysis of the residue indicated that no PPA was present after heating up to K. As for **$(2DCA^-)(2PPA^+)$•$5H_2O$** the first mass loss is assigned to the loss of water followed by the loss of 2 PPA molecules. The initial mass loss (TG) for **$(DCA^-)(DIBUAM^+)$** is due to the loss of the amine. The sharp endotherm at 401.5 K is due to the guest loss. For all the compounds, an endotherm for the decomposition of the host was observed after 600 K. Thermal analysis curves of the propylamine salts are shown in **Figure 4.5.1** and TGA and DSC results for **$(DCA^-)(DIBUAM^+)$** are represented in **Figure 4.5.2**.

A B

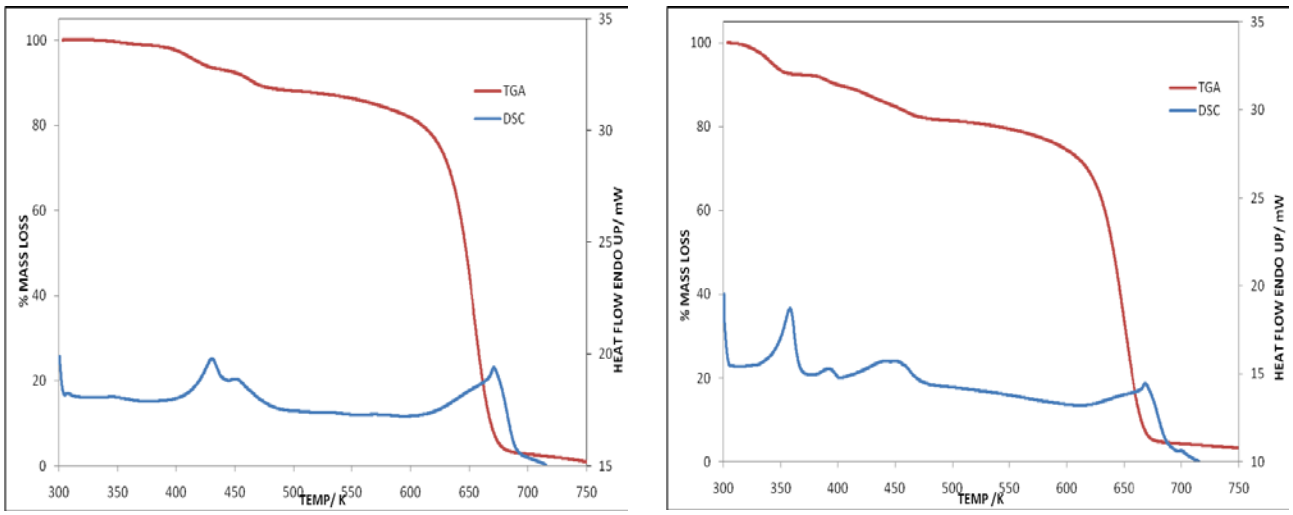

Figure 4.5.1: Thermal analysis results for DCA and PPA salts, **$(DCA^-)(PPA^+)$•ACE** (A) and **$(2DCA^-)(2PPA^+)$•$5H_2O$** (B)

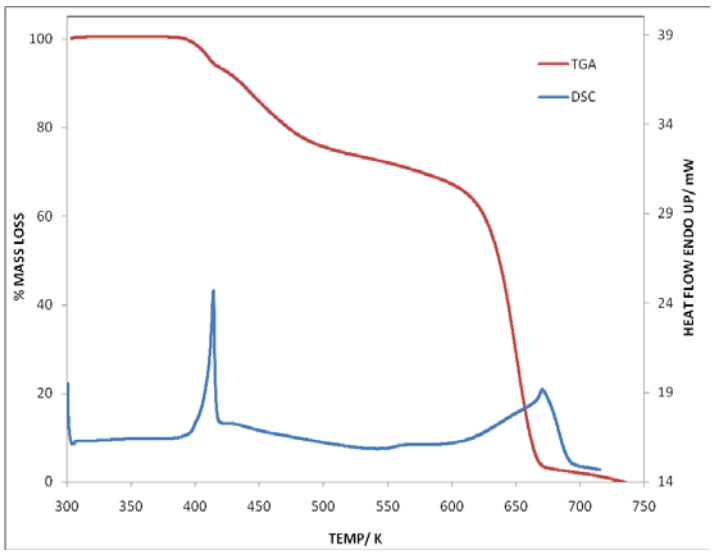

Figure 4.5.2: Thermal analysis results for **(DCA^-)($DIBUAM^+$)**

Crystals of **(DCA^-)(PPA^+)•ACE** and **(2DCA^-)(2PPA^+)•5H_2O** were heated to 473 K and the residue was analysed by proton nuclear magnetic resonance (HNMR) spectroscopy to determine the presence of the amine after heating. The results showed that 1-propylamine was not detected in the residue.

4.6 Structural analysis

Table 4.6.1: Crystal data table of DCA with achiral amines

Compound	**$(DCA^-)(PPA^+)$•ACE**	**$(2DCA^-)(2PPA^+)$•$5H_2O$**	**$(DCA^-)(DIBUAM^+)$**
Molecular Formula	$(C_{24}H_{39}O_4^-)(C_3H_{10}N^+)$•$C_3H_6O$	$(2C_{24}H_{39}O_4^-)(2C_3H_{10}N^+)$•$5H_2O$	$(C_{24}H_{39}O_4^-)(C_8H_{20}N^+)$
Molecular Mass ($gmol^{-1}$)	509.8	993.6	521.9
Data collection temp. (K)	173(2)	173(2)	173(2)
Crystal system	Monoclinic	Triclinic	Monoclinic
Space group	$P2_1$	P1	$P2_1$
a (Å)	11.0361 (11)	7.7287 (6)	14.0430 (3)
b (Å)	7.7101 (7)	11.5210 (9)	7.8258 (16)
c (Å)	17.9654 (18)	15.5589 (13)	14.0550 (3)
α (°)	90.00	81.143 (2)	90.00
β (°)	105.750 (2)	79.051 (2)	100.94 (3)
γ (°)	90.00	89.485 (2)	90.00
Volume ($Å^3$)	1471.3 (2)	1430.03 (19)	1516.5 (6)
Z	2	2	2
D_c, Calculated density ($g\ cm^{-3}$)	1.151	1.186	1.143
Final R indices	R_1= 0.0531	R_1= 0.0516	R_1= 0.0443
[I>2sigma(I)]	wR_2=0.1285	wR_2=0.1339	wR_2=0.1007
R indices (all data)	R_1= 0.0740	R_1= 0.0602	R_1= 0.0704
	wR_2=0.1407	wR_2=0.1414	wR_2=0.1162
Largest diff. peak and hole ($eÅ^{-3}$)	-0.302; 0.648	-0.338; 0.556	-0.212; 0.264

$(DCA^-)(PPA^+)$•ACE and **$(DCA^-)(DIBUAM^+)$** were found to crystallize in the monoclinic crystal system; space group $P2_1$. **$(2DCA^-)(2PPA^+)$•$5H_2O$** crystallized in the triclinic crystal system, space group P1. Z = 2 was obtained for all the structures. All compounds gave host-guest ratios of 1: 1. A single molecule of acetone is also trapped in **$(DCA^-)(PPA^+)$•ACE**. The propylamine in the structure of **$(2DCA^-)(2PPA^+)$•$5H_2O$** is disordered over two positions. The structures of the respective compounds are shown in **Figure 4.6.1**. For all the structures there is a proton transfer from DCA to the guest amines.

A

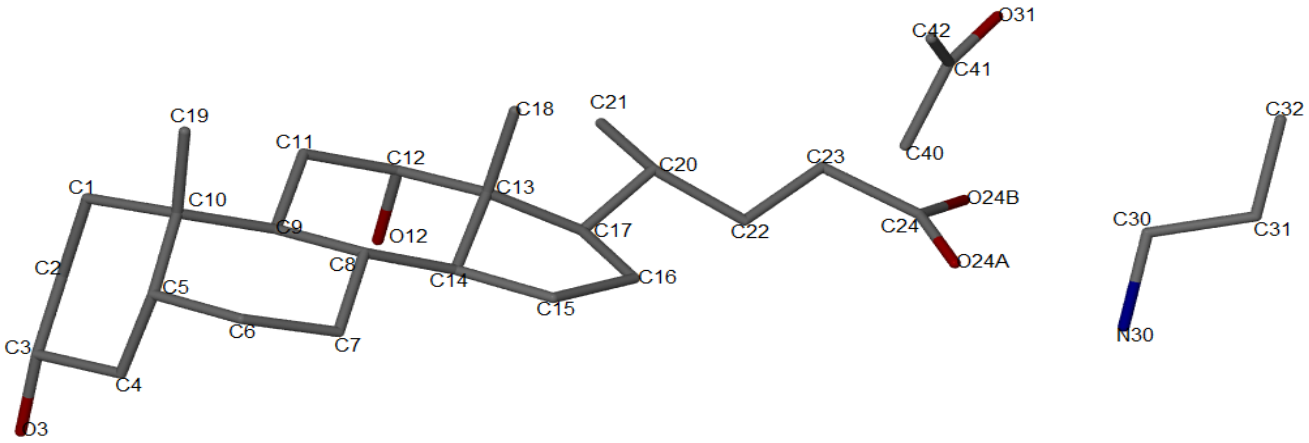

B

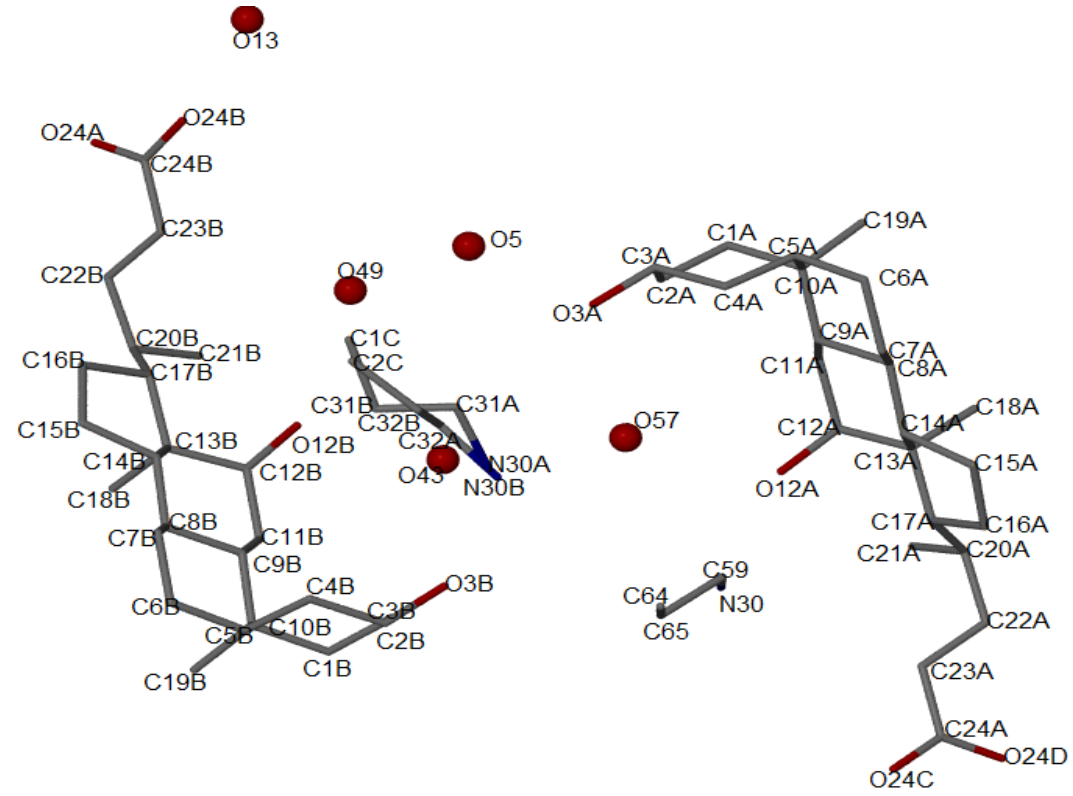

C

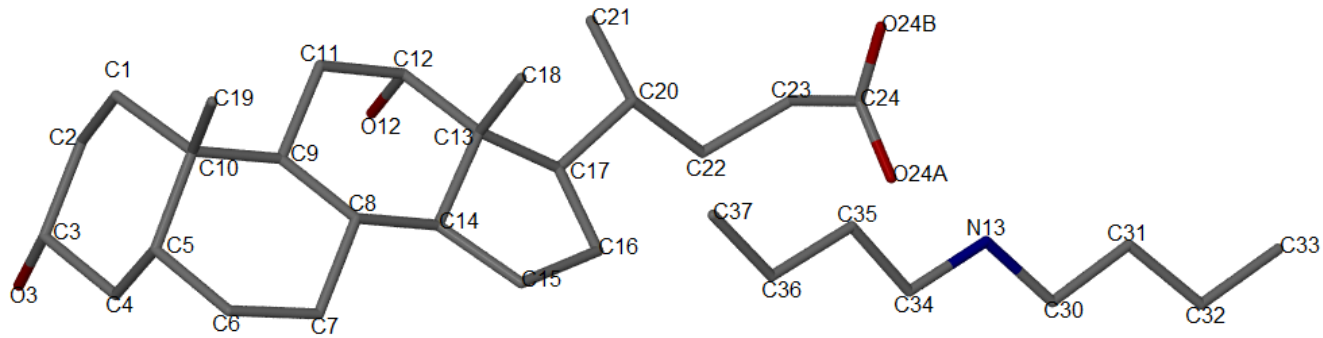

Figure 4.6.1: Formula units for the structures of **(DCA^-)(PPA^+)•ACE** (A), **(2DCA^-)(2PPA^+)•5H_2O** (B) and **(DCA^-)($DIBUAM^+$)** (C)

Hydrogen bonding is the main form of interaction in all the structures. See **Figure 4.6.2.**

A

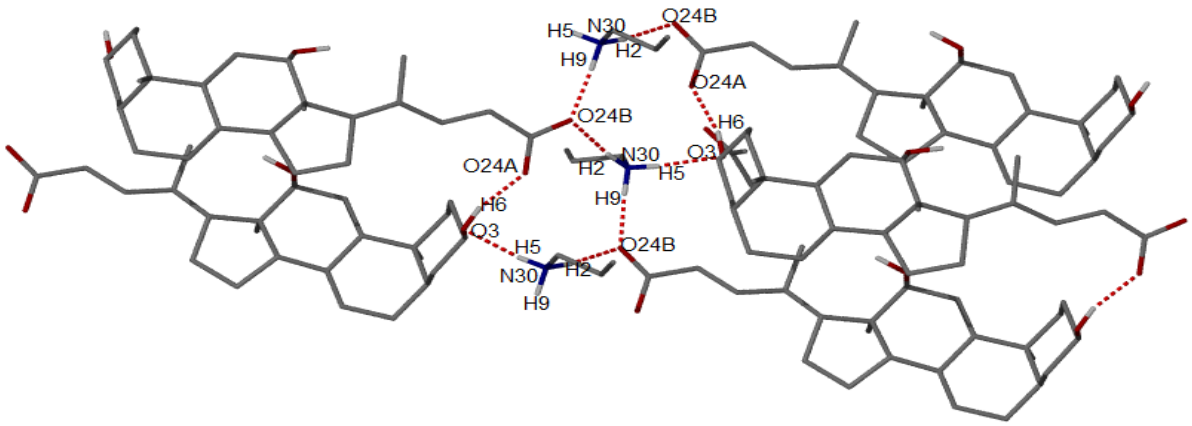

B

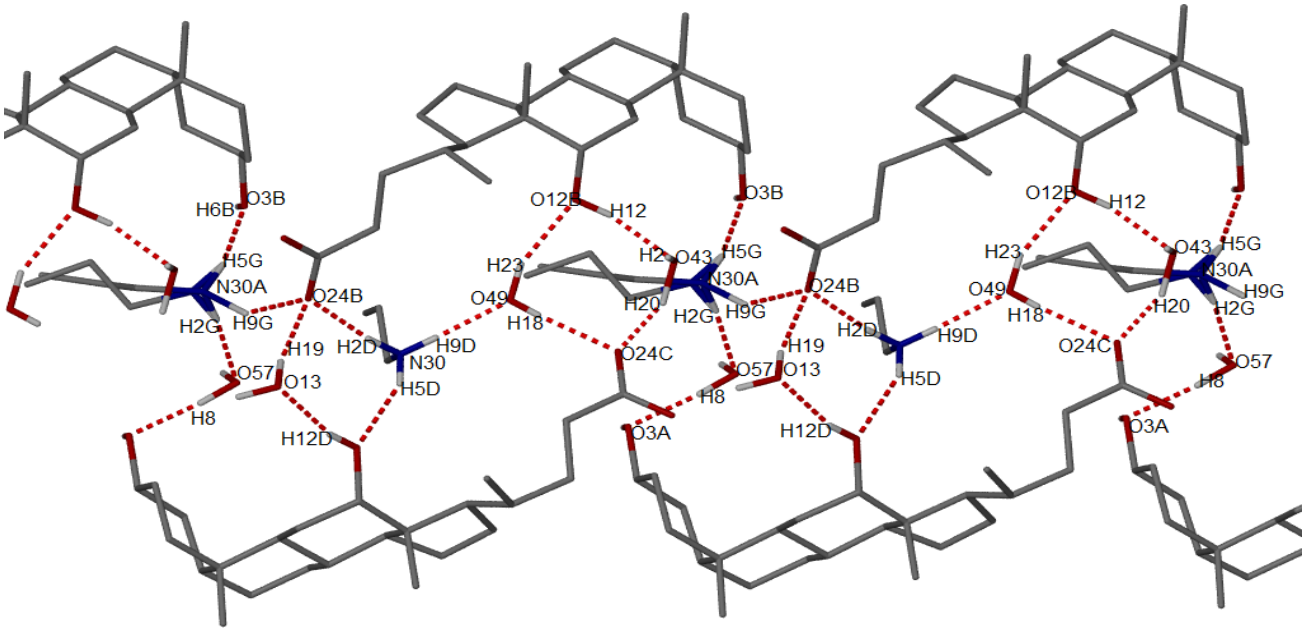

C

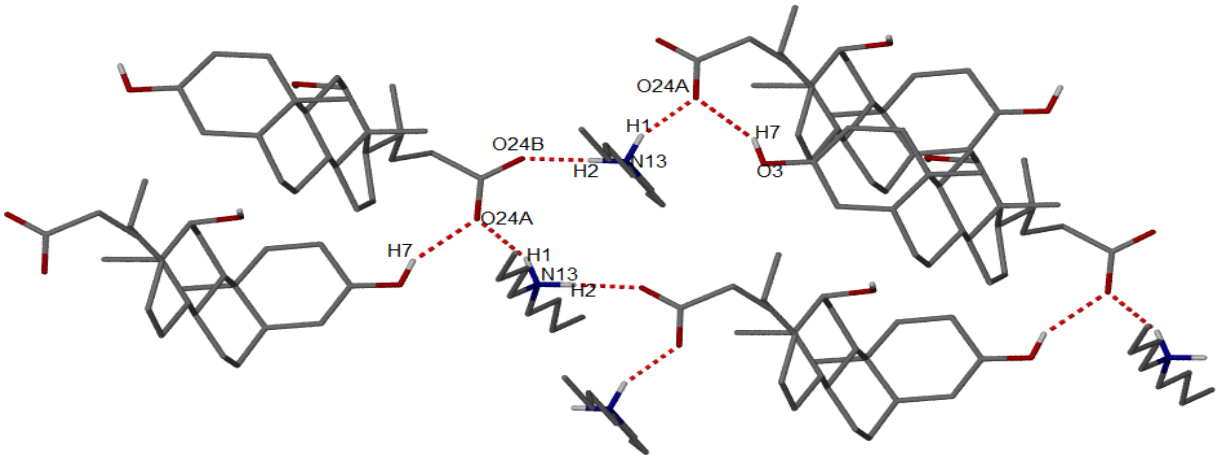

Figure 4.6.2: Hydrogen bonding diagram for **(DCA^-)(PPA^+)•ACE** (A), **(2DCA^-)(2PPA^+)•5H_2O** (B) and **(DCA^-)($DIBUAM^+$)** (C)

Figure 4.6.2 (A) shows hydrogen bonding observed in **(DCA^-)(PPA^+)•ACE**. All hydrogen atoms around the protonated N30 are involved in hydrogen bonds. A protonated N atom of the amine forms hydrogen bonds with O atoms (O24B) of two carboxylate moieties and O3 of the hydroxyl group on the next DCA^- ion. A three centre hydrogen bond is formed at the oxygen of the carboxylate (O24B). The O3-H6 of the anion acts as a hydrogen bond donor to the oxygen on the carboxylate (O24A). The hydrogen bonding can be described with the graph set $N_1 = R_5^4(12)$. There are no hydrogen bonds observed around the acetone molecule. Weak C-H···O hydrogen bonds, approximately 3.622 Å to neighbouring PPA ions are observed. The acetone molecule is not hydrogen bonded and has been omitted for clarity.

Hydrogen bonding in **(2DCA^-)(2PPA^+)•5H_2O** is shown in **Figure 4.6.2** (B). Several hydrogen bonds are formed in the structure; this is due to the large number of water molecules trapped in the crystal system. The hydrogen atoms around the protonated nitrogen atoms are involved in hydrogen bonding. The nitrogen atoms hydrogen bond to the OH groups of the anion, water molecules and O24B of the carboxylate moiety. A four-centre hydrogen bond is observed at O24B. This oxygen acts as a hydrogen bond acceptor for the two nitrogen atoms and a water molecule. The hydrogen bonds O3B-H6B···O24A and O3A-H6A···O24D connect the layers formed. A three-centre bond occurs at H9G of the disordered cation.

A three centre bond is formed at O24A of the carboxylate in the structure of **(DCA^-)($DIBUAM^+$)** as shown in **Figure 4.6.2** (C). The oxygen atom forms hydrogen bonds with the O3-H7 of the closest anion and N13-H1 of the cation. N13-H2 also forms a hydrogen bond with O24B of the carboxylate. Hydrogen bonding parameters for the respective structures are reported in **Table 4.6.2**.

Table 4.6.2: Hydrogen parameters of different structures

COMPOUND	D-H···A	D···A (Å)	D-H (Å)	H···A (Å)	D-H···A (º)
(DCA^-)(PPA^+)•ACE	N30-H2···O24B	2.759 (3)	0.90 (1)	1.87 (1)	174 (3)
	N30-H2···O24A	3.291 (3)	0.90 (1)	2.63 (1)	131 (1)
	N30-H5···O3[a]	2.876 (3)	0.95 (3)	1.93 (3)	171 (3)
	N30-H9···O24B[b]	2.731 (3)	0.91 (3)	1.83 (3)	171 (3)
	O3-H6···O24A[c]	2.627 (2)	0.74 (4)	1.90 (4)	169 (4)
a = x, y, -1+z; *b* = 2-x,½+y,-z; *c* = 2-x,-½+y,1-z					
($2DCA^-$)($2PPA^+$)•$5H_2O$	N30-H5D···O12A	2.833 (3)	0.84 (4)	2.07 (4)	155 (4)
	N30-H9D···O49[a]	2.833 (4)	0.89 (4)	1.93 (4)	176 (4)
	O12B-H12···O43	2.736 (3)	0.87 (5)	1.91 (5)	167 (4)
	O49-H18···O24C[b]	2.759 (3)	0.73 (5)	2.02 (5)	175 (5)
	O49-H23···O12B	2.957 (3)	0.94 (6)	2.07 (5)	157 (4)
	O13-H12C···O24D[c]	2.665 (3)	0.94 (7)	1.79 (7)	164 (6)
	N30-H2D···O24B[a]	2.743 (3)	0.88 (1)	1.85 (1)	173 (3)
	O3B-H6B···O24A[d]	2.698 (3)	0.73 (4)	1.96 (4)	168 (4)
	O57- H8···O3A	2.813 (3)	0.98 (6)	1.86 (6)	178 (5)
	O57- H13···O13[d]	2.832 (4)	0.86 (7)	1.99 (7)	162 (6)
	O3A-H6A···O24D[e]	2.692 (3)	1.08 (5)	1.69 (6)	146 (5)
	O43-H20···O24C[b]	2.657 (3)	1.23 (7)	1.63 (7)	134 (5)
	N30A-H5G···O3B	2.809 (8)	0.99 (5)	1.84 (5)	171 (4)
	N30A-H2G···O57	2.787 (9)	0.88 (5)	1.91 (5)	176 (4)
	O13-H19···O24B	2.773 (3)	0.82 (9)	1.91 (9)	167 (8)
	O12A-H12D···O13[a]	2.736 (3)	0.80 (4)	1.94 (4)	166 (3)
	N30A-H9G···O43	2.909 (9)	1.43 (12)	2.13 (6)	135 (5)
	N30A-H9G···O24B[a]	3.088 (9)	1.43 (12)	2.34 (6)	132 (5)
a = x, 1+y, z; *b* = x, -1+y, z; *c* = x, -2+y, z; *d* = -1+x, 1+y, z; *e* = -1+x, -1+y, z					
(DCA^-)($DIBUAM^+$)	N13-H1···O24A	2.672 (2)	0.88 (1)	1.85 (1)	156 (2)
	N13-H2···O24B[a]	2.706 (2)	0.93 (2)	1.78 (2)	174 (2)
	O3-H7···O24A[b]	2.852 (2)	0.81 (3)	2.13 (3)	150 (2)
a = 1-x,-½+y,2-z; *b* = -x,½+y,1-z;					

Unit cells and packing diagrams of the respective structures are shown in **Figure 4.6.4**. **Figure 4.6.4** (A) shows the view down [010] of **(DCA^-)(PPA^+)•ACE** and **Figure 4.6.4** (B) is the packing diagram of the host shown in van der Waals radii viewed down [010] with the propylammonium and acetone omitted. The small chain of bile acids is regarded as the tail and the opposite OH end is the head as shown in **Figure 4.6.3**.[5]

Figure 4.6.3: Representation of the head and tail of bile acids

The host ions arranged in bilayers, anti-parallel (head-to-tail) on the hydrophilic faces forming channels. The acetone and cations reside in channels formed down [010].

A

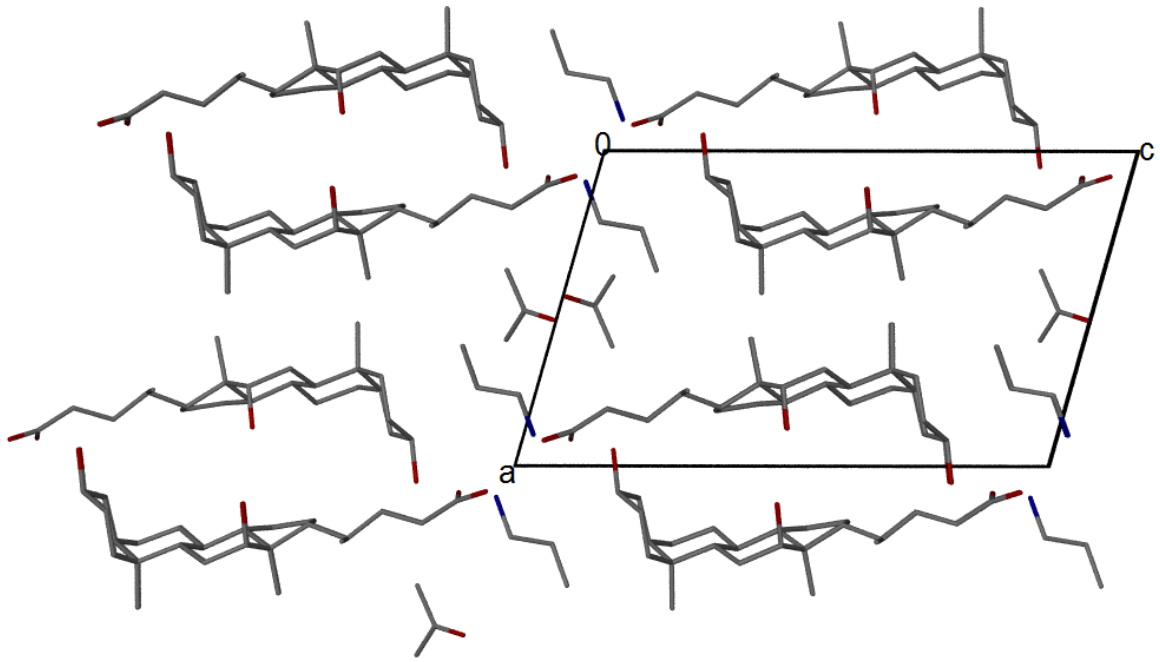

B

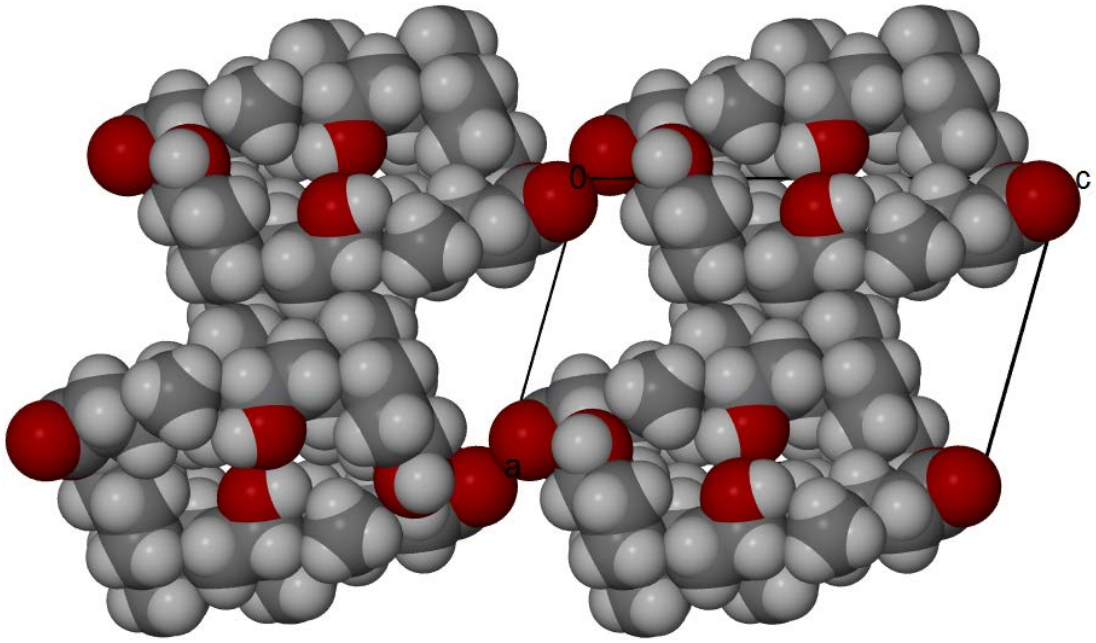

Figure 4.6.4: Packing diagram (A) and channels (B) of **(DCA^-)(PPA^+)•ACE** viewed down [010]. The guests are omitted and the host ions are shown in van der Waals radii.

The packing diagrams for **(2DCA^-)(2PPA^+)•5H_2O** are represented in **Figure 4.6.5**.

A

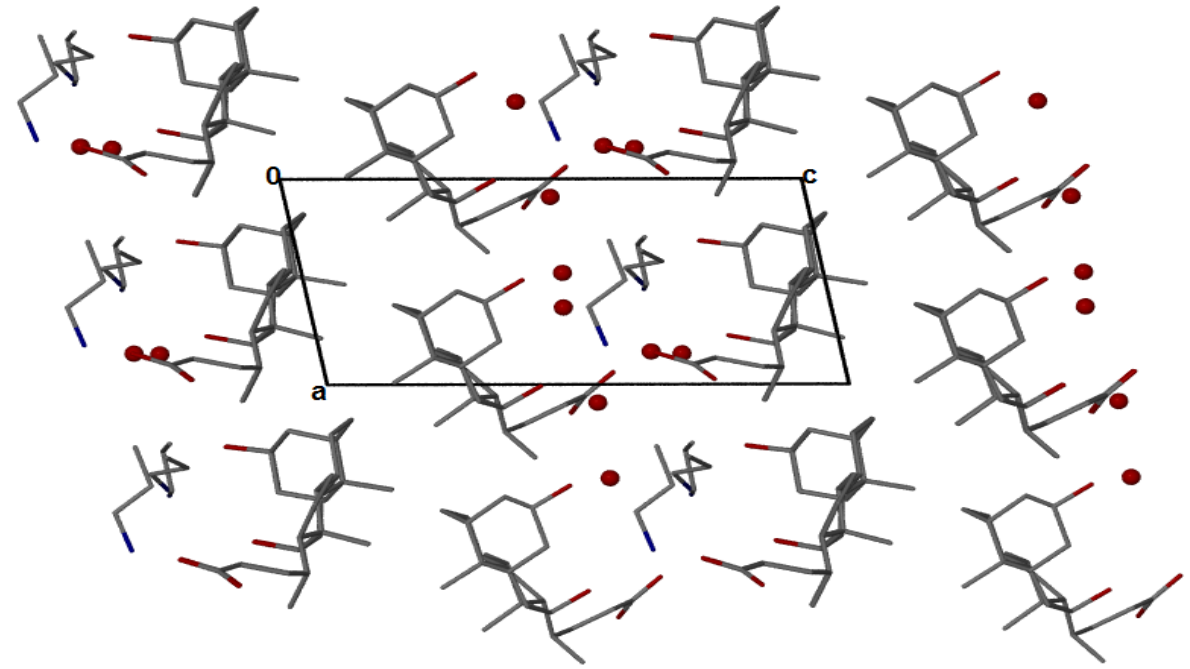

B

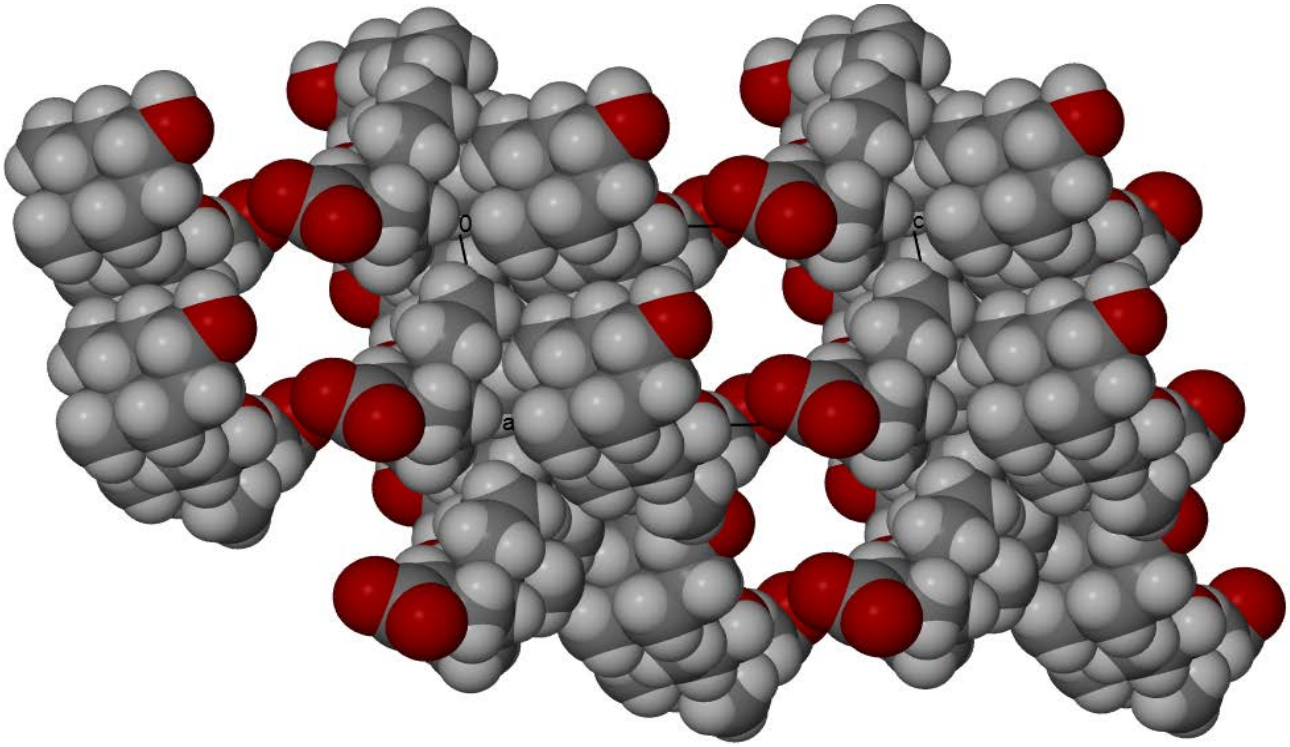

Figure 4.6.5: Packing diagram down [010] of **(2DCA$^-$)(2PPA$^+$)•5H$_2$O** (A) and channels down [010] (B) with the guest omitted and the host viewed in van der Waals radii

The host ions arrange in parallel bi-layers with their hydrophobic faces pointing towards each other. The guest and the water molecules reside in between the hydrophilic faces as represented in **Figure 4.6.5** (A). The channels formed down [010] are shown in **Figure 4.6.5** (B).

Figure 4.6.6 displays the packing diagram (A) and the packing of the host ions in **(DCA$^-$)(DIBUAM$^+$)** (B). The packing of the host is similar to the previous structures in that the host ions arrange in double layers, anti-parallel on hydrophilic faces. They arrange such that the carboxylate and hydroxyl head moieties are close to the N atom of the cation for hydrogen bonding. The guest ions lie in pairs on the lipophilic faces of the host as presented in **Figure 4.6.6** (A). The unit cell contains two formula units. The guest ions lie in the [001] plane. A space filling diagram is shown in **Figure 4.6.6** (B) with the guests omitted. The open structure of (DCA$^-$)(DIBUAM$^+$) is responsible for the low activation energies reported in the kinetics of desolvation.

A

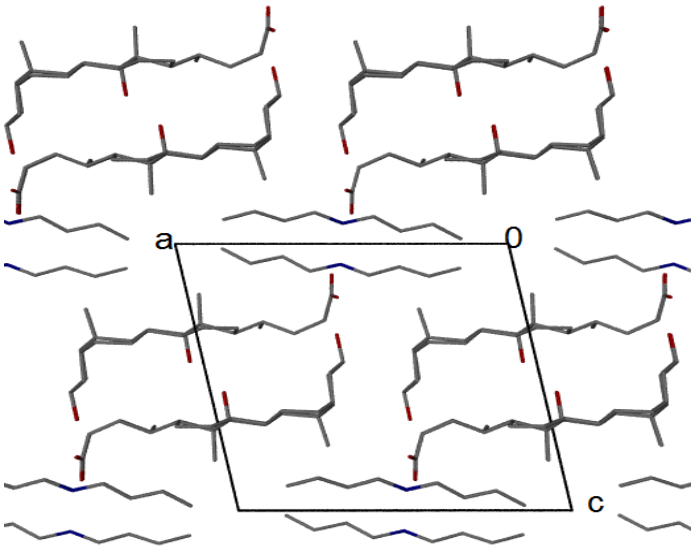

B

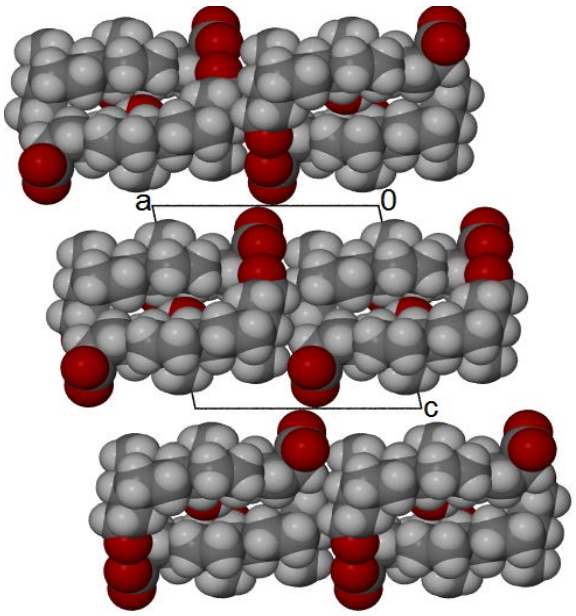

Figure 4.6.6: Packing diagram viewed down [010] for **(DCA$^-$)(DIBUAM$^+$)** (A) and space filling diagram down [010] with the host anions shown in van der Waals radii, guest omitted (B)

REFERENCES

[1]Cambridge Structural Database (CSD), Version 5.32 (November 2010), http://ccdc.cam.ac.uk.

[2] Flynn, J. H. & Wall, L. A. (1966), A Quick, Direct Method for the Determination of Activation Energy from Thermogravimetric Data, *Journal of Polymer Science, Polymer Letters*, Vol.4: 323-328.

[3] Ozawa, T. (1965), A New Method of Analyzing Thermogravimetric Data, *Bull. Chem. Soc. Jpn*. Vol. 38: 1881-1886.

[4]Coleman, A. W. (1998), Molecular recognition and inclusion, Kluwer Academics Publishers, The Netherlands.

[5]Miyata, M., Sada, K. & Yoswathananont, N. (2004), Deoxycholic acid, cholic and apocholic acids, *Encyclopedia of Supramolecular Chemistry*, Ed: Atwood, J. L. & Steed, J. W., Vol. 1:441-451.

CHAPTER 5

DCA AND CHIRAL *sec*-BUTYLAMINE COMPOUNDS

The salt of (+)-deoxycholic acid (DCA) with (*R*)-(-)-*sec*-butylamine (*R*-BUAM), **(DCA$^-$)(*R*-BUAM$^+$)** was obtained by dissolving the host in a minimum amount of racemic *sec*-butylamine while **(DCA$^-$)(*S*-BUAM$^+$)** was obtained by dissolving the host in a minimum amount of (*S*)-(+)-*sec*-butylamine (*S*-BUAM). The solutions were left to crystallize at room temperature. Thermal and structural analyses of the crystals were performed. Thermal analysis results are reported in **Table 5.1.1** and **Figure 5.1.1**.

5.1 Thermal analysis

Table 5.1.1 shows a record of the mass losses and endotherms obtained from thermal analyses of the resultant crystals.

Table 5.1.1: Thermal analysis results for inclusion compounds of DCA with *sec*-butylamine

Compound	**(DCA$^-$)(*R*-BUAM$^+$)**	**(DCA$^-$)(*S*-BUAM$^+$)**
H:G ratio	1:1	1:1
$Endo_1$ (T_{on}, K)	341.6	–
$Endo_2$ (T_{on}, K)	406.2	395.4
$Endo_2$ ranges (K)	406.2- 477.5	395.4- 508.8
1st Experimental % mass loss	7.0	–
Theoretical % mass loss	–	–
2nd Experimental % mass loss	15.7	15.3
Theoretical % mass loss	15.7	15.7

The diagrams below show the DCA and TGA curves for **(DCA$^-$)(*R*-BUAM$^+$)** and **(DCA$^-$)(*S*-BUAM$^+$)**

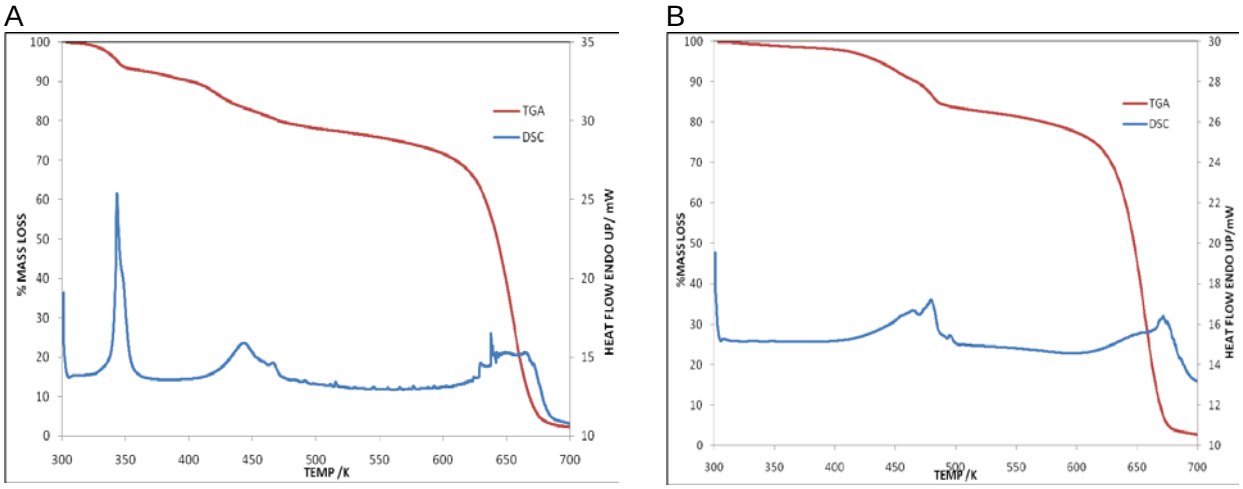

Figure 5.1.1: Thermal analysis curves of **(DCA$^-$)(*R*-BUAM$^+$)** (A) and **DCA$^-$•*S*-BUAM$^+$** (B)

The first endotherm and the first mass loss that occurs at 340 K on the curve of **(DCA$^-$)(*R*-BUAM$^+$)** is assigned to the loss of surface solvent. The crystals were sticky so drying them completely was a challenge. The second mass loss and endotherm can be correlated to loss of (*R*)-BUAM trapped in the crystal structure and concomitant melt. Thermal analysis of **(DCA$^-$)(*S*-BUAM$^+$)** showed a single endotherm and a one step mass loss is correlated to the loss of (*S*)-BUAM. The experimental mass losses obtained are close to the theoretical values and correspond to those obtained from the powder experiments in Chapter 4. Decomposition of the host occurs after 600 K.

We note that the onset temperature for the *R*-BUAM compound is 406.2 K which is 11 K higher than that of the *S*-BUAM compound. This is a measure of the higher stability of the former compound and serves as an indication of why it is selected by DCA from the racemic modification.

5.2 Structural analysis

Table 5.2.1: Crystal data table of DCA with *sec*-butylamine

Compound	**(DCA$^-$)(*R*-BUAM$^+$)**	**(DCA$^-$)(*S*-BUAM$^+$)**
Molecular Formula	$(C_{24}H_{39}O_4^-)(C_4H_{12}N^+)$	$(C_{24}H_{39}O_4^-)(C_4H_{12}N^+)$
Molecular Mass (gmol^{-1})	465.8	465.8
Data collection temp. (K)	173(2)	173(2)
Crystal system	Monoclinic	Monoclinic
Space group	*C*2	$P2_1$
a (Å)	23.5110 (4)	10.1547 (11)
b (Å)	7.6318 (12)	7.5678 (8)
c (Å)	18.1960 (3)	17.6450 (2)
α (°)	90.00	90.00
β (°)	123.029 (2)	90.915 (3)
γ (°)	90.00	90.00
Volume (Å^3)	2737.4 (7)	1355.8 (3)
Z	4	2
D_c, Calculated density (g cm^{-3})	1.128	1.141
Final R indices [I>2sigma(I)]	R_1= 0.0514	R_1= 0.0464
	wR_2= 0.1155	wR_2= 0.1102
R indices (all data)	R_1= 0.0793	R_1= 0.0585
	wR_2= 0.1302	wR_2= 0.1181
Largest diff. peak and hole (eÅ^{-3})	-0.235; 0.372	-0.174; 0.268

The structure of **(DCA$^-$)(*R*-BUAM$^+$)** was obtained by resolving the racemic mixture of *sec*-butylamine with (+)-deoxycholic acid. The compound crystallized in the monoclinic crystal system, space group *C*2 with Z = 4**. (DCA$^-$)(*S*-BUAM$^+$)** was crystallised directly from (*S)-(+)sec*-butylamine. It crystallized in the monoclinic crystal system, space group $P2_1$ with the Z = 2. The structures of the formula units are represented in **Figure 5.2.1**.

A

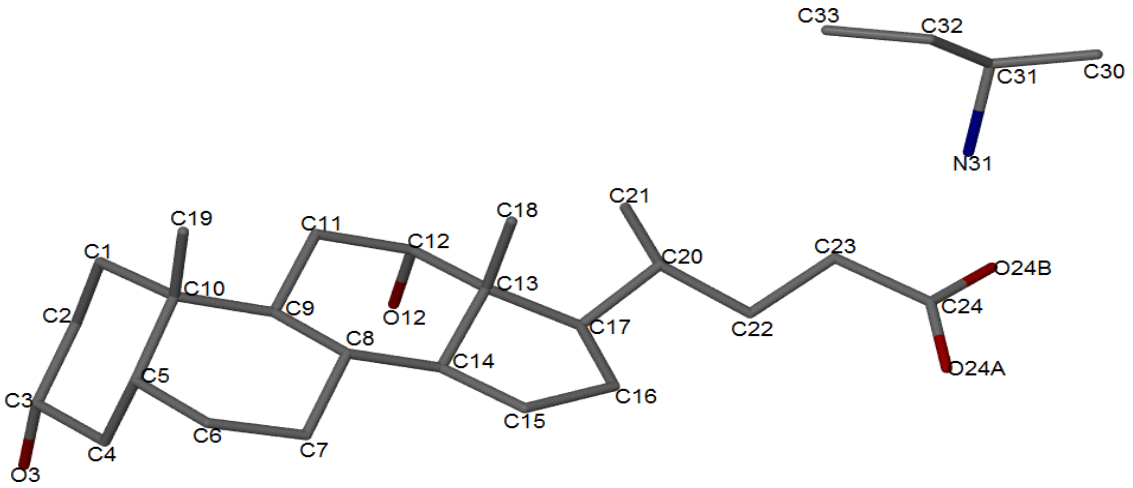

B

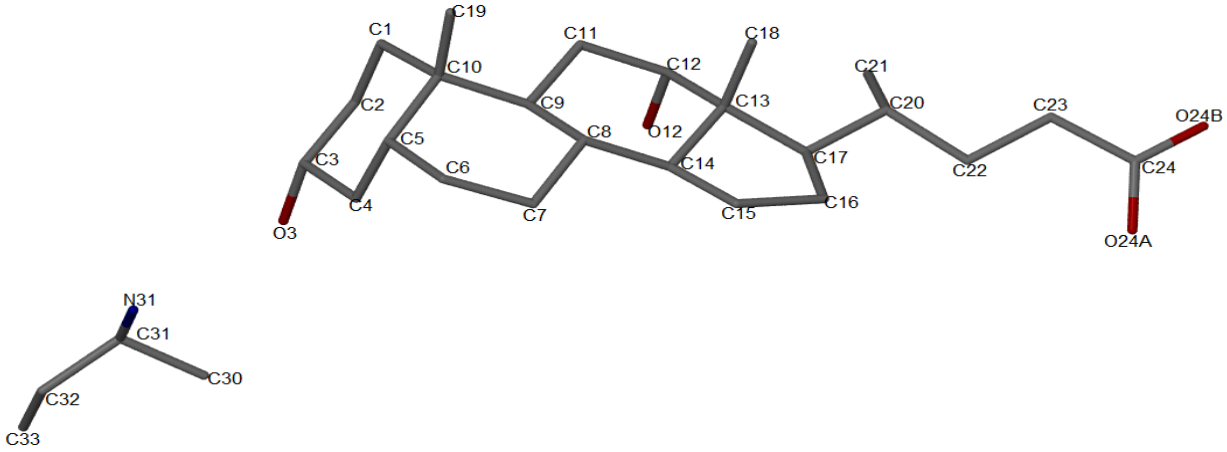

Figure 5.2.1: Formula units for **(DCA$^-$)(*R*-BUAM$^+$)** (A) and **(DCA$^-$)(*S*-BUAM$^+$)** (B)

Hydrogen bonding is the main form of interaction for both structures. Figure 5.2.2 shows hydrogen bonding observing in the structures of DCA and *sec*-butylamine.

A

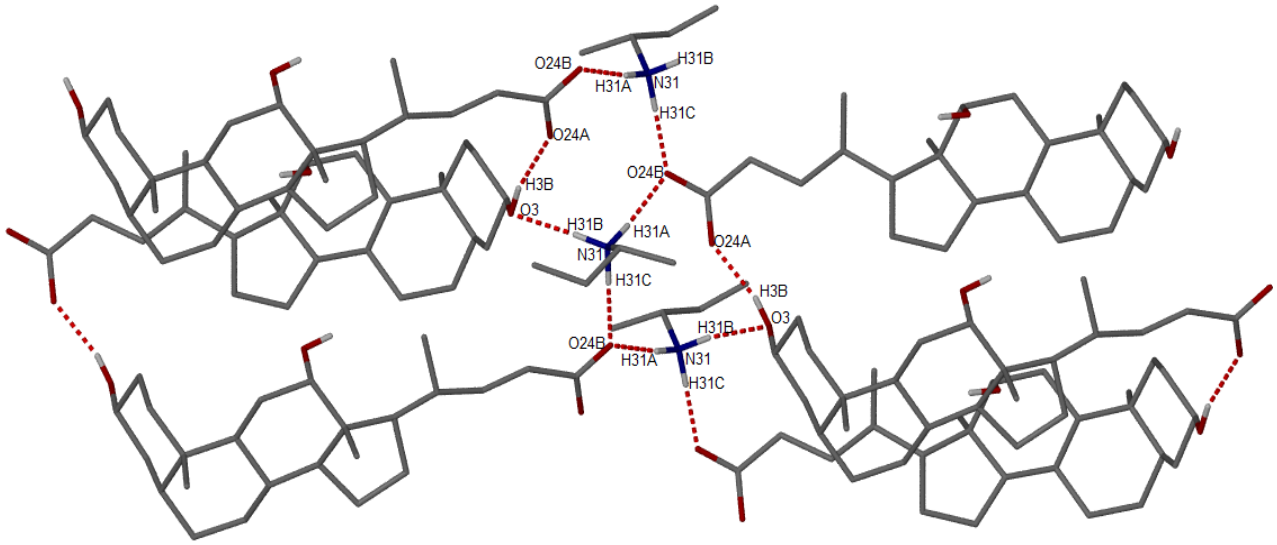

B

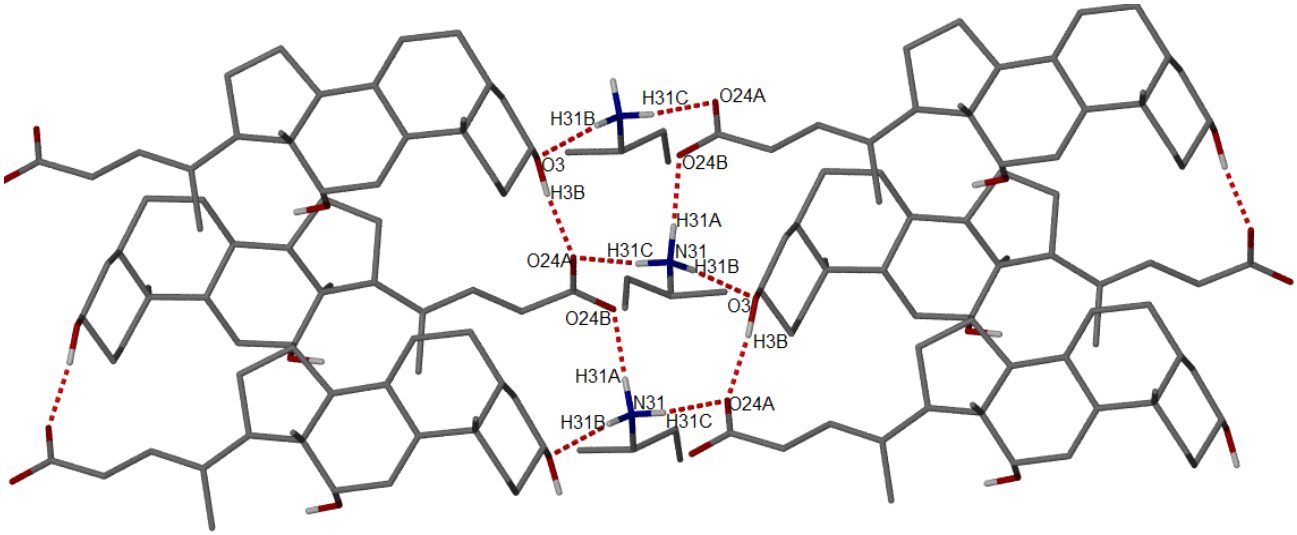

Figure 5.2.2: Hydrogen bonding in **(DCA$^-$)(*R*-BUAM$^+$)** (A) and **(DCA$^-$)(*S*-BUAM$^+$)** (B)

The hydrogen bonding in both structures is identical. A hydrogen bond ring with the graph set $R_5^4(12)$ is formed in both structures. The DCA anions arrange such that the tail of one anion hydrogen bonds to the head of the other. The carboxylate tail also hydrogen bonds to the protonated *sec*-butylamine. A bifurcated hydrogen bond is formed at O24B in the structure of **(DCA$^-$)(*R*-BUAM$^+$)** and at O24A in **(DCA$^-$)(*S*-BUAM$^+$)**. The OH tail of the anion acts as a hydrogen bond donor and acceptor on both structures. The hydrogen bond parameters are shown in **Table 5.2.2**.

Table 5.2.2: Hydrogen bond parameters in structures of DCA with *sec*-butylamine

COMPOUND	D-H···A	D···A (Å)	D-H (Å)	H···A (Å)	D-H···A (º)
(DCA$^-$)(*R*-BUAM$^+$)	N31-H31A···O24B^a	2.784 (3)	0.91 (3)	1.88 (3)	172 (3)
	N31-H31B···O3^b	2.890 (3)	0.96 (3)	1.94 (3)	170 (3)
	N31-H31C···O24B	2.753 (3)	0.89 (3)	1.86 (3)	178 (3)
	O3-H3B···O24A^b	2.636 (3)	0.81 (4)	1.84 (4)	167 (4)
	N31-H31A···O24A^a	3.230 (3)	0.91 (3)	2.60 (3)	130 (3)
a = ½-x,-½+y,-1-z; *b* = ½-x,½+y,-z					
(DCA$^-$)(*S*-BUAM$^+$)	O3-H3B···O24A^a	2.707 (2)	0.85 (3)	1.87 (3)	170 (3)
	N31-H31C···O24A^b	2.785 (2)	0.91 (2)	1.88 (2)	170 (2)
	N31-H31C···O24B^b	3.290 (2)	0.91 (2)	2.62 (2)	130 (2)
	N31-H31B···O3	2.822 (2)	0.84 (1)	2.00 (1)	167 (2)
	N31-H31A···O24B^c	2.730 (2)	0.92 (3)	1.82 (3)	168 (2)
a = -x,½+y,1-z; *b* = x, y,1+z; *c* = -x,-½+y,1-z					

The packing diagram and host arrangement in the structure of **(DCA$^-$)(*R*-BUAM$^+$)** are represented in **Figure 5.2.3**. The unit cell of the compound is shown in **Figure 5.2.3** (A) with four hosts and four guest ions enclosed inside the cell. The host ions pack in bilayers, forming channels down [001] as shown in **Figure 5.2.3** (B) and the guest occupies the constricted channels. The guest ions position themselves close to the carboxylate moieties.

A

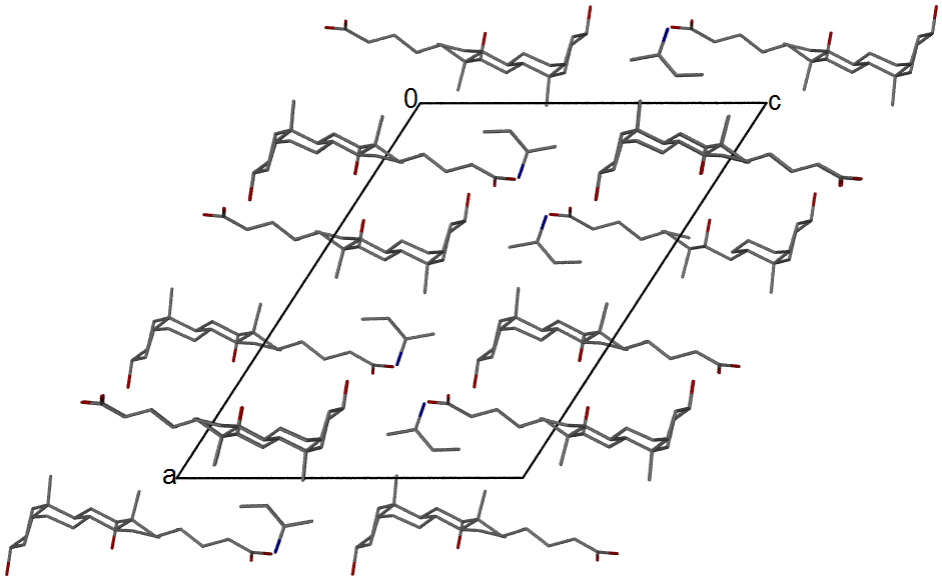

B

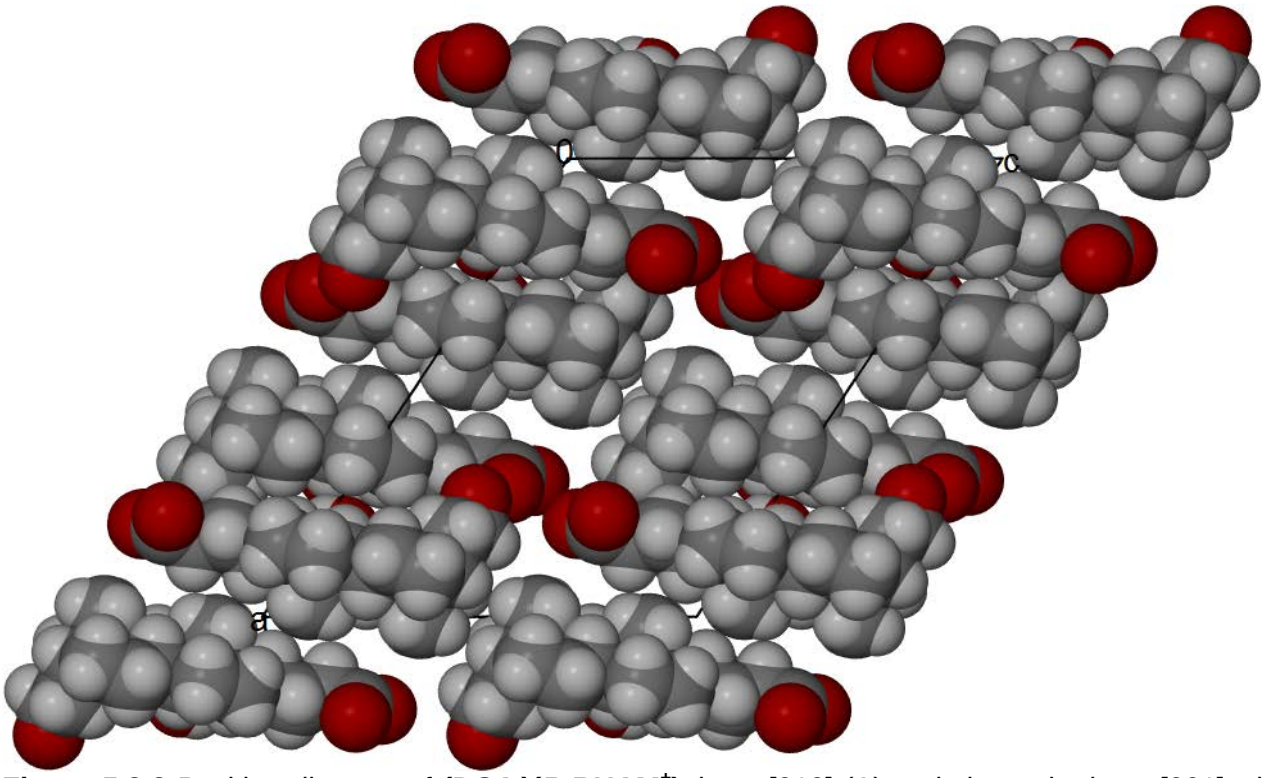

Figure 5.2.3 Packing diagram of **(DCA$^-$)(*R*-BUAM$^+$)** down [010] (A) and channels down [001] with DCA in van der Waals radii (B)

The host ions in the structure of **(DCA$^-$)(*S*-BUAM$^+$)** pack in a similar manner as the previous structure. The packing diagram of the compound is shown in **Figure 5.2.4** (A). The guest ions reside in channels formed down [010] as shown in **Figure 5.2.4** (B), guest omitted.

A

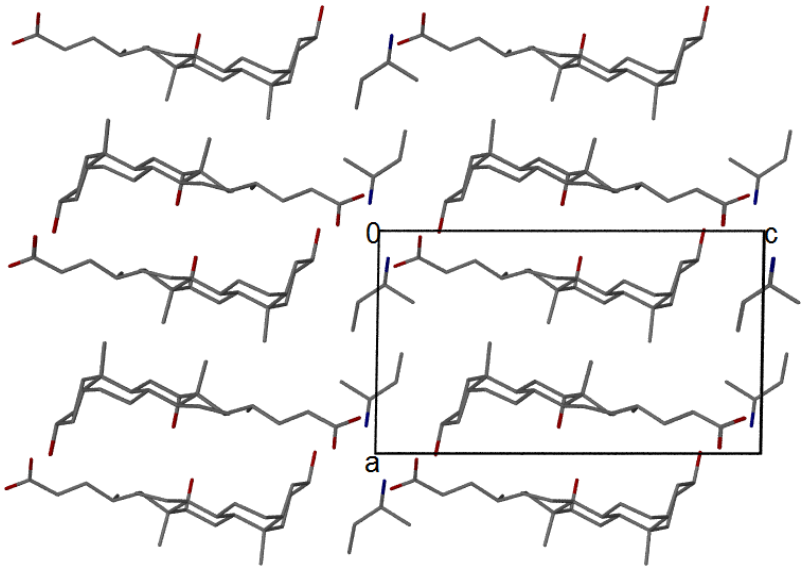

B

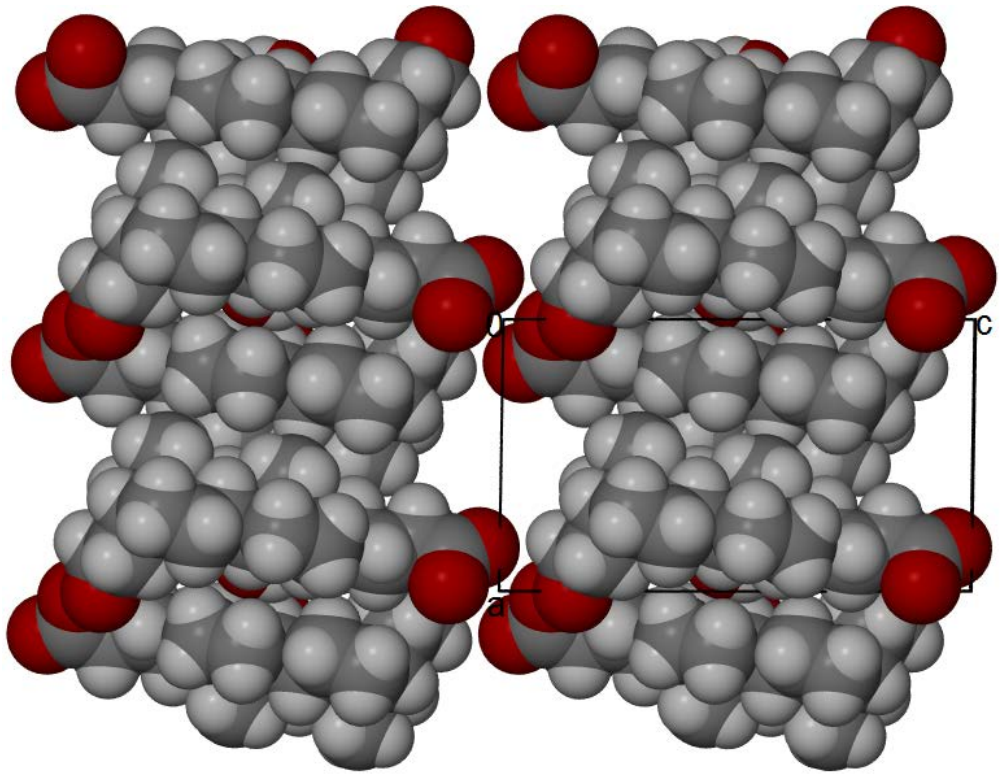

Figure 5.2.4: Packing diagram of **(DCA$^-$)(*S*-BUAM$^+$)** down [010] (A) and channels down [010] with DCA in van der Waals radii, guest omitted (B)

The channels in the structure of **(DCA$^-$)(*R*-BUAM$^+$)**, (A) are more constricted compared to those in **(DCA$^-$)(*S*-BUAM$^+$)**, (B). This would explain the higher onset temperature for the release of the guest in **(DCA$^-$)(*R*-BUAM$^+$)**. Analyses of the two structures with MSRoll[1] using a probe size 1.2 Å showed that both structures have unoccupied voids between the anions. The voids in **(DCA$^-$)(*R*-BUAM$^+$)** are larger (30.4 Å^3) compared to those in **(DCA$^-$)(*S*-BUAM$^+$)** which are 14.3 Å^3, hence a lower density of the former reported in the crystal data table. The different arrangements of the anion viewed down [001] are shown in **Figure 5.2.5**.

A

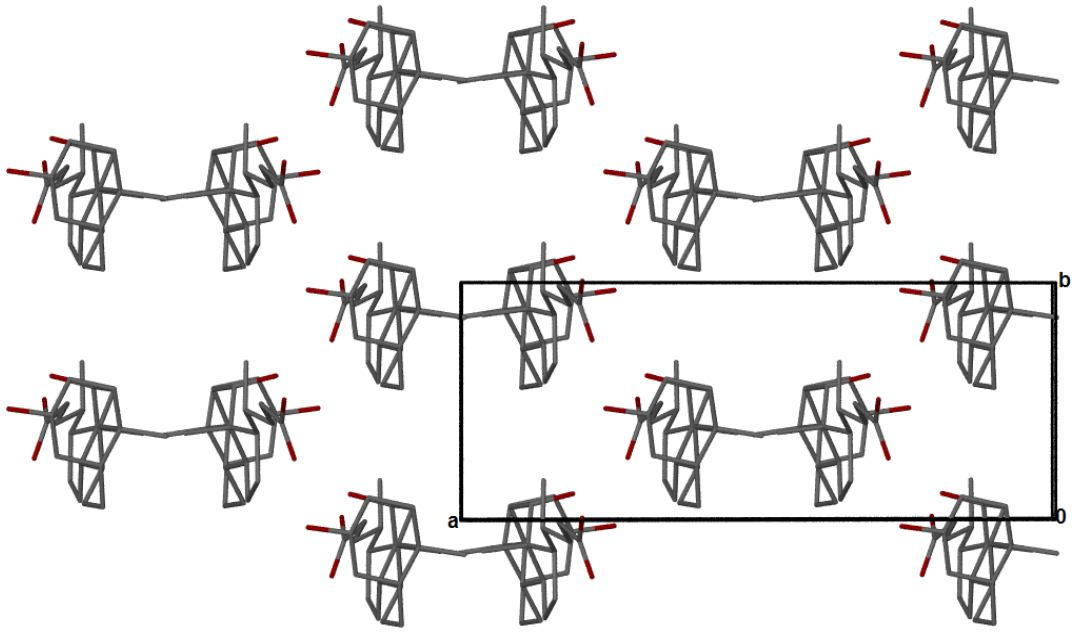

B

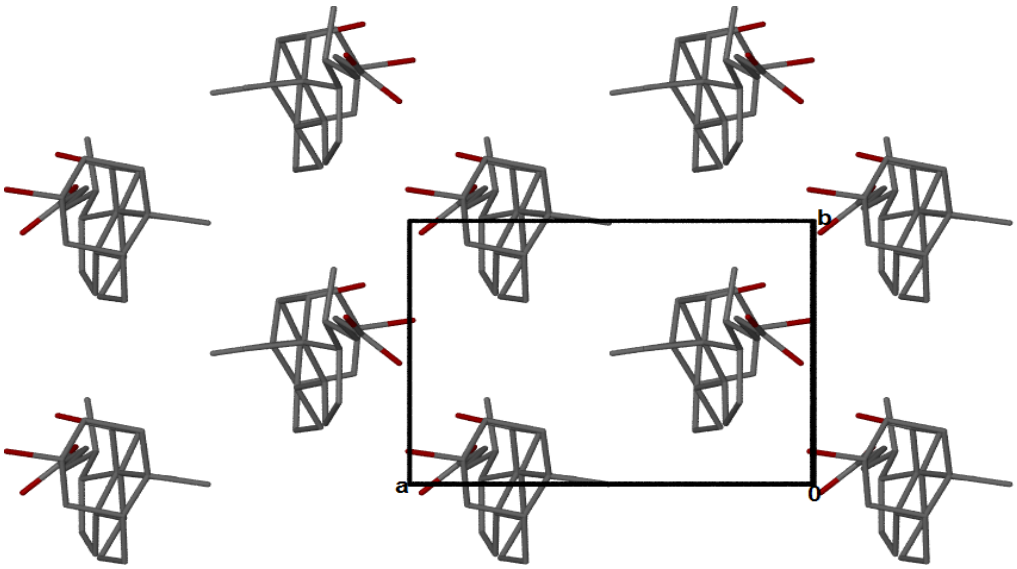

Figure 5.2.5: Anion arrangements in **(DCA$^-$)(*R*-BUAM$^+$)** (A) and **(DCA$^-$)(*S*-BUAM$^+$)** (B) viewed down [001]

Host and guest ions in the structures of **(DCA$^-$)(*R*-BUAM$^+$)** and **(DCA$^-$)(*S*-BUAM$^+$)** were overlaid using Mercury[2] for comparison. The RMSD for the host is 0.2 Å and a maximum distance of 0.66 Å was observed between the O atoms of the carboxylate for the two structures. This is because of the flexibility of the long chain bearing the carboxylate moiety. Root mean square deviation (RMSD) which is the average distance between the atoms was determined. An overlay of the guest ions yielded a higher RMSD of 0.8 Å with the maximum distance of 1.04 Å observed between C32 for the respective structures. This is caused by the opposite chirality of the guests.

The host ions pack in a similar manner in both structures, they arrange in pairs in head to tail dimers. However the supramolecular packing of the subunits is different, in the structure of **(DCA$^-$)(*R*-BUAM$^+$)**, the subunits repeat along [100] while in **(DCA$^-$)(*S*-BUAM$^+$)** they repeat vertically on the [100] axis.

5.3 Guest exchange experiment

A guest exchange experiment was performed by exposing the ground sample of **(DCA$^-$)(PPA$^+$)•ACE** to vapours of racemic 2-BUAM. The resultant powders were analysed by thermal analysis and PXRD. The results were compared to the starting material and the results for **(DCA$^-$)(*R*-BUAM$^+$)**. The DSC curves of **(DCA$^-$)(PPA$^+$)•ACE** and **(DCA$^-$)(*R*-BUAM$^+$)** are very similar and therefore the experiment could not be monitored using DSC. Hence the change in mass loss was observed using TGA. The mass loss of 15.2 % on the TG curve of the final sample matches the loss of 2-BUAM. **Figure 5.3.1** shows the comparison of thermogravimetric analysis results.

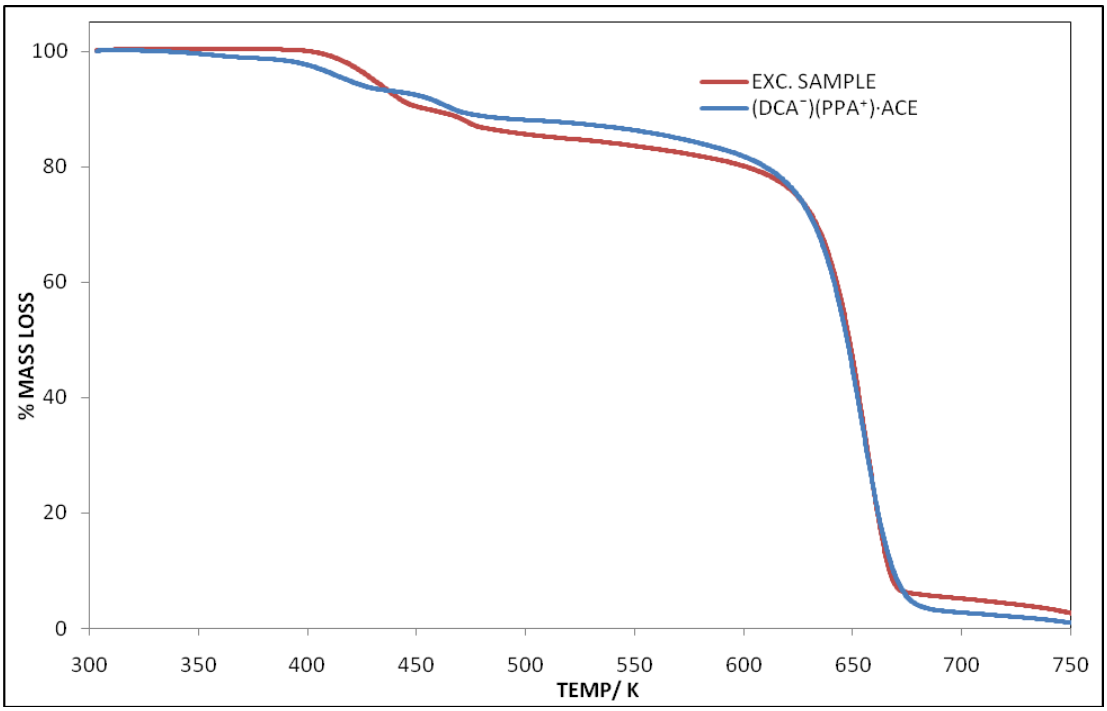

Figure 5.3.1: Overlay of the TG curves for the starting material (blue), **(DCA$^-$)(PPA$^+$)•ACE** and the final product (red) after guest exchange

The powder pattern of the final product was also compared to the PXRD patterns of **(DCA$^-$)(PPA$^+$)•ACE** and **(DCA$^-$)(*R*-BUAM$^+$)** generated from crystal structure data by Mercury[2] software. **Figure 5.3.2** shows the comparison of the generated powder patterns to that of the guest exchange sample.

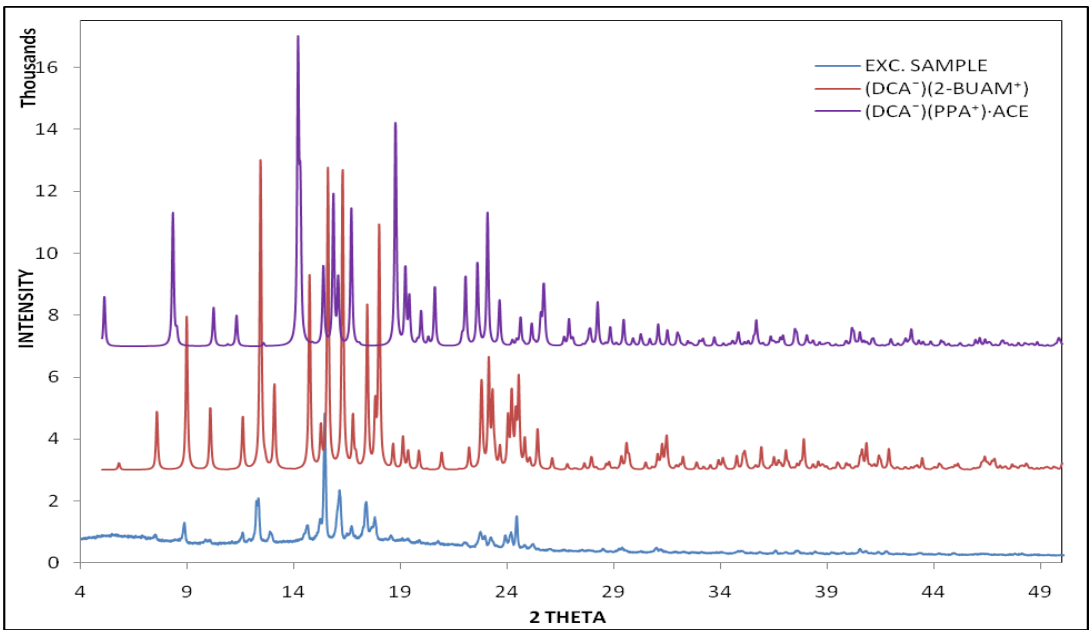

Figure 5.3.2: Overlay of the powder patterns

The powder pattern of the guest exchange sample matches that of **(DCA$^-$)(*R*-BUAM$^+$)**, therefore PPA was successfully exchanged for 2-BUAM.

REFERENCES

[1] Connolly, M. L. (1993), The molecular surface package , *J. Mol. Graphics*, Vol. 11: 139–141.

[2] Allen, F. H. & Lipscomb, K. J. (2004), The Cambridge Structural Database, *Encyclopedia of Supramolecular Chemistry*, Ed: Atwood, J. L. & Steed, J. W., Vol. 1:161-168.

CHAPTER 6

DCA AND CHIRAL 2-AMINO-3-METHYLBUTANE COMPOUNDS

6.1 Thermal analysis

The crystals of (+)-deoxycholic acid (DCA) and (*R*)-(+)-2-amino-3-methylbutane (*R*-MeBUAM) and DCA and (*S*)-(-)-2-amino-3-methylbutane (*S*-MeBUAM) were formed by dissolving small amounts (≈ 20 mg) of deoxycholic acid in a few drops of the respective amine. The white precipitates formed were dissolved in acetone with the aid of heating and stirring vigorously. The clear solutions were allowed to evaporate slowly at room temperature. An equimolar mixture of the enantiomers was prepared in the laboratory to obtain the racemic mixture and the crystals were also obtained as above. Thermal analysis was performed and the results obtained are reported in **Table 6.1.1** and **Figure 6.1.1**.

Table 6.1.1: DSC and TG results for compounds of DCA with MeBUAM

Compound	**(DCA$^-$)(*R*-MeBUAM$^+$)**	**(DCA$^-$)(*S*-MeBUAM$^+$)**
H:G ratio	1:1	1: 1
Endo (T_{on}, K)	404.9	411.7
Endo range (K)	404.9- 495.3	411.7- 502.6
Experimental % mass loss	17.8	17.8
Theoretical % mass loss	18.2	18.2

A

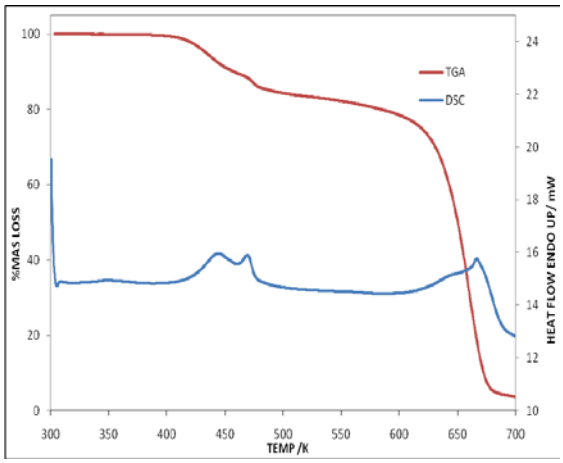

B

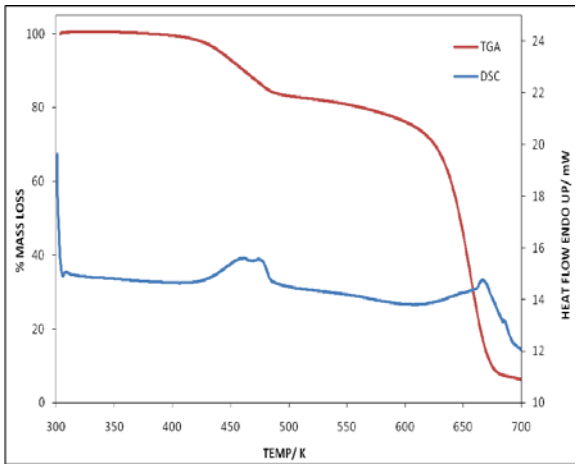

Figure 6.1.1: DSC and TG curves for **(DCA$^-$)(*R*-MeBUAM$^+$)** (A) and **(DCA$^-$)(*S*-MeBUAM$^+$)** (B)

Similar TG and DSC curves were obtained for both samples. The experimental mass losses are close to the expected values with the host-guest ratios of 1:1. The endotherms and mass losses on both curves were assigned to the loss of amine and melt. A slight difference in onset temperatures is observed. The onset temperature for the endotherm **(DCA$^-$)(*S*-MeBUAM$^+$)** is 6.8 K higher than that of **(DCA$^-$)(*R*-MeBUAM$^+$)** which is an indication of the difference in stability of the compounds

formed and could explain the selection of *S*-MeBUAM from the racemic modification. Decomposition of the host occurs after 600 K.

6.2 Structural analysis

The structures of **(DCA$^-$)(*R*-MeBUAM$^+$)** and **(DCA$^-$)(*S*-MeBUAM$^+$)** were obtained by crystallizing DCA with the pure enantiomers of MeBUAM. The efforts to resolve the racemic mixture of MeBUAM were successful because the host compound captured the *S*-enantiomer from the racemic mixture and the structure for **(DCA$^-$)(*S*-MeBUAM$^+$) (I)** was obtained. The structures obtained have identical crystal systems, space groups as well as Z values. All crystallized in the monoclinic crystal system, space group $P2_1$ with Z=2. Unlike the other two structures, the structural analysis of **(DCA$^-$)(*R*-MeBUAM$^+$)** was performed at room temperature. The formula units of the respective structures are shown in **Figure 6.2.1**. The host: guest ratio is 1: 1 for all structures. Structural analysis of the obtained crystals was also performed and the data displayed in **Table 6.2.1.**

Table 6.2.1: Crystal data table of DCA with MeBUAM

Compound	**(DCA$^-$)(*R*-MeBUAM$^+$)**	**(DCA$^-$)(*S*-MeBUAM$^+$)**	**(DCA$^-$)(*S*-MeBUAM$^+$)(I)**
Molecular Formula	$(C_{24}H_{39}O_4^-)(C_5H_{14}N^+)$	$(C_{24}H_{39}O_4^-)(C_5H_{14}N^+)$	$(C_{24}H_{39}O_4^-)(C_5H_{14}N^+)$
Molecular Mass ($gmol^{-1}$)	479.8	479.8	479.8
Data collection temp.(K)	296 (2)	173 (2)	173 (2)
Crystal system	Monoclinic	Monoclinic	Monoclinic
Space group	$P2_1$	$P2_1$	$P2_1$
a (Å)	11.5010(2)	11.026 (2)	11.080 (2)
b (Å)	7.7042(15)	7.5245 (15)	7.5757 (15)
c (Å)	17.175 (4)	17.160 (4)	17.614(4)
α (°)	90.00	90.00	90.00
β (°)	106.189 (4)	105.26 (3)	106.661 (3)
γ (°)	90.00	90.00	90.00
Volume ($Å^3$)	1461.5 (5)	1408.7 (5)	1416.8 (5)
Z	2	2	2
D_c, Calculated density ($g\ cm^{-3}$)	1.090	1.131	1.125
Final R indices [I>2sigma(I)]	R_1= 0.0516 wR_2= 0.1282	R_1= 0.0440 wR_2= 0.0897	R_1= 0.0720 wR_2= 0.1903
R indices (all data)	R_1= 0.0887 wR_2= 0.1500	R_1= 0.1138 wR_2= 0.1349	R_1= 0.1297 wR_2=0.2306
Largest diff. peak & hole ($eÅ^{-3}$)	-0.156; 0.225	-0.285; 0.254	-0.354; 0.848

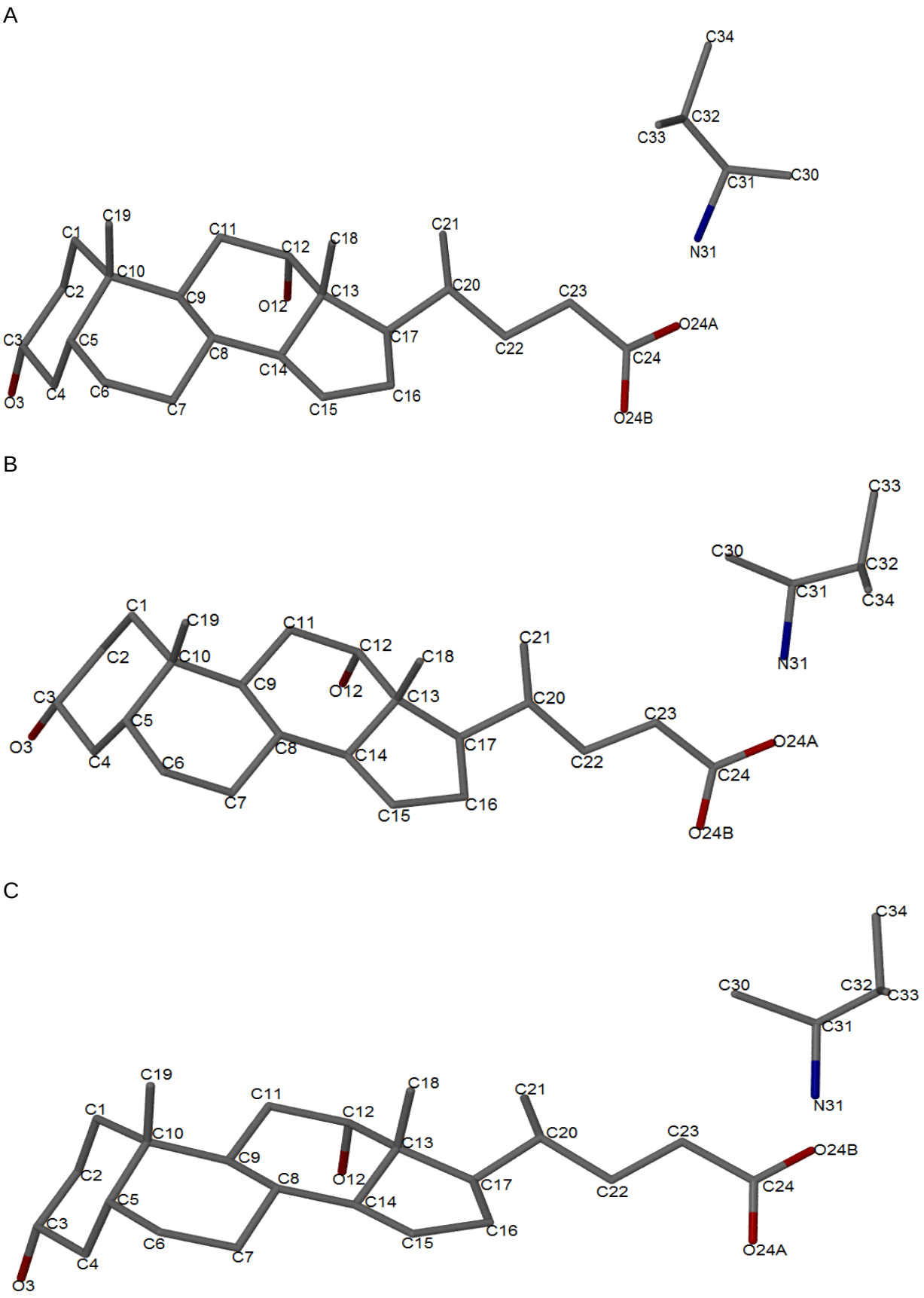

Figure 6.2.1: Formula units of **(DCA^-)(*R*-MeBUAM$^+$)** (A), **(DCA^-)(*S*-MeBUAM$^+$)** (B) and **(DCA^-)(*S*-MeBUAM$^+$)(I)** (C) with the hydrogen atoms omitted for clarity

Hydrogen bonding is the main form of interaction in the structures obtained. Their hydrogen bonding networks are represented in **Figure 6.2.2**. The host ions in all the structures arrange such that they hydrogen bond head to tail. In the structure of **(DCA$^-$)(*R*-MeBUAM$^+$)**, three centred hydrogen bonds are formed at H31A, O24A and O24B. H31A forms hydrogen bonds with both oxygen atoms of the carboxylate moiety, (O24A and O24B). O24A then hydrogen bonds to H31B from another guest molecule and O24B hydrogen bonds to H3B from the OH head of the nearby host molecule. The OH head is the hydrogen bond donor as well as the acceptor. Hydrogen bond rings with the graph set $R_5^3(10)$ $R_1^2(4)$ hold the ions together.

The structures of **(DCA$^-$)(*S*-MeBUAM$^+$)** and **(DCA$^-$)(*S*-MeBUAM$^+$)(I)** are held together by hydrogen bond rings with the graph set $R_5^4(12)$**.** All the hydrogen atoms around the N atom of the guest are involved in hydrogen bonding. A three centre bond is formed at O24B on both structures. **Table 6.2.2** shows the hydrogen parameters of the different structures.

A

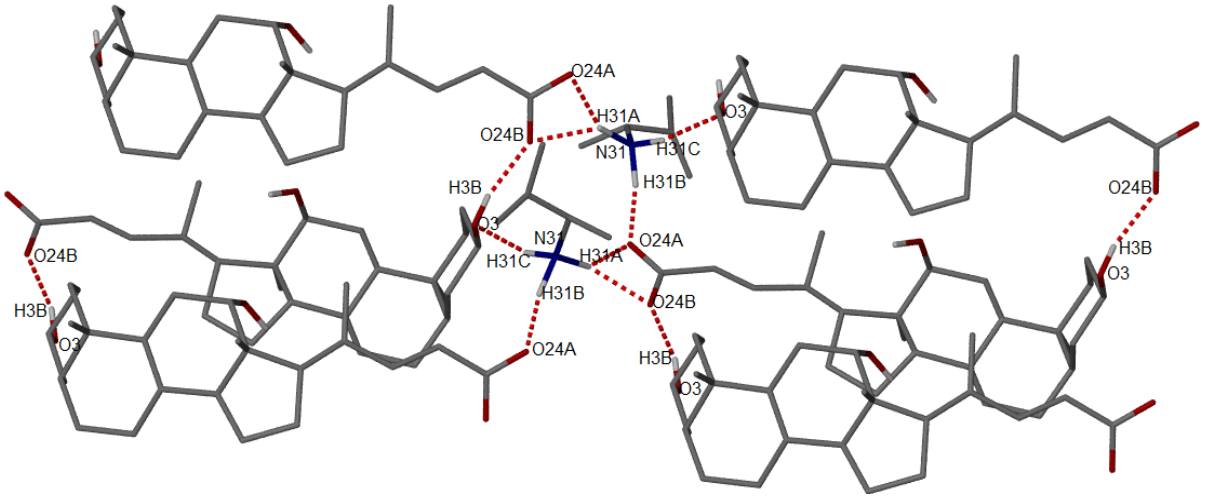

B

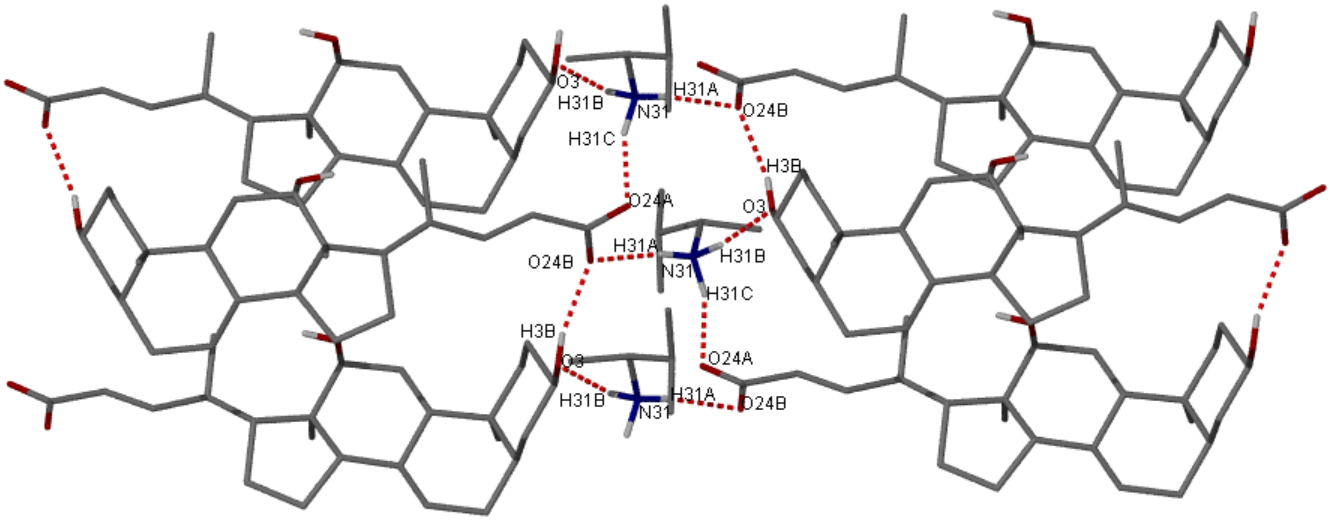

C

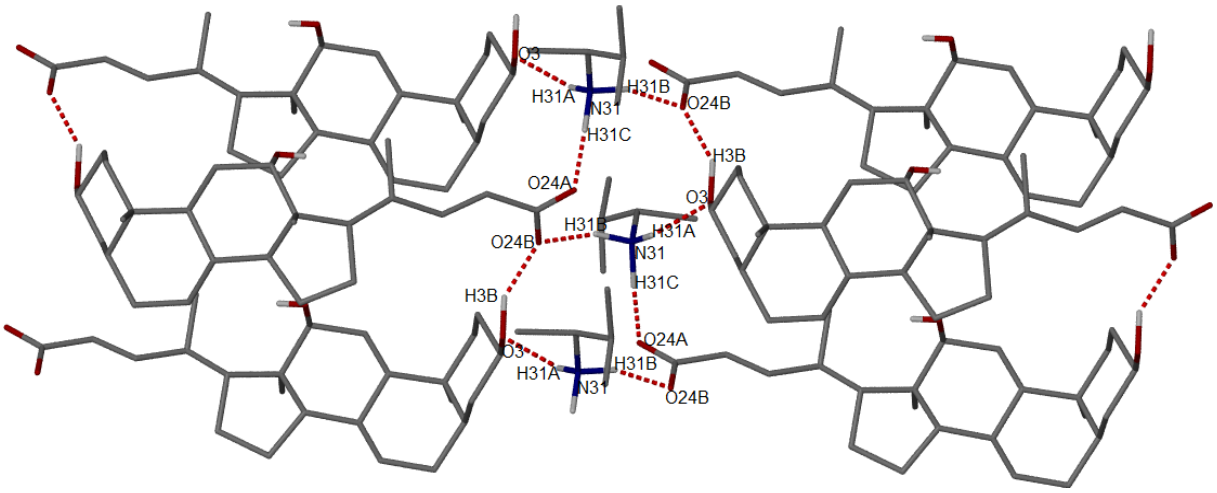

Figure 6.2.2: Hydrogen bonding interactions in **(DCA$^-$)(*R*-MeBUAM$^+$)** (A), **(DCA$^-$)(*S*-MeBUAM$^+$)** (B) and **(DCA$^-$)(*S*-MeBUAM$^+$)(I)** (C)

Table 6.2.2: Hydrogen parameters in structures of DCA with MeBUAM

Compound	D-H···A	D···A (Å)	D-H (Å)	H···A (Å)	D-H···A (º)
(DCA$^-$)(*R*-MeBUAM$^+$)	N31-H31B···O24A	2.739 (4)	0.94 (2)	1.81 (2)	169 (3)
	N31-H31C···O3^a	2.868 (4)	1.19 (5)	1.67 (5)	176 (4)
	N31-H31A···O24B^b	3.007 (4)	0.87 (4)	2.17 (4)	161 (4)
	N31-H31A···O24A^b	2.992(4)	0.87 (4)	2.27 (4)	140 (4)
	O3-H3B···O24B^a	2.682 (4)	0.66 (4)	2.02 (4)	176 (6)
a = 2-x,½+y,2-z; *b* = 1-x,½+y,1-z					
(DCA$^-$)(*S*-MeBUAM$^+$)	N31-H31C···O24A	2.736 (5)	1.01 (5)	1.82 (5)	149 (3)
	N31-H31B···O3^a	2.808 (4)	1.06 (4)	1.79 (4)	161 (3)
	N31-H31A···O24B^b	2.778 (4)	0.90 (1)	1.89 (1)	170 (3)
	N31-H31A···O24A^b	3.301 (4)	0.90 (1)	2.62 (2)	133 (3)
	O3-H3B···O24B^a	2.724 (4)	0.76 (5)	1.98 (5)	167 (5)
a = -x,-½+y,-z ; *b* = -x,-½+y,1-z					
(DCA$^-$)(*S*-MeBUAM$^+$)(I)	N31-H31C···O24A	2.732 (4)	0.95 (1)	2.09 (7)	123 (7)
	N31-H31A···O3^a	2.826 (4)	0.86 (1)	2.03 (2)	154 (4)
	N31-H31B···O24B^b	2.771 (4)	1.09 (1)	1.72 (1)	160 (4)
	N31-H31B···O24A^b	3.287 (4)	1.09 (1)	2.47 (3)	130 (4)
	O3-H3B···O24B^a	2.718 (4)	1.05 (1)	1.92 (4)	130 (4)
a = 1-x,-½+y,1-z; *b* = 1-x,-½+y,2-z					

The packing diagrams of **(DCA$^-$)(*S*-MeBUAM$^+$)** and **(DCA$^-$)(*S*-MeBUAM$^+$)(I)** are similar and the former was chosen for comparison with the packing diagram of **(DCA$^-$)(*R*-MeBUAM$^+$)**. An overlay of the *S*-MeBUAM structures is shown in **Figure 6.2.3.** The structures were found to have RMS = 0.1, which indicates their high degree isostructurality.

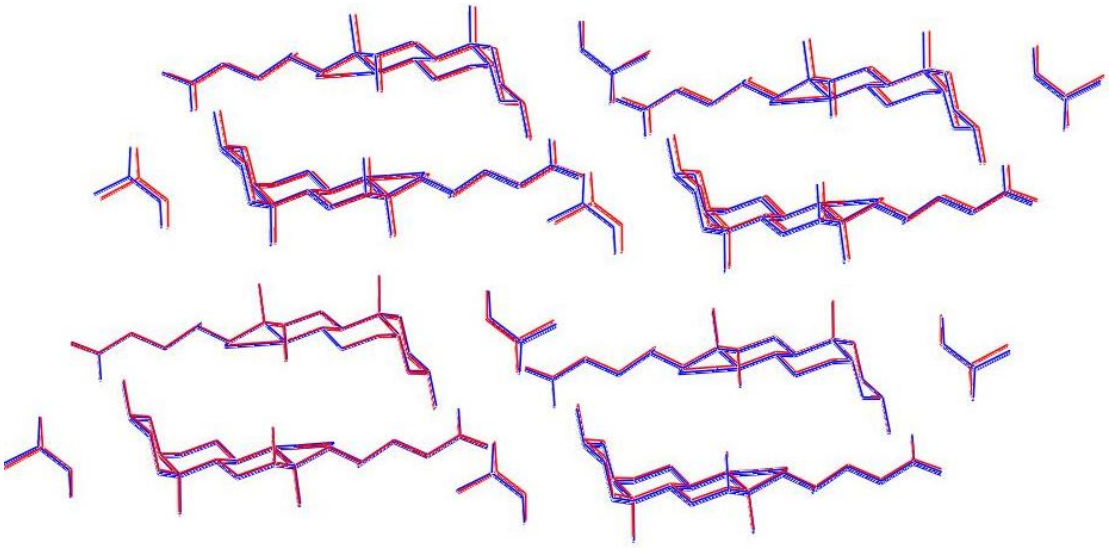

Figure 6.2.3: Overlay of **(DCA$^-$)(*S*-MeBUAM$^+$)** in blue and **(DCA$^-$)(*S*-MeBUAM$^+$)(I)** in red

The packing diagrams are shown in **Figure 6.2.4**.

A

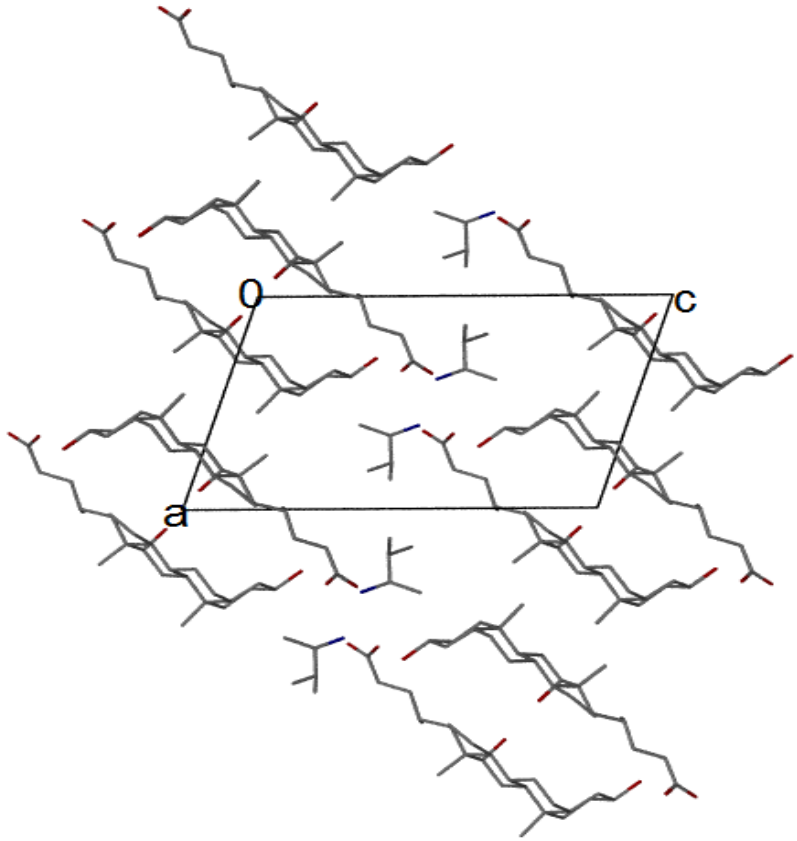

B

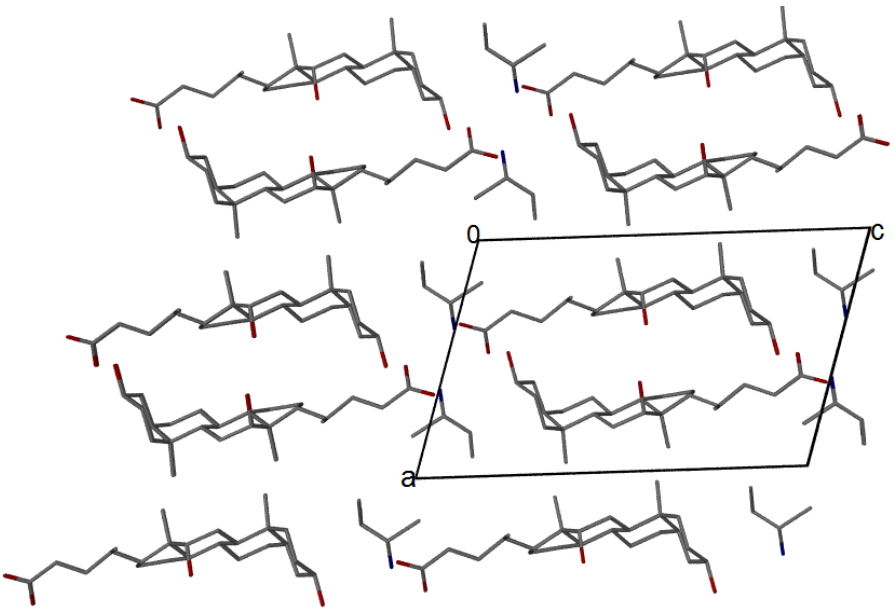

Figure 6.2.4: Packing diagrams of **(DCA$^-$)(*R*-MeBUAM$^+$)** (A) and **(DCA$^-$)(*S*-MeBUAM$^+$)** (B) viewed down [010]

The packing diagrams of the two salts are similar in that they both have two host and guest ions inside the unit cell.

The host ions in both structures arrange in parallel pairs on the hydrophilic faces. The pairs form channels down [010]. In the structure of **(DCA$^-$)(*R*-MeBUAM$^+$)**, channels are more elongated than in **(DCA$^-$)(*S*-MeBUAM$^+$)**. The channels formed by the host ions viewed down [010] are shown in **Figure 6.2.5**.

A

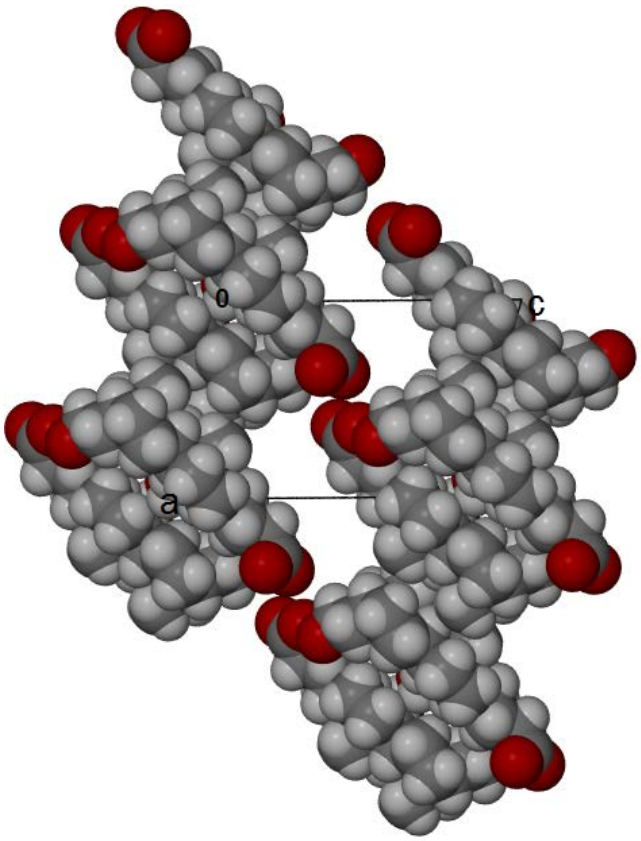

B

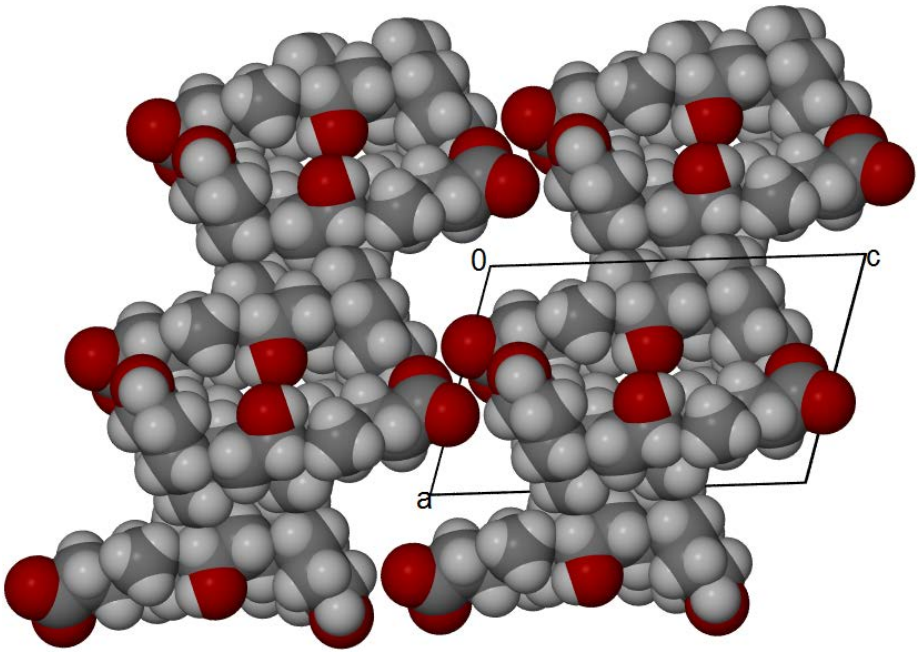

Figure 6.2.5: Channels of **(DCA$^-$)(*R*-MeBUAM$^+$)** (A) and **(DCA$^-$)(*S*-MeBUAM$^+$)** (B) viewed down [010], the host ions are depicted in van der Waals radii

There is a difference in the sizes of the channels. The volumes of the voids were calculated using MSRoll[1] using a probe size of 1.2 Å. The void in the *R*-MeBUAM structure was found to be 373.1 Å^3 and 301.6 Å^3 was obtained for the *S*-MeBUAM structure.

The overall packing factors of the unit cells for **(DCA$^-$)(*R*-MeBUAM$^+$)** and **(DCA$^-$)(*S*-MeBUAM$^+$)** are 64.7 % and 67.7%, respectively. The packing factors of the guest sites were determined and the results are reported in **Table 6.2.3**.

Table 6.2.3: Packing factors for **(DCA$^-$)(*R*-MeBUAM$^+$)** and **(DCA$^-$)(*S*-MeBUAM$^+$)**

	(DCA$^-$)(*R*-MeBUAM$^+$)	**(DCA$^-$)(*S*-MeBUAM$^+$)**
$V_{guest\ mol}$ (Å^3)	101.8	104.4
V_{void} (Å^3)	373.1	301.6
V_{mol}/V_{void} = PF%	27.2	34.3

$V_{guest\ mol}$ - guest volume and V_{void} - void volume

The results show that the *S*-enantiomer is more tightly packed within the structure than that of the *R*-enantiomer. The larger packing factor for the *S*-isomer structure correlates to the densities obtained in **Table 6.2.1**, 1.090 g cm^{-3} for **(DCA$^-$)(*R*-MeBUAM$^+$)** and 1.131 g cm^{-3} for **(DCA$^-$)(*S*-MeBUAM$^+$)**. Small unoccupied voids were also found in the structures that make the volumes of the voids larger, hence low guest site packing factors. These voids are 62.6 Å^3 for **(DCA$^-$)(*R*-MeBUAM$^+$)** and 34.2 Å^3 for **(DCA$^-$)(*S*-MeBUAM$^+$)**.

The host and guest ions from the two structures were overlaid and molecular isostructurality was determined using Mercury[2] software. The average distance between the atoms was calculated and expressed in Å as the RMSD. An RMSD value of 0.1 Å was obtained for the host and a maximum distance of 0.44 Å was found at the O atoms of the carboxylate. Guest overlay gave a higher RMSD value of 0.6 Å with a maximum distance of 0.97 Å between C32 atoms. A larger difference is correlated to the configuration and flexibility of the guest ions.

The crystal packing of the two compounds were overlaid as shown in **Figure 6.2.6** with the structure of **(DCA$^-$)(*R*-MeBUAM$^+$)** in red and **(DCA$^-$)(*S*-MeBUAM$^+$)** shown in blue. The host packing is similar, the cations are found at a common site and this resulted in similar channels formed by the hosts. RMS, which gives measure of divergence of structures, was found to be 0.9, indicating a good structural fit.

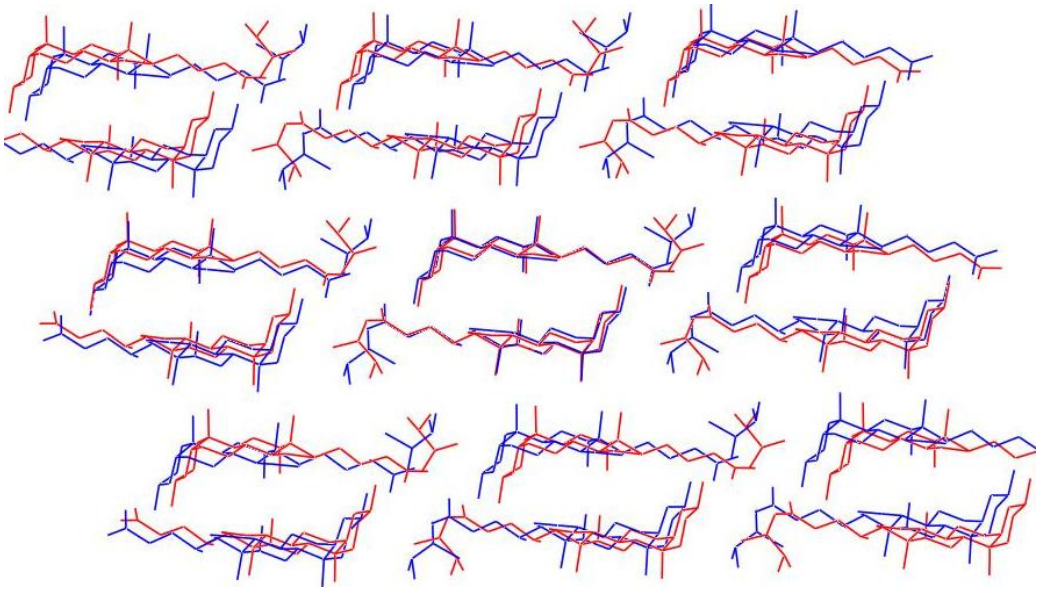

Figure 6.2.6: Overlay of **(DCA$^-$)(*R*-MeBUAM$^+$)** in red and **(DCA$^-$)(*S*-MeBUAM$^+$)(I)** in blue viewed down [010]

REFERENCES

[1] Connolly, M. L. (1993), The molecular surface package , *J. Mol. Graphics*, Vol. 11: 139–141.

[2] Allen, F. H. and Lipscomb, K. J. (2004), The Cambridge Structural Database, *Encyclopedia of Supramolecular Chemistry*, Vol. 1:161-168.

CHAPTER 7

CONCLUSION

Understanding the mechanism of chiral resolution of a racemic modification via diastereomeric salt formation is of fundamental importance. Application of resolution techniques is also of direct importance in the pharmaceutical, food and fine chemical industries.

Successful resolution was attained with (+)-deoxycholic acid (DCA). The host compound was able to resolve racemic *sec*-butylamine, (capturing the *R* isomer from a racemate) and racemic 2-amino-3-methylbutane where the *S*-enantiomer was selected.

Significant difference was observed in the structures of **(DCA^-)(*R*-$BUAM^+$)** and **(DCA^-)(*S*-$BUAM^+$)**. The two structures crystallized in different space groups. **(DCA^-)(*R*-$MeBUAM^+$)** and **(DCA^-)(*S*-$MeBUAM^+$)** were structurally similar.

There were similarities in the packing of DCA for all the structures. However, different packing patterns of the host were observed in the structures of **(DCA^-)($DIBUAM^+$)** and **(2DCA^-)(2PPA^+)•5H_2O**.

The structures of **(2$QUIN^+$)(*L*-MA^{2-})•2H_2O** and **(2$QUIN^+$)(*D*-MA^{2-})•2H_2O** were compared. The two crystals showed very similar structural arrangement of the cations. The anions are entrapped in a crystallographically related position (both are sitting on a two-fold axis), however careful investigation of the void shows subtle differences. Structural analysis of the quininium cations demonstrates slight adjustment of the crystal packing to the entrapped malate anions. This delicate change in the crystal structure is related to the fine discrimination between *D*-(+)-malic acid and *L*-*(-)*-malic acid. Unfortunately the discrimination is not good enough to enable resolution of the racemic mixture because both *D* and *L* isomers were captured in the crystal structure after crystallizing the racemic mixture with QUIN.

Solvents being used during crystallization showed to play a role in the interaction of the guest and the host. Completely different structures of QUIN and *D*-(+)-malic acid were obtained from two solvents, **(2$QUIN^+$)(*D*-MA^{2-})•2H_2O** from ethanol and **($QUIN^+$)(*D*-MA^-)•H_2O** from water.

Notable differences in unit cell packing factors were observed in compounds where selectivity occurred. The unit cell packing factors for **(DCA^-)(*R*-$MeBUAM^+$)** and **(DCA^-)(*S*-$MeBUAM^+$)** were 27.2 % and 34.3 %, respectively while (**2$QUIN^+$)(*D*-MA^{2-})•2H_2O** and (**2$QUIN^+$)(*L*-MA^{2-})•H_2O** were 71.8 % and 70.9 %, respectively.

Kinetics results for **(DCA$^-$)(2-BUAM$^+$)** and **(DCA$^-$)(DIBUAM$^+$)** were correlated to the structures obtained. The structure of **(DCA$^-$)(DIBUAM$^+$)** shows that the guest ions reside in open channels hence lower activation energies reported. In the structure of **(DCA$^-$)(2-BUAM$^+$)**, the guest ions reside in constricted channels and this relates to the high activation energies obtained from kinetics of desolvation.